DEGREE PROJECT

Tribological characterisation of turbocharger turbine sealing rings in heavy duty diesel engines

Alex Gousskov
Alin Dumitru Durac

Mechanical Engineering, master's level
2018

Luleå University of Technology
Department of Engineering Sciences and Mathematics

LULEÅ UNIVERSITY OF TECHNOLOGY

Abstract

This work investigated the wear mechanisms of turbocharger components in heavy duty diesel engines. By understanding the wear mechanisms that are occurring in turbochargers the life time of the turbocharger components can be improved. For better understanding, as to why the components are worn out, an analysis of several turbocharger components and tribological tests were carried out.

The contact surfaces between turbocharger and sealing rings were analysed. Surfaces are analysed by several methods, including chemical composition of the surface. Influence of different parameters such as contact pressure, sliding velocity, temperature, and distance on friction and wear behaviour are established by performing tribological tests. Pin on disc sliding wear tests were carried out at both room temperature and at high temperature of 300˚C. The pin and the disc, that were used during the tribological tests, were made of the same materials that are used in turbocharger components.

Analysis of pins and discs from tribo-tests and turbocharger components (turbine sealing rings and shafts) show abrasive and adhesive wear on the worn surfaces of the components, from both the tribological tests and the turbochargers respectively. An increase of the temperature resulted in a reduced friction due to the formation of oxide layers on the sliding surfaces of pins and discs. In the turbocharger, traces of lubricant between the sliding surfaces was found, in addition to plastic deformations on the worn surfaces of the shafts and adhesive and abrasive wear on both worn surfaces that were in contact with each other. On the other hand, on the worn surfaces of the turbine sealing rings some cracks were observed that were perpendicular to the sliding direction, which indicates presence of a fatigue process. The presence of fatigue cracks is probably due to the way the trucks were operated, the increase and decrease of temperature and pressure in the turbocharger is probably the cause of these cracks.

To minimize the wear mechanisms that occurs in turbocharger components such as sealing rings and shafts, there are some parameters such as contact pressure between the sliding surfaces of the components that can be minimized. By minimizing the contact pressure between the sliding surfaces, the lifetime of turbocharger can be improved. A better surface finishing and geometry of the contacting surfaces can also improve the sealing rings and shafts lifetime. To minimize the relaxation of turbine sealing rings, materials that can better keep the mechanical properties of the sealing rings at high temperatures must be used.

Table of contents

1. Introduction

1.1 Tribology

Tribology is the science and technology of interacting surfaces in relative motion and of related subjects and practise. The word tribology comes from the Greek word *τρίβω* (tribo) meaning rubbing. The study focuses on friction, wear mechanisms and lubricants.

One of the earliest tribological thinking is found in old Egypt circa 1880 BC. Egyptians poured lubricant in front of a sled to be able to move the colossus El-Bersheh. Approximately 170 slaves were used to pull the 60 ton statue. It was possible due to the lubricant which lower the coefficient of friction down to 0.27 [1]. The coefficient of friction itself was introduced by Renaissance engineer-artist Leonardo da Vinci, who defined it as ratio of friction force that resisted sliding to normal load applied on the surface.

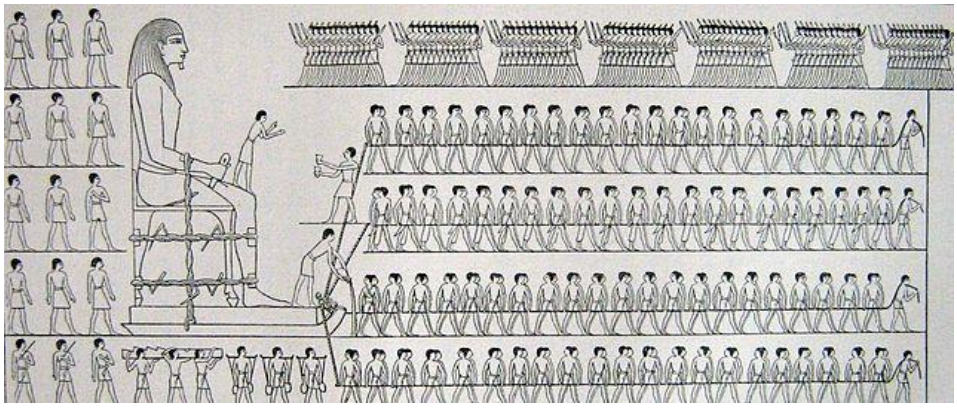

Figure 1. Egyptian using lubricant to aid movement of colossus, EL-Bersheh, ca 1880 B.C.

1.2 Tribological testing

Measurement of friction and wear is termed tribotesting and consist of four basic elements: simulation, acceleration, specimen preparation and friction and wear measurements. Good simulation is a correct prepared test that replicate the wear mechanisms in actual system. The simulation includes type of motion, speed, load, lubrication condition, and operating environment (humidity, temperature etc..). Acceleration of the test is used to minimize the cost by reducing lubricant or increasing load, speed or temperature. It is crucial to keep the same wear mechanism that occurs in real application. Specimen preparation is important for getting repeatable results from the test.

In laboratory testing, there are three types of contact geometries that are typically employed: conforming (area) contact, line contact and point contact. Conformal contact provides uniform and stable contact area after the parts has worn in. This result in accurate measurements data for validation. The point contact changes the contact area during the test but do not need alignment. There are various numbers of tribological tests that exist today. Some examples are:

Pin on disc (rotational)

Pin on disc tribological test is commonly used to measure the friction force and wear of materials. The test gives possibilities to vary load, temperature, lubricant even during the test. Usually the disc is made of a harder material than the pin to avoid the problem with the pin cutting through the disc instead of continuous wear. One of the most common problems with this type of test is the small oscillation or vibration during lubricated or boundary-lubricated conditions [2].

Pin on flat (reciprocating)

Pin on flat test uses an oscillation motion to evaluate friction and wear behaviour of the test material. This test is widely used to evaluate the friction behaviour of cylinder liner and piston rings, but other applications are also possible such as the replacement of shoulder joint. The test has an advantage of study of friction during start stop conditions and evaluate wear in human shoulder joints.

Taber abrasion test

Taber abrasion test evaluate a wear resistance in sliding rotational movement. This movement causes a specific rub-wear action which evaluate a resistance of surface to outside conditions. It is used to evaluate the effective strength of fabrics or the forces required to brake a specific width of fabric. Other application like determination of coating behaviour is also common.

Mar-Resistance Abrasion test

Mar-resistance abrasion test uses different techniques to evaluate the resistance to scratching of a material. The samples are usually high gloss rigid surfaces. It measures the difference in colour before and after which can be taken as measurement of resistance to scratch. The technique uses to evaluate the home electronics like flat screens.

1.3 Wear mechanisms

Wear constitutes the main limitation of the technical and economical service life of a machine. The wear is defined as the progressive loss of material from one or both the contacting surfaces, this is occurring because of the normal load and the relative motion between two surfaces [3].

There are four basic wear processes, *Adhesive wear, Abrasive wear, Surface fatigue* and *Corrosive wear* [3-4].

***Adhesive wear**:* occurs when the two surfaces are sliding relatively to each other, the contact between interacting asperities lead to micro-welding, material from the lower wear resistant surface removes to the other surface. This type of wear is dependent on both chemical and physical aspects, such as material properties and corrosive atmosphere of chemicals. Specific forms of *adhesive wear* are *scuffing*, *scoring* and *galling* [3-4].
Several steps that are leading to Adhesive wear:

- Deformation of the contacting asperities
- Adhesive junction forms
- Transfer of material during the failure of the junctions.

The way of preventing/avoiding *Adhesive wear*, is to choose two different materials that are not metallurgically compatible to each other, in turn this decrease the friction and the wear will be reduced [3-4].

Abrasive wear*:* the abrasive wear is divided into two types of abrasive wear which means that this type of wear occurs in two modes, two and three body abrasive wear:

Two body abrasive wear: occurs when hard particles or grid remove material of the opposite surface, there the harder surfaces asperities are penetrating the softer surface and removing material throw a plugging or cutting operation [4].

Three body abrasive wear: occurs when the third body is present, usually small hard particles that are in between two surfaces that are sliding relatively to each other. These small particles are able to slide down and roll on the surfaces and by that damage the surface that has a lower hardness [4].

The abrasive wear can be minimized/prevented by:

- The difference of the hardness less 10% of the two surfaces
- Both surfaces should have a high hardness.
- Implementing a harder layer in the softer surface
- Keeping clean or removing the hard particles from the surfaces

Surface fatigue: this type of wear occurs in rolling contact possibly with some slip, the surface fatigue manifest generally after a very large number of contacting cycles. Because of these cycles particles of material breaks away from the sliding surface with rolling bearing, cams and gears. The surfaces fatigue is also known as pitting, small pits are formed on the contacting surfaces, these pits are of different sizes, if it`s delamination or spalling, the pit seizes are in order of 1000 µm other ways the pit sizes are in order of 30 µm [3-4].

The surface fatigue can be minimized by:

- Reducing the contact pressure
- High hardness of both surfaces
- Finishing/polishing the surfaces in contact, low roughness
- By hardening the surface, carburizing flame or induction hardening (not nitriding)

Corrosive wear: occurs under reaction of the products in corrosive environment, which means that under presence of a corrosive liquids or gases, the reaction products are formed on the surfaces which in turn strongly affects the wear process. The most common form of corrosive wear is the oxidation. Most metals react with oxygen in air or water to form an oxide layer [3-4]. The reaction of steel with oxygen builds up a thin oxide layer that is often more brittle than the base material. During the sliding this thin oxide layer brakes and if the oxide debris are softer than the base material then the debris are like a solid lubricant and minimize the friction. If the oxide debris are more brittle than the base material then these oxide debris increase the abrasive wear.

The corrosive wear can be decreased by taking care of the environment and the dynamic interactions between the mating surfaces. Protection against chemical attack from environment. can prevent corrosive wear.

1.4 Wear characteristics of tool steels

Tool steels are complex iron-base alloys of carbon, chromium, vanadium, molybdenum or tungsten, in different combinations thereof. In some cases, tool steels can have a substantial amount of cobalt, cobalt dissolves in iron and strengthens it whilst and at the same time is imparting the temperature strength, the temperature of the cutting surface can sometimes even be 850°C. These different alloys are balanced to give a high resistance to wear, high resistance to thermal softening and a good toughness for effecting cutting operations in different industries. The main influence factors that are preventing the wear in tool steels are: the carbide forming elements, the microstructure and the hardness of the material [5] [6]. The friction and wear of tool steels are temperature dependent. The friction decreases with increasing temperature while the wear increases with increasing temperature.

The governing wear mechanisms that occurs in machine elements there the tool steels are used are adhesive and abrasive wear. Adhesive wear is often described as a severe wear, is generally the starting point for a wear process developing between two metal surfaces that are sliding against each other. It is a process where the softer surfaces mechanically adhere or bond, which in turn is identified by tearing or material displacement, this in turn can produce debris in a loose form.
The abrasive wear arises from the penetration of asperities of harder surface into the softer surface during the sliding against each other, this is called two-body abrasive wear. Even the debris that are coming from material displacement between the sliding surfaces from adhesive wear lead to three-body abrasive wear [7].

Often the tool steel is used at elevated temperatures, tool steels have better hardness properties than other steels at elevated temperatures. Even for tool steels there are several problems that are encountered at elevated temperatures such as thermal fatigue and oxidation [8]. If tool steel machine elements are frequently exposed to high cyclic temperatures and mechanical loads. These severe conditions will eventually lead to surface damage. One of the most common failure mechanisms is crack initiation caused by heat checking, which is a network of surface cracks that are created by friction heating of contacting surfaces and it is followed by rapidly cooling of the surfaces and is usually influenced by oxidation and creep [9].

1.5 Wear mechanisms at high temperatures

In many applications, the machine components are exposed to severe conditions such as high working loads, sliding speeds and temperature. These type of machine elements are mostly found in aerospace, mining, metal working industries and automotive. The high temperature tribology is therefore focused on how the temperature affects the friction and wear behavior and how to control these [10].

The wear mechanisms at relatively high temperature are mainly abrasive and adhesive wear. Mechanical systems exposed to high temperatures can increase the severity of these wear mechanisms and thereby increase the wear rate [11].

The adhesive wear is initiated by the formation of bond between the asperities of sliding surfaces. At higher temperatures, the strength of the materials decreases (materials get softer), the materials

get more ductile and the number of bonds starts to increase and the severity of the adhesive wear increases under a given load [12].

During sliding, the detached asperities (from the sliding surfaces or abrasive particles from outside environment, debris) may get accumulated and builds up particles [12]. These particles can embed into one of the surfaces causing grooves by ploughing in the counter surface and two body abrasive wear occurs. Due to the build-up particles, three body abrasive wear at high temperature can also occur, due to the presence of hard particle/oxides wear debris [12], [13].

At high temperature the materials get softer, by that the abrasive particles that are between the sliding surfaces can get embedded into the softer surface and that in turn can form a tribo-layer on the surface which increases the resistance to wear. Such layers are sometimes called glaze oxide layers [14].

The oxide layers are present on almost all metals in presence of oxygen. The interaction of this chemical reaction occurs when the oxygen and metal ions react. The rate of the chemical reactions and the formation of oxides increase with increasing of temperature. These oxides have a higher forming rate not only during the heat that is generated the contacting asperities but also due to the heat that is generated from the surrounding environment (high ambient temperature) [15]. This rate of oxidation increases at higher temperature due to the higher diffusion rate of ions.

While increasing the ambient temperature the rate of oxidation increases and in turn a total oxidation of the sliding surfaces can occur. At high ambient temperature, the stability of the oxide layers on the substrates will be affected by changes in the coefficient of thermal expansion of the metal substrate and the oxide layer [16-19]. While increasing the ambient temperature the oxide layers are less adherent to the metal substrate, which in turn increases the formation of oxide debris/particles between the sliding surfaces [19].

Another important factor that also influence the appearance of the oxide particles in the tribosystem, is the thermal diffusivity value. If the thermal diffusivity of the oxide layer is higher than that of the counter surface and in turn will rapidly cool down by transferring the generated heat into the counter surface, then the oxide layer will become hard and brittle, and these hard and brittle oxide layers will easily produce abrasive particles in the contact [19].

1.6 Fundamentals of internal combustions engines and turbochargers

Internal Combustion Engine

The Internal Combustion Engine (ICE) is a thermal engine where the combustion of a fuel occurs with an oxidizer, the oxidizer is usually air which in turn mixes with the fuel in a combustion chamber. The expansion of high-pressure gases and high-temperature in the combustion chamber applies a direct force on engine components (pistons), the components starting to move in order to convert thermal energy into mechanical energy [20].
The most common internal combustion engines are four-stroke engines (four-cycle engine). The four-stroke engine is an engine in which the piston completes four separate strokes while turning a crankshaft, the length of a stroke is the full travel of the piston along the cylinder.

1. The intake stroke begins at top dead center and ends at bottom dead center. In this stroke, the intake valve is open, the piston pulls an air-fuel mixture into the cylinder.

2. Compression stroke starts at bottom dead center, in this stroke the valves are close and the piston compresses the air-fuel mixture in preparation for ignition.

3. Ignition stroke or power stroke, starts at top dead center and the air-fuel mixture is ignited, then forcefully the piston moves to bottom dead center. This stroke produces mechanical work from the engine to turn the crankshaft.

4. Exhaust stroke starts from bottom dead center of the cylinder and ends at top dead center while the exhaust valve is open and the exhaust gases are evacuated from the cylinder.

There are two different four-stroke internal combustion engines, diesel engines and gasoline engines. Both diesel engines and gasoline engines are converting the chemical energy of the fuel into mechanical energy through a series of combustions. In a gasoline engine, the fuel is mixed with air, compressed by the piston and then is ignited by spark from a spark plug. In a diesel engine, the air is compressed first then the fuel is injected, while the air heats up during the compression, the fuel ignites.

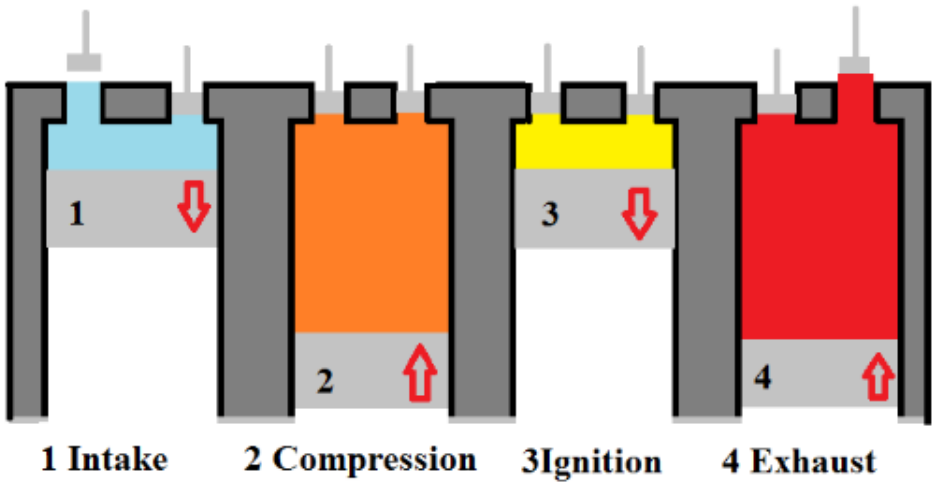

Figure 2. How a four-stroke internal combustion engine works.

The materials that are used to manufacture the internal combustion engines must be reinforced, the reinforcement of these metals can have many different objectives.
Increase the yield strength and tensile strength at room temperature and high temperature while maintaining minimum ductility or toughness and other objectives such as increase the fatigue strength at elevated temperatures, improvement of thermal chock resistance, improvement of corrosion resistance, increase of Young`s modulus and reduction of the thermal elongation [19].

Turbocharger

The engine power can be boosted if the air entering the cylinder has a density that is higher than the pressure at ambient conditions. If the air density is higher, then the air mass flow rate is higher and a higher fuel mass flow rate can be burnt in the same displacement volume [21]. The purpose is to increase the engine power. To be able to compress the air entering the cylinder and to increase the engine power a *turbocharger* is required. The *turbocharger* uses the exhausted gases energy to rotate a turbine wheel which in turn rotates the compressor [21]. The compressor wheel pressurizes the air into the combustion chamber of an internal combustion engine. The turbine wheel is connected to the compressor wheel through a shaft. The shaft has axial and radial bearings to hold it in place in the central housing of the turbocharger. Between the central house of the turbocharger and the turbine house there are sealing rings to prevent the exhaust gases from entering into the central house and contaminate the oil, and on the other hand prevent the oil leaking from the central housing of the turbocharger [21].

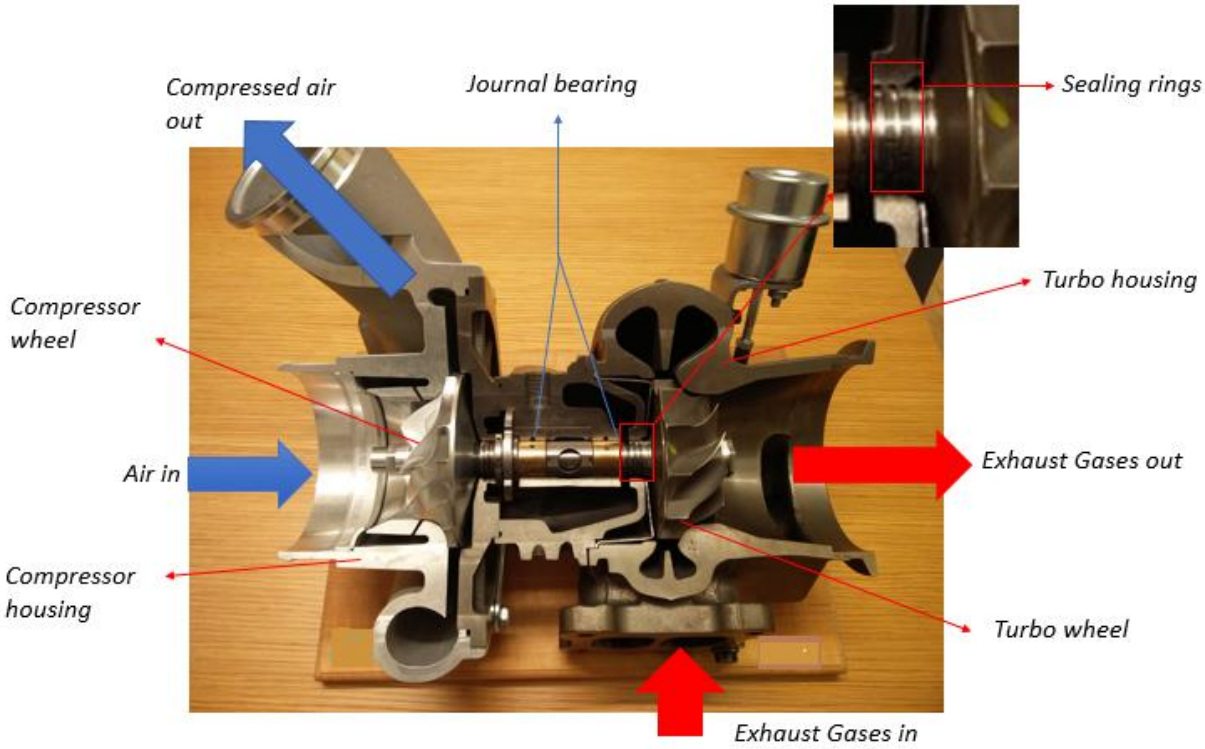

Figure 3. Cross-section view of turbocharger with components description, how the exhaust gases rotate the turbo wheel and how the air is then compressed through a compressor wheel.

1.7 Wear of turbochargers

Modern trucks are regulated by many requirements for emissions and demands for lower fuel consumption. This leads to a higher demand for more efficient engines as well as turbochargers. It is well known that the turbocharger increases the thermodynamic efficiency of the combustion engine [22]. To minimize losses further the turbocharger itself should become more efficient, without sacrificing its durability.

The turbocharger has several components whose combination can provide a durable system to increase the engine efficiency including heavy-duty diesel engines. The failure of one of the component can lead to seizure of turbocharger and damage the engine. FABIŚ-DOMAGAŁA [23] have conducted FMEA research to determine a probability of failure of each component.

To secure turbocharger durability it is important to focus on sealing rings and bearings. A common practice today is using a floating bearing to support a turbine shaft [24]. The bearing is silent and have advantage in rotor dynamics because of its damping ability due to the oil film between the shaft and the bearing. The rotodynamic have been extensively studied [24,25-28] and validation of models have been done [27]. Papers describe influence of oil feed, oil pressure, whirl, bearing clearance on the stability of the rotor and friction behaviour. The one study on floating bearing in turbochargers investigates air as the separating media [28] and nano-magnetorheological fluids instead for oil [29].

The second alternative to decrease frictional losses in turbochargers is to replace the trust bearing with a ball bearing [30,31]. Several designs of ball bearings have been evaluated, from different sizes to material selection. There are many questions about the dynamics and durability of the new designs that are main subject of research.

This work focuses on wear of sealing rings. One of the main problem it is discussed that the main problem of poor sealing performance is increased blow by. The exhaust gases, which passes through the sealing rings, flows in to the bearing house. The oil drain pipe of the turbocharger leads the gases further to the oil chamber. Extensive leakage through the sealing rings builds up a pressure, first in the bearing house, then in the oil drain. This lead to problems of the engine system. High pressure in the oil chamber creates several problems. The high-pressure forces oil through the sealing for example in engine head which leads to a risk of fire. Another problem is that high pressure in the oil chamber prevents oil draining from the turbocharger. Oil then stays in the turbocharger causing problems with lubrication of the shaft bearings which leads to severe damage and potential seizure of the bearing.

1.8 Wear models for turbochargers

Based on Scania internal research one of the latest wear models to describe wear of sealing rings is based on Archard's wear equation. Archard have in the 1950's described wear as function $Q = \frac{K W L}{H}$. The equation describes wear Q proportional to normal load W, sliding distance L and a wear constant K. The model also takes in account the hardness of softer material H.

The parameters to apply to the wear equation were determent by using data accumulated by Scania. The normal load W and sliding distance L are described by knowing pressure and rotational speed in the turbocharger. The hardness of material H varies with temperature but in the wear model for turbocharger have taken as a constant value. The value of the constant K is estimated by available data from existing measurements. The model shows some promising results, but its limitations are discussed.

One of the challenges is to determine the conditions in the turbocharger. Measurements of required pressure to move the sealing ring are not taken. The friction generated between sealing rings and a bearing house is measured at disassembled turbocharger. This gives some uncertainties in the model.

1.9 Knowledge gaps

The uncertainties of today's wear model of sealing rings based on Archard's equation gives an area for a deeper research. There have not been found information about wear mechanisms that occur in the sealing of turbocharger. It is mentioned before that the working conditions are not determined either. It has not been found an available data on measured temperature, pressure or content of fluid around sealing rings.

This thesis work will cover the analyze of gliding surfaces of sealing rings and shaft. Performing a visual, hardness, EDS and profile analyses will give better understanding of conditions that may occur in the sealing area. Performed analyses will help to determine wear mechanisms, which are crucial for the models based on Archard's equations. Furthermore, there will be performed several tribological tests to evaluate conditions influence on wear mechanisms and wear rate.

2. Aim, objectives and limitations

Aim of the project

The aim of this project is to identify the dominant wear mechanisms of the inner sealing rings and shafts of turbochargers in heavy duty diesel engines. Tribological experiments will be carried out to identify which parameters that influence the wear. Analysis of data from trucks used in the field will be analysed to assess which driving conditions that are most damaging for the components of the turbochargers. The long-term aim is to use this information to prevent the damage of the components of turbochargers.

Objectives

The objectives of the project are:

1) Literature studies about different types of wear, at different conditions such as wear at high temperature and literature studies about the wear that occurs in turbochargers.

2) Investigations about the contact conditions that are occurring between the turbocharger shafts and the sealing rings. These investigations are focussed on temperature, contacting pressure, sliding velocity and the wear and friction between the sliding surfaces.

3) Identify the dominant wear mechanisms that are occurring in the turbocharger components (sealing rings and shafts) and how these mechanisms are influencing the turbocharger components lifetime.

4) Carry out tribological experiments to understand the influence of operating conditions such as contact pressure, sliding velocity and temperature on friction and wear.

Limitations

The analysis of worn turbocharger components from field use were limited to four selected vehicles. These were selected based on randomly chosen turbochargers. Two of the turbochargers came from Netherlands, one from Australia and one from Great Britain. The trucks were used for hauling a general cargo, mostly highway. Trucks have different mileage and work conditions for better comparison.

Limitations in tribological tests

The extreme conditions (high sliding speeds and temperatures) in the turbocharger are difficult to simulate in the laboratory. The pin on disc TE67 machine can run up to 2000 RPM and with the maximum disc radius the sliding speed is limited to 11 m/s. This is lower than the actual application but can still provide an indication about the effect of sliding speed.

3. Experimental work

3.1 Material and specimens

Turbocharger

The sealing rings of turbochargers are commonly made of tool steel HS 6-5-2. The hardness of the sealing ring material is around 620 HV and the chemical composition of the material can be seen in Table 1 below.

Table 1.The chemical composition of the sealing rings material.

Element	C	Cr	Mo	W	V	Fe
wt%	0.9	4.2	5.0	6.4	1.8	Balance

The shaft is made of carbon steel, with the designation ASIS 4140 (UNS G87400) and the hardness is around 412 HV. In Table 2 below, the chemical composition of the shaft is given.

Table 2.Chemical composition of shaft material.

Element	C	Mg	Cr	Mo	Si	P	S	Fe
wt%	0.40	0.80	0.55	0.22	0.27	0.02	0.02	Balance

Tribological test specimens

The discs for tribological experiments are made of the tool steel HS 6-5-2, same as the ring material. The diameter of the discs is Ø120 mm and 8 mm thick with a Ø10 mm hole in the middle for attachment to the tribological machine.

The shaft of the turbocharger is made from carbon steel UNS G87400. The same material is used in pins supplied for tribological experiments. The pins are Ø4 mm in diameter and 4 mm in length. They have chamfered edges on both sides to prevent cutting effects that may occur during the tribological test when using flat-on-flat contacts.

Data from customer trucks

During the project, data from approximately 60 customer trucks was made available. Logged data was downloaded from trucks and presented as a matrix. This matrix included the truck serial number, mileage, number of gearshifts, country, percentage of use at each load interval within RPM interval. Trucks used the same engine with different truck application. The information was used to evaluate parameters influence on wear resistance.

The turbochargers were removed from trucks. All the turbochargers were in working conditions before they were removed. The turbochargers were taken apart to remove the sealing rings. Wear of both outer and inner sealing rings was measured at three different points and an average value was calculated for each sealing ring. The data was then added to the matrix from trucks and supplied by Scania.

3.2 Experimental technique

The turbocharger components

Turbocharger components that had been chosen for analyses came from trucks which had been used by costumers. Differentiation of turbochargers in analyses had been done by writing the chassis number of each truck, where the turbochargers had been used. The components of turbochargers that had been analysed are turbocharger shafts and turbo sealing rings. In Figure 4 below it can be seen how the shafts had been cut for analyses. In image a) the entire turbocharger shaft is shown with the turbo wheel and the red highlighted surface is the surface where the inner sealing ring had been in contact with the shaft. In image b) it can be seen how the shaft had been cut, the cut had been done to better analyse the worn surface of the shaft. While in image c) it is shown how the shaft had been cut along the axial direction for cross-section analysis.

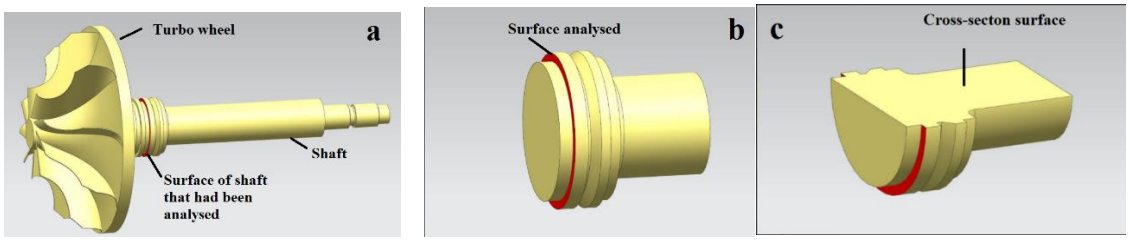

Figure 4. Shows how the shaft had been prepared for surface and cross-section analysis.

Before the surface analyses the turbochargers components (sealing rings and shafts) had first been ultrasonically cleaned with ethanol and then with acetone.

The sealing rings was also surface analysed. The surface analysis had been done with Light Optical Microscope, 3D Surface Profiler and Electron Microscope. The sealing rings have a gap as it can be seen in Figure 5 below. Due to the ring gap, the worn surface of the sealing rings differs along the length. Therefore, the analysis of the sealing rings had been done at two different positions as shown in Figure 5 below.

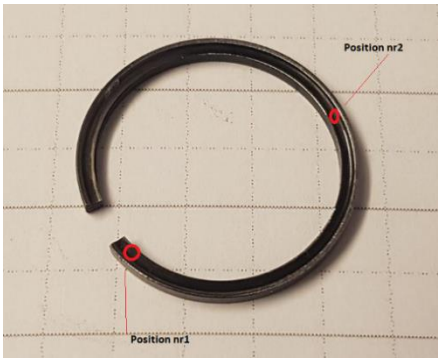

Figure 5. Position 1 and 2 respectively where the sealing ring surface analyses had been done.

Cross-section analyses of sealing rings and shafts had been done to measure the hardness depth profiles of sealing rings and shafts. The hardness measurements had been done across the cross-section of the sealing rings and shafts to identify how the hardness had changed after the components had been used. In Figure 6 below it can be seen where the hardness had been measured along the cross-section of the sealing rings and shafts. The shafts had been analysed along the cross-section, the hardness measurements were started from the worn surface that had been in contact with the surface of the inner sealing rings and it is marked with 1 in Figure 6 while for inner sealing rings the hardness measurements had been done from the surface that had worn during the contact with the shaft and is marked with 2. The hardness of outer sealing rings had been done at two positions, 3 and 4 respectively where the hardness of the outer sealing rings had first been measured at position 3 where the outer ring had been in contact with the shaft and at position 4 where the outer rings had mostly been influenced by the pressure and the temperature of the exhausted gases.

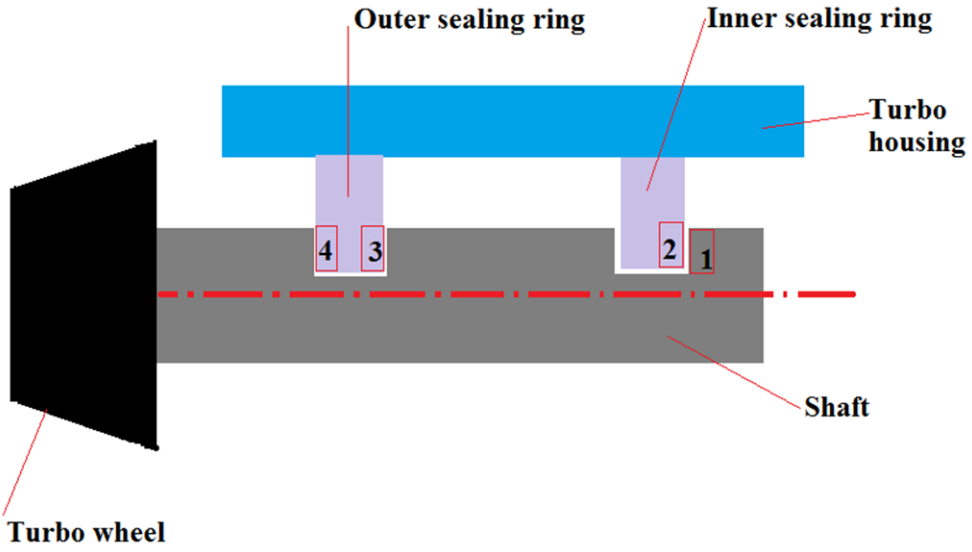

Figure 6. Schematic cross-section of the turbo components.

The red area marked with 1 shows where the hardness of the shafts had been measured along the cross-section, 2 shows where the hardness measurements of the inner sealing rings was measured across the cross-section, and positions 3 and 4 respectively shows where the hardness of outer sealing rings was measured across the cross-section.

Before the cross-section analysis of the sealing rings and shafts was done, the parts shown in Figure 7 a) was hot mounted with *Press implement 1000* and it was heated up to 150 °C under high pressure in polymer powder (Phenocure) which has a green color and it can be seen in Figure 7 a) below.

The sealing rings were cold mounted with a mixture of two different thermosets, *epoxi* and *durocite* respectively which is a transparent thermoset mixture shown in Figure 7 (b). These mounting processes were done because it was difficult to hold the small samples during the grinding and polishing.

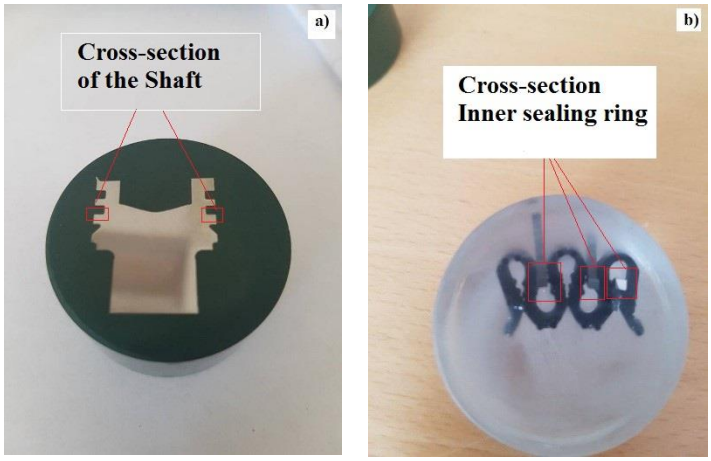

Figure 7. In a) molded cross-section of the shaft and in b) the cross-section of the sealing ring.

Tribotests

The pin on disc machine Phoenix Tribology TE67 was used to perform tribological tests. The tests evaluate the tribological behaviour during the rotational motion between two surfaces. In this project, the test is used to specify the influence of different parameters, such as load, speed and temperature, on wear behaviour of the materials in turbocharger.

The pin on disc machine TE67 have several possibilities to apply load in different ways. There is a pneumatic bellow that can be mounted for high load or variable loads during the test. For measurement during these tests a dead weight system will be used instead. It is placed on top of the pin as shown in Figure 8 . Thermo couples were placed in the middle of inlet air channel to measure the inlet air temperature. The temperature of the disc is measured by a pyrometer which is adjusted before tests. A lid is placed on top of the chamber during the heating and testing at high temperature, see Figure 8. The friction sensor measures the friction force in Newton up to 10 measurements per second.

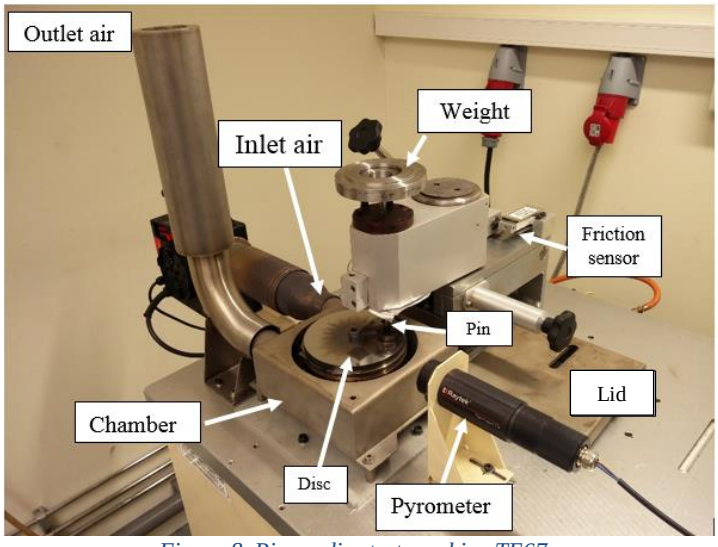

Figure 8. Pin on disc test machine TE67.

There were five discs and 29 pins available. Besides the discs/pins mentioned above some additional tests were carried out on another disc to decide the test parameters like speed and duration of the test before running the actual test.

The tests are varying three parameters: load, speed and temperature. Two measurements at each combination were performed to verify the results. The first set of tests is designed to evaluate the influence of speed on wear. Two measurements at 3 m/s and at 11 m/s were performed. The diameter of wear track is Ø30 and Ø48 mm for 3 m/s test and Ø110 mm for 11 m/s.

The second set of tests evaluated the influence of load on wear. The first setup of tests uses the load of 0.2 kg. The second setup perform additional tests at 0.9 kg load. Measurements at 3 m/s were performed at diameter Ø30 and Ø48 mm and the 11 m/s were carried out at Ø110 mm diameter. The third set of tests evaluated the influence of temperature on wear and friction. There performed measurements at every load and speed that is mentioned above but the discs are heated up to 300 °C.

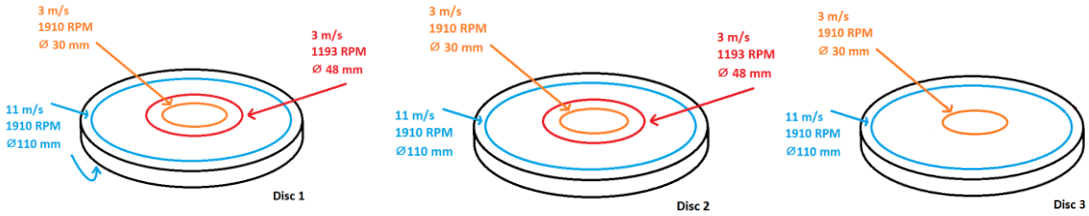

Figure 9. Example of wear tracks on disc surfaces.

The tests resulted in 2 loads at 2 speeds at 2 different temperatures. There were 2 or more measurement at each combination to verify the result. The result consists of a total of 19 measurements, which can verify the influence of each parameter on wear and friction.

3.3 Test parameters

Calculations are performed to get the sliding conditions of the contact between shaft and sealing rings in the actual turbocharger. These are then compared with the possibilities of the tribological equipment. The decision of the test conditions for tribological experiments is made to replicate the conditions of the turbocharger as much as possible in laboratory environment. The parameters are contact pressure, relative speed and distance.

Contact pressure

There are several methods used to calculate the pressure drop over the sealing rings. The first method is to simulate the flow that goes through the rings. During the project a CAD model of the turbocharger was created in the CAD software Siemens NX. The dimension is taken from the turbocharger commonly used in trucks.

A variable mesh of air that surrounds the component of turbo was generated. The air is marked blue in Figure 10. The simulation needs some estimations to create the solution. It is decided that the is no rotation of the turbocharger and air is an ideal gas at temperature 300°C. The boundary condition is the pressure drop of 6 bar between exhaust side and the oil chamber. The sealing ring is mounted 10 µm from the surface of the shaft where the wear of sealing ring occurs.

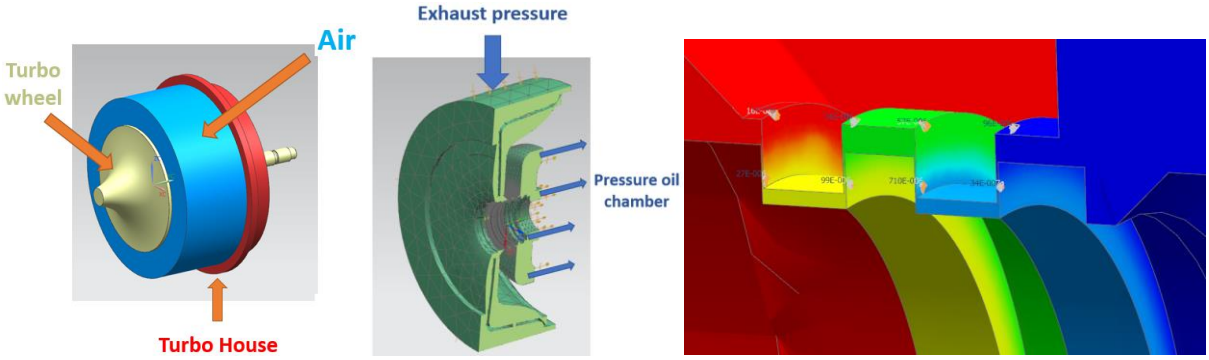

Figure 10. Simulation of pressure over the rings.

The result from the simulation gives the same pressure drop for both rings which is unlikely. This is the reason that this method is not used to calculate the contact pressure for tribological experiment.

An aditional version of the flow simulation througth sealing rings was made. In this case the geometry is simplified compared to the first version. The sealing rings are placed in the middle of the groove on the shaft. The simulations were done in Ansys software to create a mesh and simulation, see Figure 11. The result are similar to the previous one and is not used for further analysis.

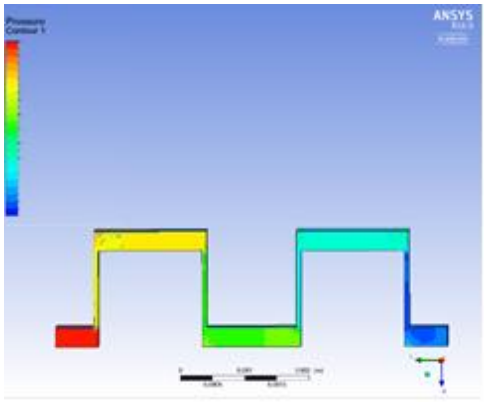

Figure 11. The pressure drop over the sealing rings.

The second method to evaluate the pressure drop over the sealing rings uses the model used by Scania. The model simplified two sealing rings as a strangulation of flow, see Figure 12.

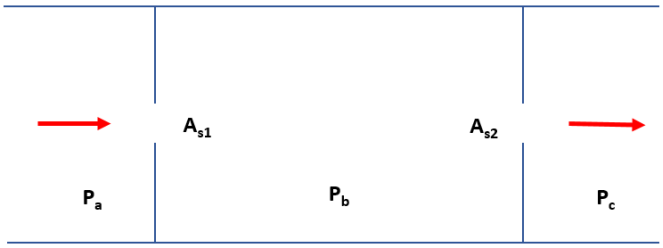

Figure 12. Simplified model of flow through the sealing rings.

The calculation gives the pressure difference over sealing ring of 2.7 and 3.8 bar over the outer and inner sealing ring respectively where the pressure drop is 6 bar over both sealing rings.

The second step is calculation of contact pressure. The pressure drop over ring is not the same as the contact pressure because of geometry. This pressure drop P_1 applies over area A_1 of the sealing ring and generates the force F_1. The shaft is preventing the sealing movement and generate the pressure P_2 over the area A_2 which generates the force F_2, which resist force F_1, see Figure 13. The pressure P_2 is the contact pressure of two surfaces in the tribological experiment.

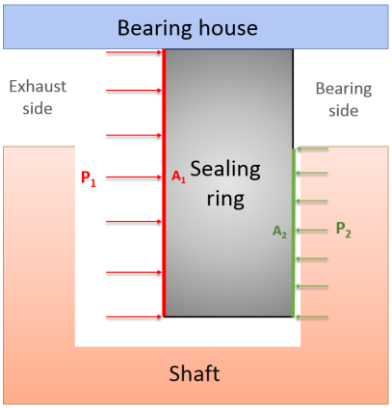

Figure 13. Cutting section of sealing ring mounted in place.

The equilibrium between forces $F_1 = F_2$ gives the equation of contact pressure P_2 dependency on pressure drop P_1 over the sealing ring:

$$P_2 = \frac{A_1 * P_1}{A_2} = \frac{A_1}{A_2} * P_1$$

Measurements of the inner- and outer diameters of the new ring mounted in a turbo house were taken. This gives an expression for the area A_1:

$$A_1 = (D_{out}^2 - D_{in}^2) * \pi/4$$

where D_{out} is outside diameter and D_{in} is the inside diameter of the mounted ring. The area A_2 is calculated from the wear diameter D_{wear}

$$A_2 = (D_{wear}^2 - D_{in}^2) * \pi/4$$

The wear diameter D_{wear} is taken from measurement of surface topography where the width of the wear track on the sealing ring can be measured. This results in:

$$P_2 = \frac{(D_{out}^2 - D_{in}^2) * \pi/4}{(D_{wear}^2 - D_{in}^2) * \pi/4} * P_1 = \frac{D_{out}^2 - D_{in}^2}{D_{wear}^2 - D_{in}^2} * P_1$$

The equations above give the influence of geometry to the difference between pressure drop over the sealing ring and the actual contact pressure between sealing ring and shaft.

In the tribological tests, the minimum contact pressure is given by the lowest dead weight that is available which is 0.2 kg. The second weight is 0.9 kg which corresponds to a pressure drop over the sealing ring of 15 bar.

Sliding speed

There are two relative speeds used in tribotests. The tribological test machine TE67 can run up to 2000 rpm. The disc, which is used in these tests, have a diameter of Ø120 mm. The maximum diameter for placing a pin on disc is settled to Ø110 mm. The minimum diameter of the wear track is 30 mm. The highest achievable relative speed between two surfaces at minimum diameter is:

$$Speed = 2\pi r * RPM = 2\pi * 15\,mm * 2000\,RPM \approx 314\frac{m}{min} \approx 3\,m/s$$

The highest relative speed achieved if pin placed on the highest radius of Ø110 mm:

$$Speed = 2\pi * 110\,mm * 2000\,RPM \approx 11\,m/s$$

The relative speed at which the sealing ring slide against the turbo shaft in the turbocharger is calculated for 80000 RPM:

$$Speed = 2\pi r * RPM = 2\pi * 10e^{-3} * 80000 \approx 5000\frac{m}{min} \approx 84\,m/s$$

Sliding distance

Different sliding distances were evaluated to decide the sliding distance for tribological test. The trial tests showed that the pin can withstand 6000 m at high wear rate and be long enough distance to produce a measurable wear. That lead to a conclusion of the total sliding distance of 6000 meters. The sliding distance of 6000 meters for an engine correspond to a 20 minutes' drive if the engine is operating at 1200 RPM and 30% engine load.

3.4 Test procedures

Preparation before tribological test.

The pins are cleaned in industrial petrol in an ultrasonic cleaner, rinsed with acetone and dried. The discs are wiped with paper rinsed with acetone before mounting them in place. A dial gauge is used to level the disc by placing shims under the disc. The calibration allowed the fluctuation up to 1 µm of outer radius of the disc, see Figure 14. The discs are additionally wiped with acetone before a test.

Figure 14. Levelling of disc before test.

There are two friction sensors available. The first sensor is designed to take loads up to 100 N and the second one takes 5 kg (49 N). The second sensor is used during the tests because the friction forces do not exceed the load limit. The sensor is more sensitive at the chosen loads, which results

in more accurate data. The friction force is calibrated with a dead weight of 2020 gram which is supposed to represent the double of friction force generated during the test.

A thermocouple of type K was used to calibrate the pyrometer, which is used to heat the test specimens during the tribological tests. The calibration is performed at 300 °C. The thermocouple was placed on top of the disc surface to get reading of the temperature which the pyrometer is calibrated to.

The disc is rotated at 120 RPM during the heating. The heater delivers a 600 °C inlet air until the pyrometer reaches the reading of 300 °C. After this, the pin is lowered and loaded against the disc to perform the high temperature tests.

3.5 Microstructural analysis

The equipment that have been used to analyse the worn turbocharger components (sealing rings and shafts) and the test specimens from the tribological tests are presented in this chapter. Descriptions about the function of these apparatus and how the turbocharger components were prepared for these analyses are presented below.

3D surface profilometry

The analyses of the field-tested samples (rings and shafts of turbo chargers) were started with the 3D surface profile measurements, the machine that had been used for doing these experiments is a *Wyko NT1100* shown in Figure 15. It uses interferometry to measure a surface. This surface profiler has two main features, VSI which means *Vertical* Sc*anning Interferometry* and the second feature is PSI that it means *Phase Shifting Interferometry*.

Figure 15. 3D Optical surface profiler.

In VSI mode, it utilizes scanning white light interferometry which is a white and dark pattern that results from splitting of a beam where one part is reflected against a very smooth reference surface and the other part reflected against the specimen. After the reflection, the beams are recombined in the interferometer and an interface pattern occurs. In turn, the pattern is then photographed by a CCD camera and then it is saved in the computer for analyses (3D profile).

PSI mode, is like the VSI mode but it uses filtered light and the reference surface is translated instead of the objective. It also uses the difference in intensity instead of fringes for height data acquisition. The data that is acquired is then used to generate a 3D image for the surface. The computer software Vision 32 enable advanced calculations of various surface parameters and image processing.

Light optical microscope (LOM)

The analysis of the samples were continued with the Light Optical Microscope LOM, the analyses of the worn surfaces of rings and shafts that had been sliding against each other were analysed to get an overview of the surface damage and potentially see if there were any lubricant residues between these sliding surfaces of the samples.

The light optical microscope, is a microscope which uses visible light and a system of lenses to magnify the images of the samples. The image of the samples from an optical microscope can be captured by normal light sensitive cameras to generate a micrograph. A micrograph is a digital image taken trough microscope to show a magnified image.

The LOM that had been used to do the analyses is *Nikon SMZ1270*, which is a microscope that can magnify the image up to 80 times. The software that had been used to take the pictures with is *NIS-Elements D*.

Figure 16. The Light Optical Microscope, Nikon SMZ1270.

The analysis of the turbocharger components with the LOM had been done on the worn surfaces of the inner sealing rings and shafts. On the sealing rings, the photos had been taken at two different positions, Position 1 and 2 respectively shown in Figure 5. The analyses with LOM had been done at magnification 60X and 80X respectively for both sealing rings and shafts.

Vickers hardness testing

The hardness is a characteristic of a material, hardness is defined as the resistance of the material to indentation and is determined by measuring the depth of indentation.
The hardness tests of the specimens was done with a *microhardness tester*, the hardness tester is shown in Figure 17. A fixed force (load) and a given indenter is used and the smaller the indentation the harder the material.

Figure 17. Microhardness tester.

The Vickers hardness tester is based on an optical measurement system. The test procedure, specifies a range of light loads using a diamond indenter, a square base pyramid shaped diamond is used for testing in the Vickers scale.

The indentations were measured using an optical microscope with a digital camera and then the area that was measured with help of the computer software had automatically been converted by the software to the hardness value (HV). The test indentation is very small for Vickers tests.

The *microhardness tester* has a range of load from 10g up to 1000g. The software that was used to measure the hardness is OmniMet (Manual Microindetation Hardness testing). The load that was used during the hardness measurements for turbocharger components was 10 grams and the distance between the hardness measurements across the cross-section of the samples was 10 µm. The hardness measurements had been repeated three times at each depth under the surface of the samples and the mean value was calculated as the hardness of the material at respectively depth.

Scanning Electron Microscope.

SEM is an abbreviation for Scanning Electron Microscope. The optical microscope uses the light to create an image. The SEM use electrons to create an image.

The electron gun generates the electron beam inside the SEM. The beam first passes through the anode to attract the electrons towards the specimen. Some electrons will be absorbed by the anode, but remaining electrons will have a velocity and direction towards specimen. The beam has a direction, but it is not focused. The light microscope uses lenses to focus the light. The electrons cannot pass a lens and they are instead moved by a magnetic field. There are two magnetic fields that adjust the electron beam in different directions this is called stigma. By changing the stigma, the magnetic field is changed which adjusts the beam. Then the electron beam passes through the objective lens to focus the beam at specific point at specimen surface, see Figure 18 a).

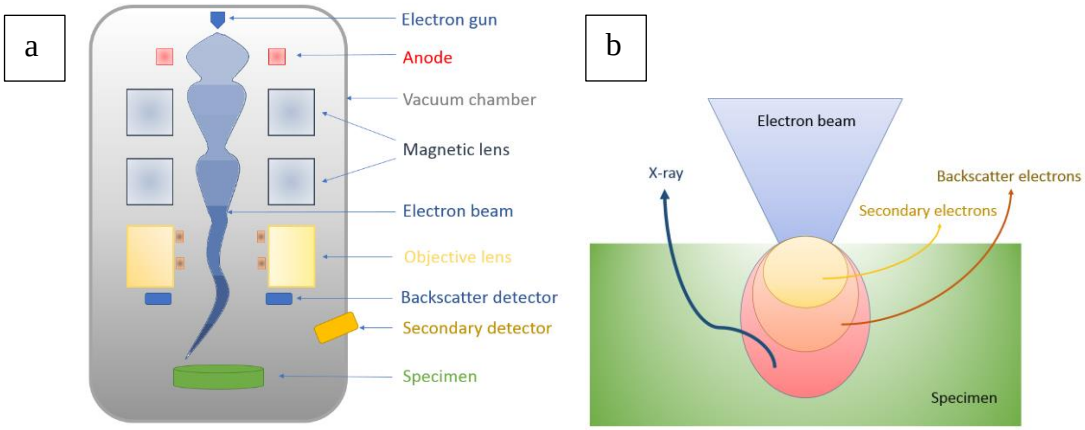

Figure 18. Scanning Electron Microscope.

When the beam reaches the surface, it excites the specimen's electrons to generate secondary electrons, backscatter electrons and X-rays. Secondary electrons have lower energy and they are closer to the surface than backscatter electrons. Electrons that penetrate the surface deep enough, so they cannot be reflected, release the energy by creating x-ray, see Figure 18 b).

The secondary and backscatter electrons are used to create an image. X-ray electrons are used to perform EDS analyse, which show the atomic content of the sample material. The result of SEM and EDS analyse is used to analyse the rings, shafts and tribological specimens in this project.

Analysis of tribological specimens.

The pins were weighed five times each to get the average weight before and after the test. The difference between measurements show the weight loss of the pins during the test. The discs cannot be weighed because they exceed the total mass of 200 grams, which is the limit of the semi-microelectronic weighing balance.

The wear of the discs were evaluated by 3D optical profile measurements instead. The 3D optical profile is taken at four different points at the wear track. It is taken five to six measurements across the wear track.

Figure 19. Example of wear measurement across discs wear track.

The values that comes from measurement is recalculated to get the wear depth at each point. The evaluation subtracts the geometrical triangle above the wear track to get the depth value. The triangle is marked orange in Figure 20 a). When the depth at each point is calculated the average depth at each radius is taken. In other words, one blue point on Figure 20 b) is average of four measurements along the wear track.

a

b

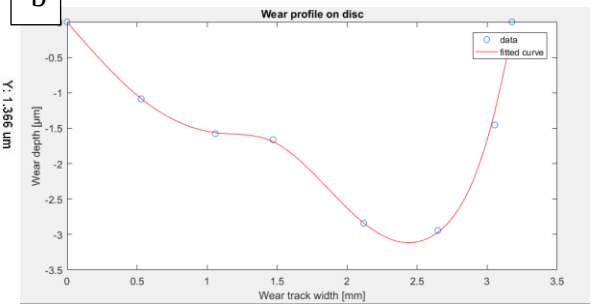

Figure 20. Calculation of disc wear.

The curve is fitted through measured values. The function of the curve is integrated to get the worn area. The area is multiplied with wear tracks circumference and density of material to get the mass loss of the disc. The result gives the possibility to compare the wear between soft and hard material involved in the tribological experiment.

Data analysis

The data provided by Scania was analysed to find correlation between the working conditions of the trucks and wear of sealing rings. Due to the big scatter in the working conditions a filter is added to find the trucks with similar load conditions. There is data available on load and RPM conditions of the engine. The parameters which are analysed are mileage, number of km in high load, number of km during exhaust brake and number of gearshifts. After filtering, only mileage was used to find correlation with wear.

4. Results and discussion

4.1 Wear and failure analysis of turbocharger components

4.1.1 LOM analysis of turbocharger components

The analysis of turbocharger components was started with the new ring and shaft. The surfaces that were analysed are the surfaces of the inner sealing ring that is in contact with the surface of the shaft. The surfaces of the new shaft and sealing ring are shown in Figure 21. Grooves on the shaft surface are from the machining of the component. The surface of the new sealing ring does not have any grooves and presented a smooth surface which appeared to be polished to a surface texture without orientation.

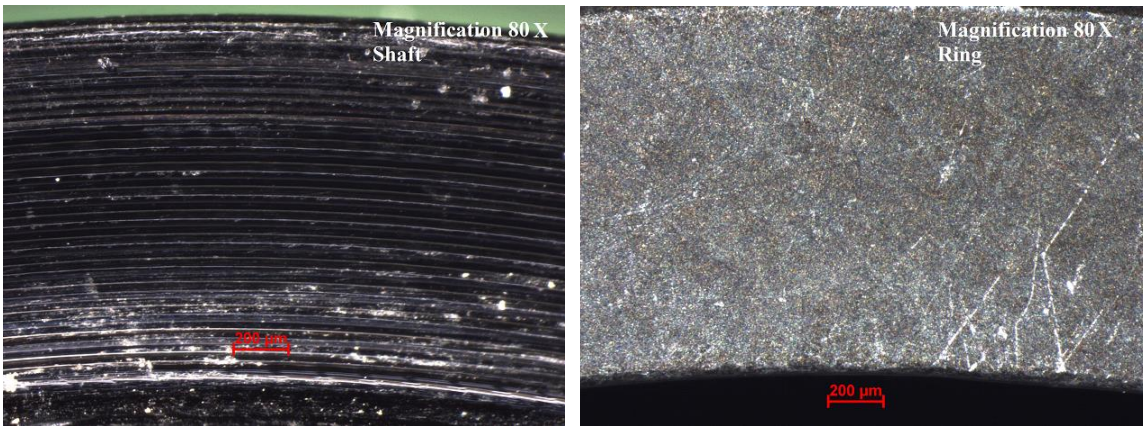

Figure 21. Illustrates the surface of the new sealing ring and shaft at magnification 80X.

The used inner sealing rings that were chosen to be analysed came from trucks number:1, 2, 3 and 4. Figure 22 below shows a worn surfaces of inner sealing rings of the trucks, close to the ring gap at position 1 in Figure 5**.**

In Figure 22 below each inner sealing ring has the chassis number and the magnification illustrated along with the sliding direction in the upper left corner. The analyses are done close to the inner ring gap to see how the worn surfaces between these inner sealing rings are differing. As it can be seen in Figure 22**,** there are black layers on all worn surface indicating that there had been an interaction with the lubricant during the operation of these inner sealing rings. As it can be seen in Figure 22 b) which has the chassis number 3 below, there is a black layer over the entire worn surface of the inner sealing ring. The other sealing rings have thinner black layer over the entire surface. The inner sealing ring number 3 is an inner sealing ring that had been on a truck, which represent an average time at max load and high exhaust gas pressure. This truck had the longest proportion of drivetime at high exhaust pressure compare to the other thee trucks that have been analysed.

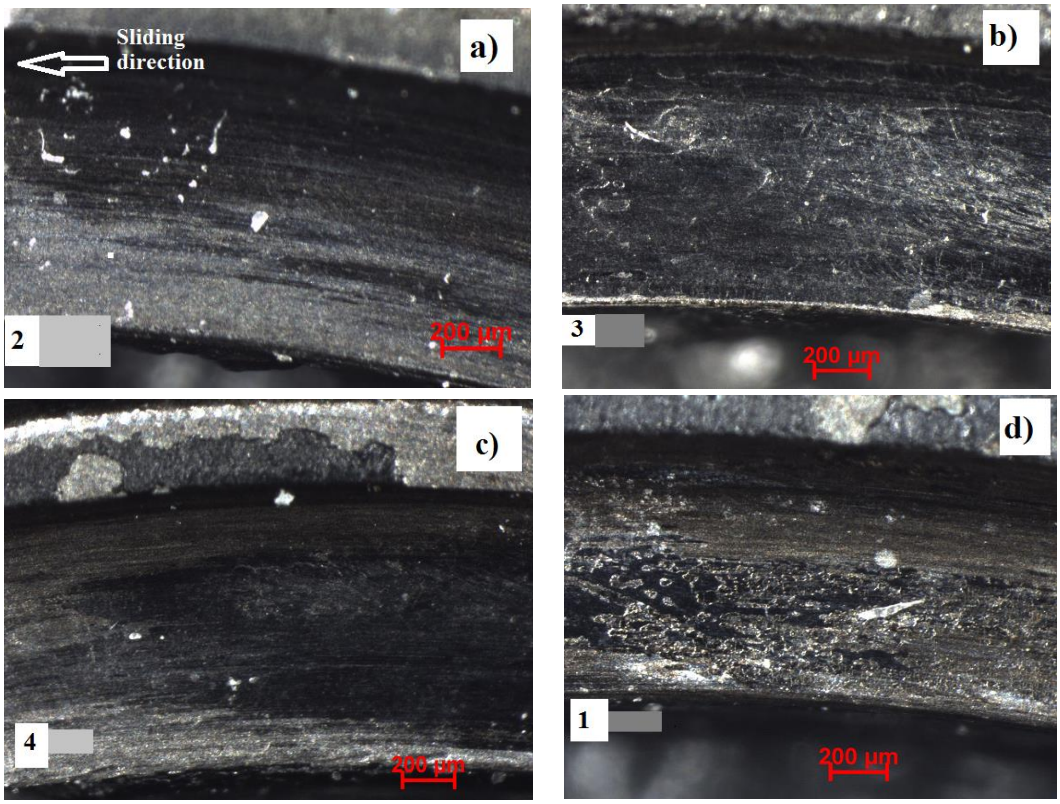

Figure 22. Illustrates images of the worn surfaces of the rings at magnification 80X close to the inner ring gap (Position 1). The sliding direction is the same for all sealing rings, therefore the sliding direction is indicated with white arrow only in the image 2.

The analysis at position 2 (Figure 5) shown in Figure 23. On each worn surface of the inner sealing rings at position 2 below it can be seen similar black layer on the surfaces as previously described. The surface of the inner sealing ring 2 in Figure 23 (c) has less coverage of the surface by this black layer. Sealing rings number 2 comes from a truck that had had been driven above average of the time at max load, which is the highest comparing to the other trucks (sealing rings) illustrated in Figure 23. The truck number 4 have the highest proportion of drivetime at high exhaust brake pressure. The second highest after 4 have the truck number 2 which was mentioned above. The sliding direction is the same for each sealing ring and it can be seen in Figure 23 (a).

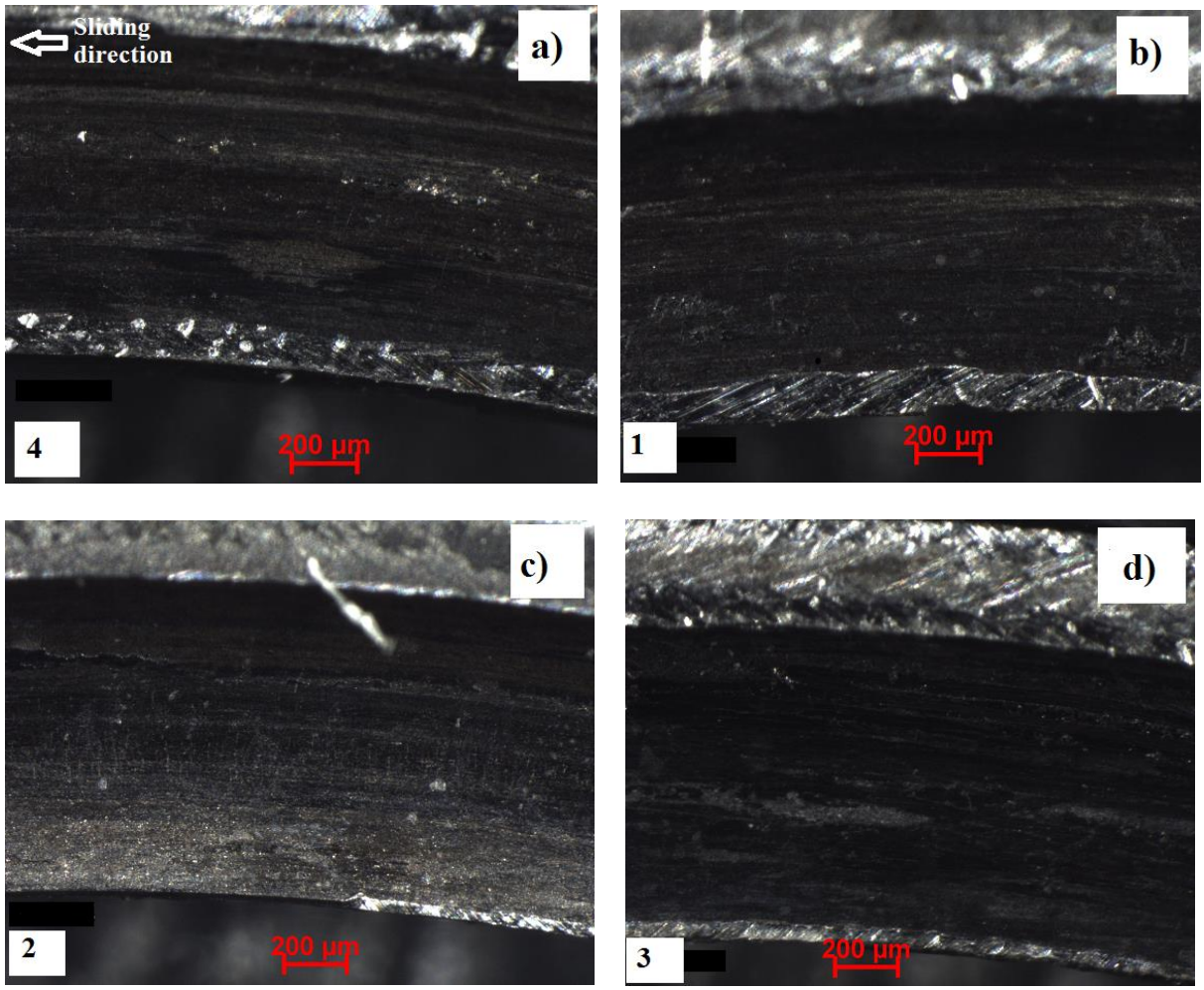

Figure 23.The inner sealing rings worn surfaces at magnification 80X and Position 2.

The surfaces of the shafts that had been into contact with the inner sealing rings 1, 2, 3 and 4 were also analysed. In Figure 24 the worn surfaces of the shafts can be seen. As it can be seen on each surface of the shafts there is a similar black layer on the worn surface as that seen on the rings. The shaft number 3 has a thicker layer on the worn surface compared to the surfaces of the other shafts. The truck has longest distance driven at highest exhaust brake, the distance is much larger comparing to the other trucks that are also illustrated in image below.

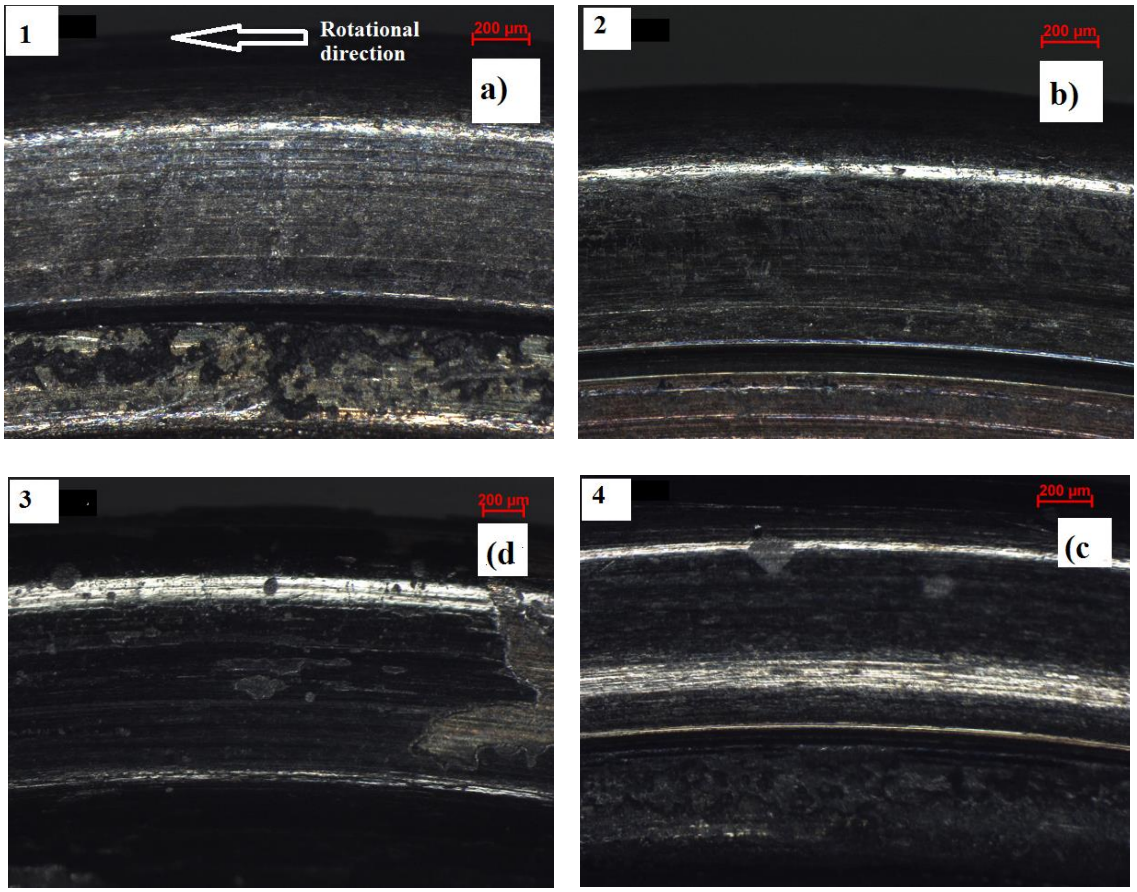

Figure 24. Images of the shafts worn surfaces at magnification 80X.

4.1.2 3D surface profile analysis

The 3D profile images had first been taken on the surfaces of the new shaft and ring and the surface roughness S_a was first calculated for the surface of the new ring. The measurements had been done at four different points on the surface and then the mean value of these measurements had been chosen as the S_a of the new sealing ring surface and the shafts. The 3D surface profile images were taken at magnification 10X and 20X respectively for both sealing rings and shafts. In Figure 25**,** the 3D profile images of the new sealing ring at magnification 10X and 20X are shown respectively. The smooth surface with random surface orientation can clearly be seen. The mean value of the surface roughness of the new sealing ring at magnification 10X and 20X respectively were:

- Roughness of the new sealing ring surface at magnification 10X: $R_a = 390\,nm$. The standard deviation STDEV is 1.2754.
- Roughness of the new sealing ring surface at magnification 20X: $R_a = 510\,nm$. The standard deviation STDEV 1.5259.

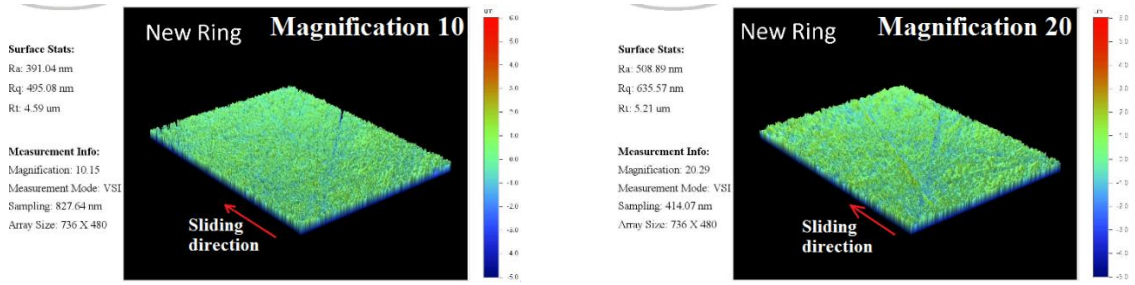

Figure 25. 3D surface profile images of the new sealing ring.

The machining marks on the new shaft surface is shown in Figure 26 and the mean value of the surface roughness Ra of the new shaft were:

- Roughness of the new shaft surface at magnification 10X: $R_a = 630\,nm$. The standard deviation STDEV is 1.354.
- Roughness of the new shaft surface at magnification 20 X:$R_a = 600\,nm$. The standard deviation STDEV is 1.285.

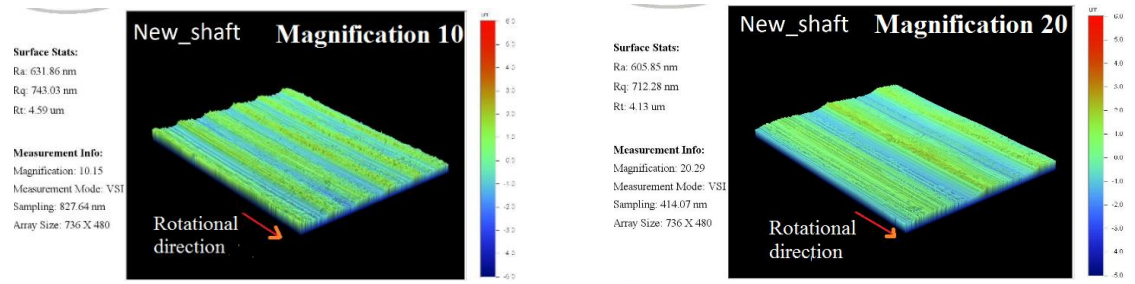

Figure 26. Illustrates the 3D surface profile of the new shaft surface at magnification 10X and 20X.

The 3D surface profile analyses of the worn surfaces was started with the surfaces of inner sealing rings at position 1 close to the ring gap. The red arrow in each image illustrates the sliding direction. As shown in Figure 27, the surfaces of the inner sealing rings had been worn more in the middle of the surface and had a shape that is more concave. The concave shape is probably due to the geometry of the inner sealing ring and shaft grooves and also due to the high pressure and friction generation between the sliding surfaces.

There was only one ring that had been worn different, the inner sealing ring from truck number 1, has a worn surface that was more flat comparing to the other inner sealing surfaces which had been analysed. The truck number 1 had been less exposed to max load and even exhaust brake pressure comparing to the other three inner sealing rings that are illustrated in Figure 27. The inner sealing ring from truck number 2 got the most concave shape perpendicular to the sliding direction. The truck has the longest time at max load comparing to the other sealing rings that are illustrated below.

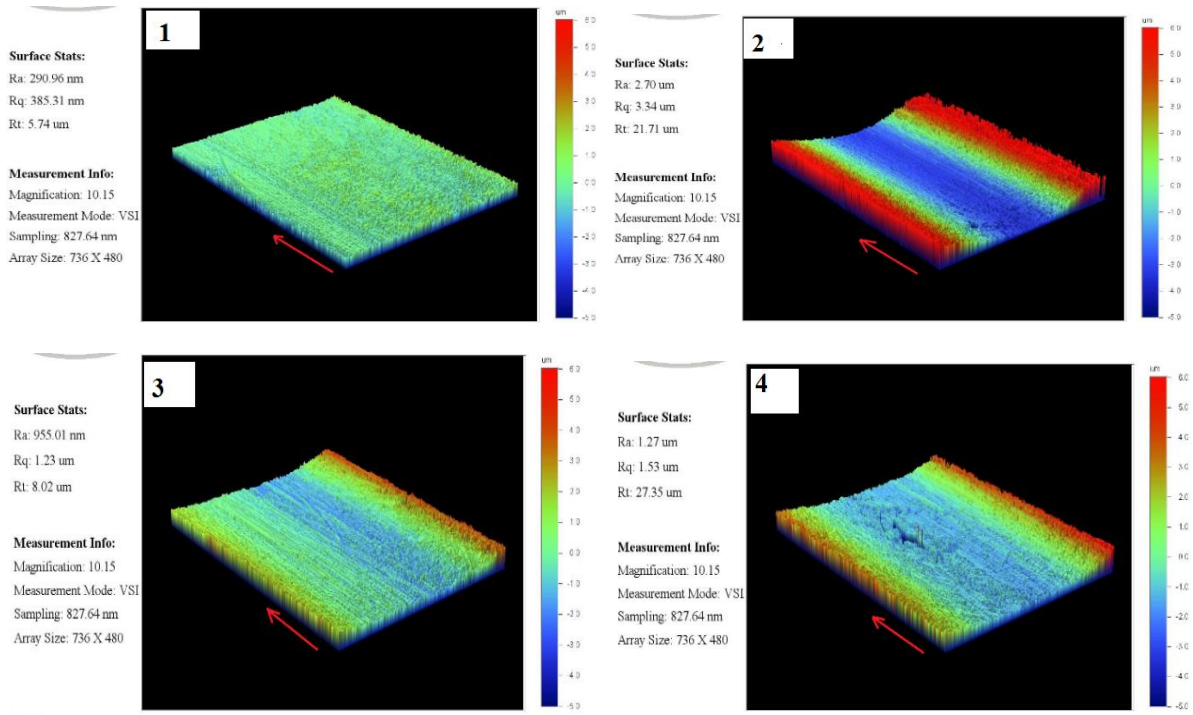

Figure 27. The 3D surface profile images of the rings at Position 1 and magnification 10X.

The 3D surface profile analysis was also done at magnification 20X. At this magnification, some grooves that are parallel to the sliding direction can be seen, these grooves can be seen in image that has the chassis number 1 up to left. The presence of these grooves on the worn surfaces of the sealing rings can indicate that there had been debris or hard abrasive particles between the sliding surfaces of the sealing rings and shafts during the operation. In Figure 28**,** the surfaces of the inner sealing rings at position 1 and magnification 20X are shown.

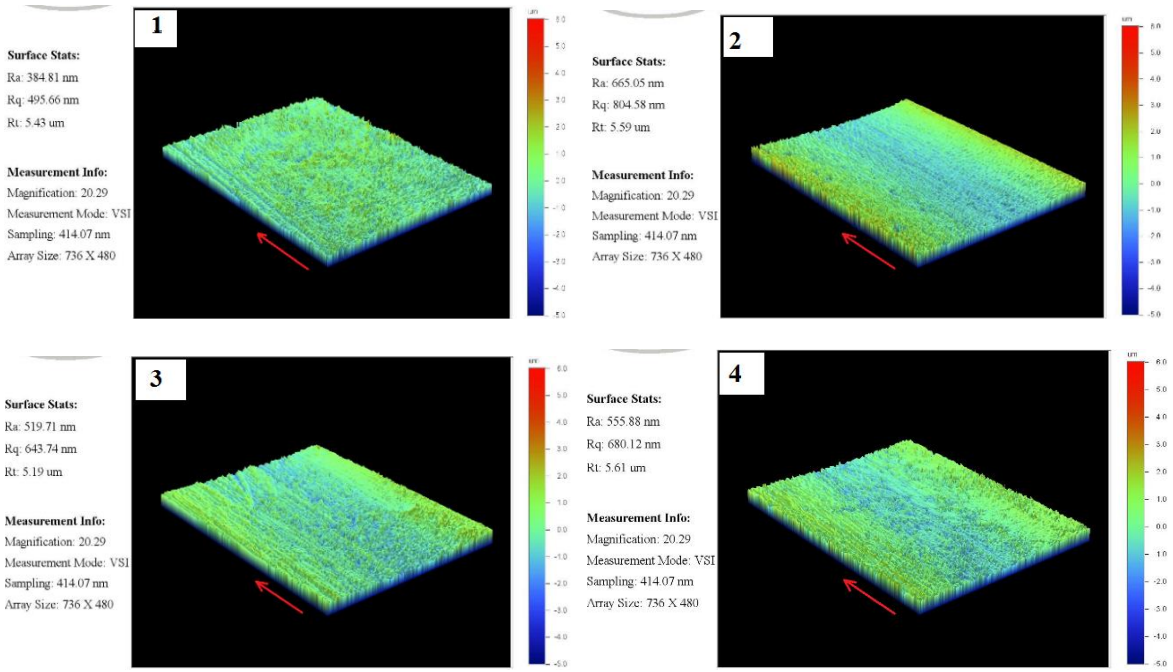

Figure 28. Rings 3D surface profile at Position 1 and magnification 20X.

The 3D surface profiles of the inner sealing rings at Position 2 and magnification 10X is shown in Figure 29. The surfaces at this position had mainly been worn in the same way as at Position 1. At this position, there were also some grooves on the worn surfaces of the sealing rings that are parallel to the sliding direction (red arrow), at magnification 20X the grooves can better be seen.

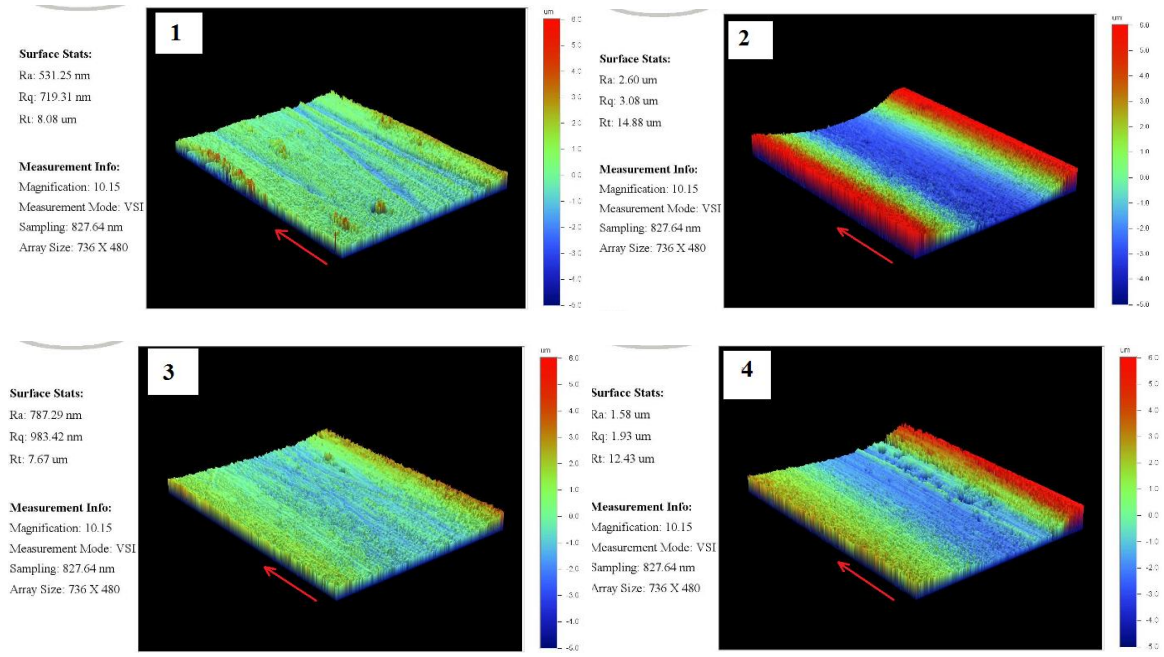

Figure 29. Surface profile images at magnification 10X and Position 2 on the worn surfaces of the inner sealing ring.

The 3D surface profile analyses of the inner sealing rings in Figure 30 below had as well been done at magnification 20X at position 2. At this magnification, the grooves on the worn surfaces can be more clearly seen. The biggest and deepest grooves on the worn surface can be seen in image that has the truck number 1.

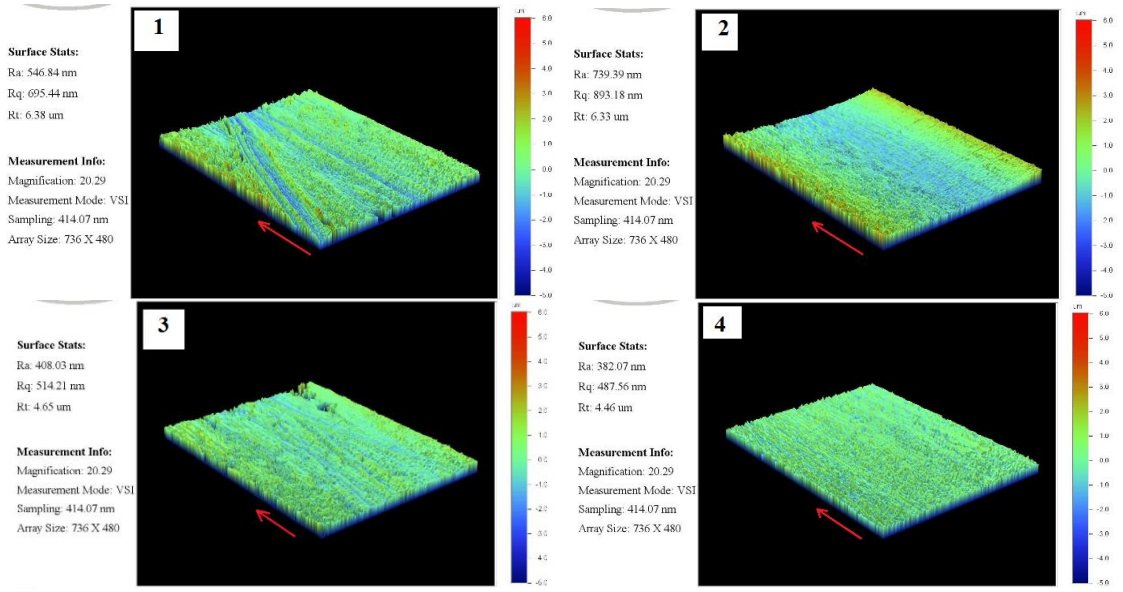

Figure 30. 3D surface profiles at magnification 20X and Position 2 on the worn surfaces of inner sealing rings, the chassis number is up to the left in each image and the red arrow shows the sliding direction.

3D surface profile analysis of worn surfaces of shafts that had been into contact with the worn surfaces of the inner sealing rings is shown below. The shafts which were analyzed have the same number as the inner sealing rings that were described above. The shafts are illustrated in Figure 31 below. The red arrows in each figure illustrates the rotational direction of the shaft. In Figure 31**,** it can be seen, the worn surfaces of the shafts have a convex shape perpendicular to the rotational direction which corresponds to the inverse shape of the sealing ring counter surface, which means that the contact between the worn surfaces of the inner sealing rings and shafts was conformal during the operation. The shaft number 1 has a flatter worn surface than the other shafts, as well the inner sealing ring from truck number 1 has a flatter surface perpendicular to the sliding direction. As it was mentioned before the truck number 1 comes from Netherlands and had been less driven at max load and high exhaust brake pressure than the other trucks that are illustrated in Figure 31 below.

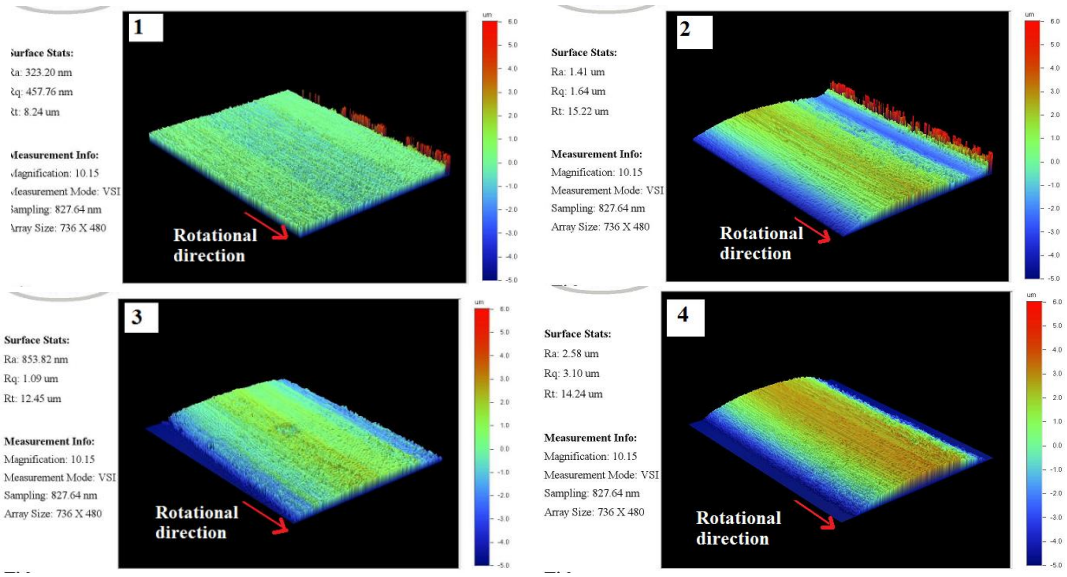

Figure 31. Illustrates the 3D surface topography of the shafts at magnification 10X.

At magnification 20X (Figure 32) some parallel grooves to the rotational direction can be observed on the worn surfaces of the shafts. The grooves are larger on the worn surfaces of the shafts compared to the worn surfaces of the inner sealing rings because the material of the shafts has a lower hardness than the hardness of inner sealing rings which had been analyzed, the presence of these grooves on the worn surfaces of the inner sealing rings and shafts indicates that there were debris or hard abrasive particles. These hard particles or debris also can indicate that there was three-body abrasive wear between the sliding surfaces during the operation.

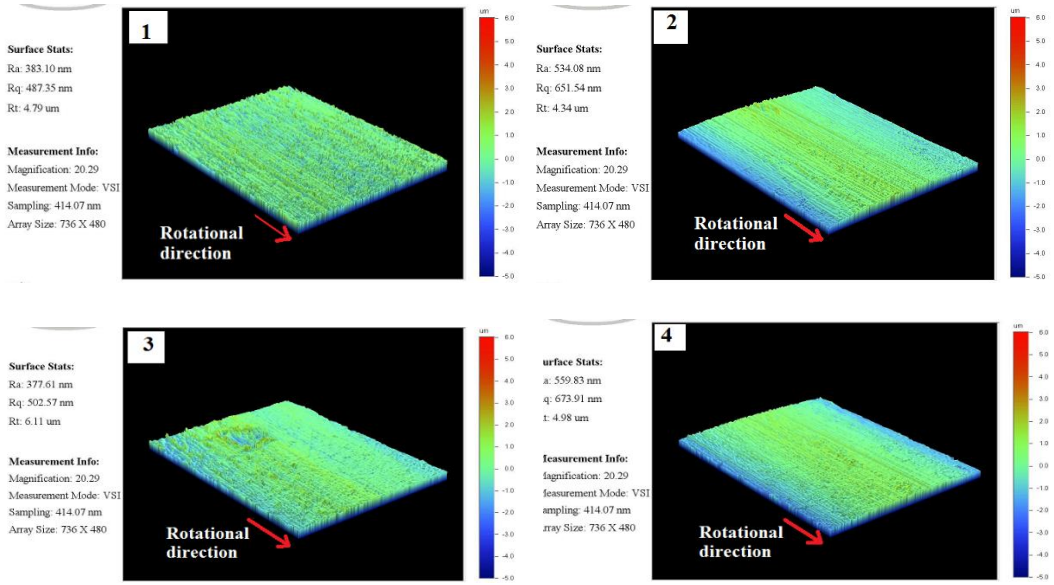

Figure 32. Illustrates the 3D surface topography of the shafts at magnification 20X.

4.1.3 Wear depth of inner sealing rings and shafts.

The wear depth of turbocharger components was calculated with help of 3D surface profile measurements. The wear depth was measured at three different positions along the worn surfaces of the sealing rings and shafts, at each position the measurements had been repeated three times and the mean value of these measurement are shown in Figure 33 with the standard deviation of these measurements at each position.

As seen in Figure 33 (a), the wear depth is very similar for all the analysed rings, Position 2 shows a slightly lower wear depth for all rings. The wear of the shafts is also very similar between the different selected shafts (Figure 33 (b)). An important observation is that the rings (harder material) shows a significantly higher wear depth compared to the shafts.

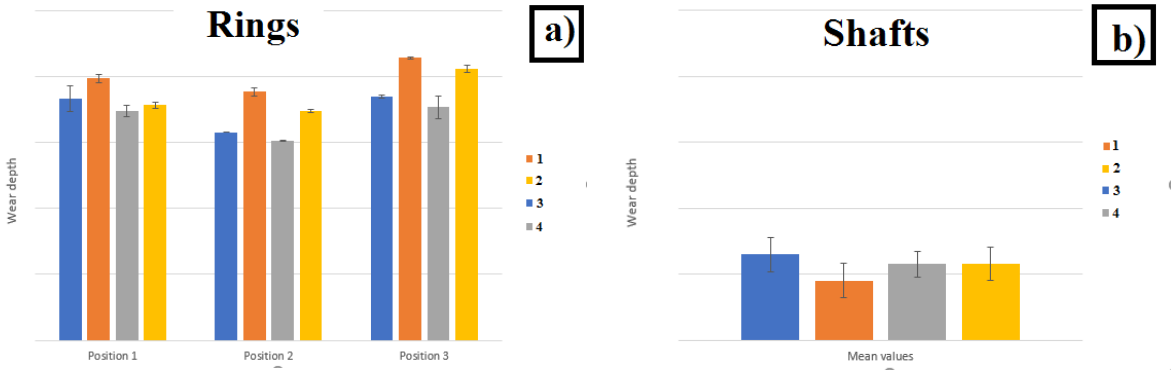

Figure 33. a) wear depth of rings, b) wear depth of shafts.

4.1.4 Hardness of new samples

The hardness of new sealing ring and shaft is shown in Figure 34. The measurements were taken along the cross-section of the sealing rings and shafts, the measurements had been repeated three times at each depth and the mean value and standard deviation of each measurement are shown in Figure 34.

As it can be seen the hardness of the new sealing ring has a hardness value around 660 $HV_{0.01}$ just below the surface and decreases to a constant hardness value around 630 $HV_{0.01}$ at a depth of approximately 60 µm. The new shaft has the hardness value around 416 $HV_{0.01}$ along the cross-section. As it can be seen in Figure 34, the hardness measurements were started at 10 µm under the surfaces of the new samples and been continued until the hardness values became constant. The positions where the hardness measurements had been done can be seen in Figure 6 where the positions are marked with 1, 2, 3 and 4 respectively. More details and measurement values can be found in Appendix E.

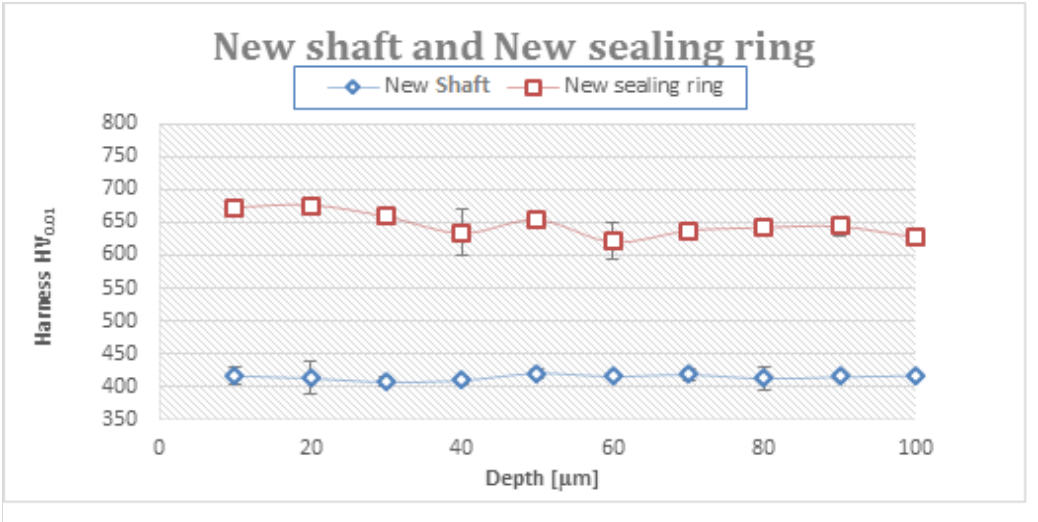

Figure 34. Hardness values of the new samples.

4.1.5 Hardness of used shafts

The hardness measurements were taken on the turbocharger shafts that come from trucks: 1, 3, 4 and 5. The hardness measurements on the shafts had been done at the positions that are marked with 1 in Figure 6**.** The hardness values of the shafts at 10 µm under the worn surfaces varies between 435 and 460 $HV_{0.01}$ and these values are decreasing along the cross-section to a constant value around 416 $HV_{0.01}$ as it can be seen in Figure 35. The hardness measurements show that there are not big differences in the hardness between the shafts that were compared in Figure 35. Mainly it can be seen that the hardness had a little increased close to the surface that had been worn, the hardness of the shafts had probably increased directly under the worn surfaces due to deformation hardening during the wear process.

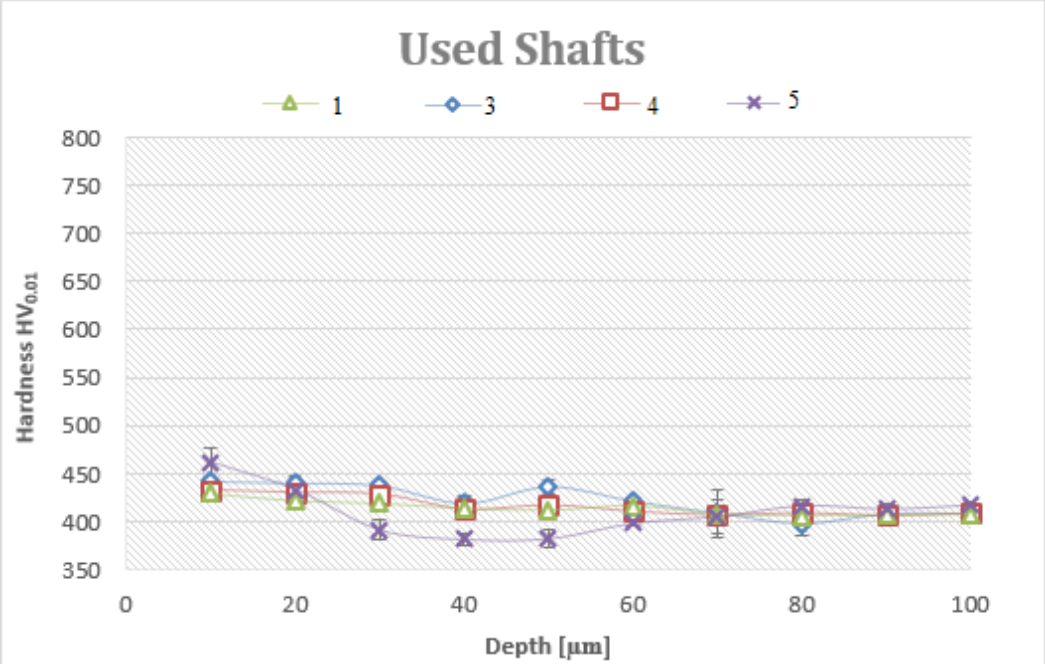

Figure 35. Hardness of used shafts.

4.1.6 Hardness of inner sealing rings

The inner sealing rings that are sitting closer to the bearing housing of the turbocharger were also analysed and the hardness values are shown in Figure 36. The hardness measurements were done at position 2 in Figure 6. The measurements were started at 10 µm under the worn surfaces and were repeated along the cross-section of the sealing rings until the hardness measurements became constant. The hardness values at 10 µm under the worn surface are between 646 $HV_{0.01}$ and 674 $HV_{0.01}$ and are then decreasing along the cross-section to a constant value around 610 $HV_{0.01}$ as it can be seen in Figure 36. In Figure 36 below it can also be seen that the inner sealing ring that comes from truck 3, has a higher hardness value even at a depth of 30 µm under the worn surface. This higher hardness value probably depends on the distance that the truck had been driven under highest exhaust brake pressure, the distance under the exhaust brake pressure is much larger than for the other sealing rings that are presented in Figure 36 below.

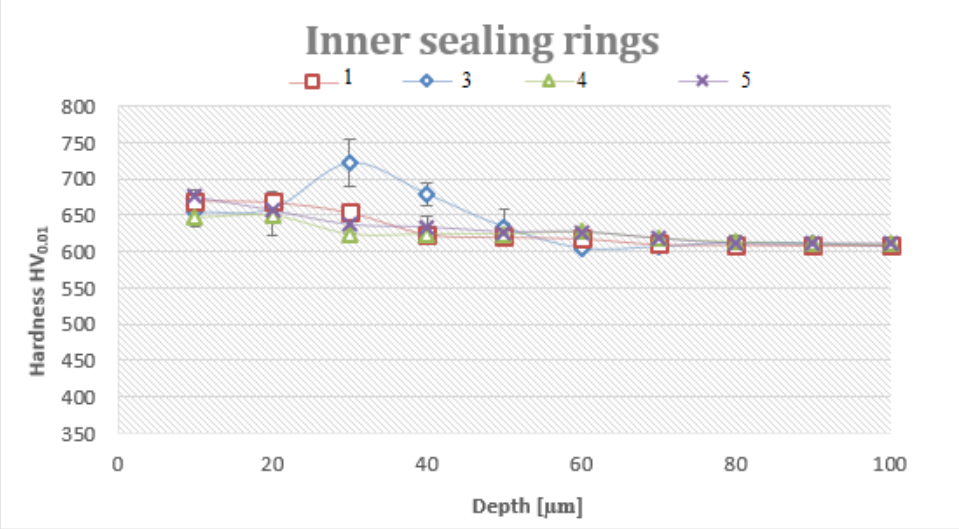

Figure 36. Hardness of inner sealing rings.

4.1.7 Hardness of outer sealing rings (in contact with shaft surfaces)

Figure 37 shows the hardness measurements of the outer sealing rings that were analysed. The hardness measurements started from the surfaces that had been in contact with shafts, the position is marked with 3 in Figure 6. In Figure 37, the hardness at 10 µm under the surfaces of the sealing rings is between 691 $HV_{0.01}$ and 770 $HV_{0.01}$ and decrease until a constant value 680 $HV_{0.01}$ along the cross section of the rings, a part of one of the rings, ring number 3 there the hardness values across the cross-section is around 625 $HV_{0.01}$, the hardness measurements values can be seen in Figure 37. As it can be seen in Figure 37 below, the hardness of outer sealing ring from truck number 4 is higher comparing to the hardness of the other outer sealing rings in the graph. The truck that has the number 4 comes from a truck that was used in Germany, from truck analyses it can be seen that the inner sealing ring of the turbocharger that had been used on truck number 4 had the largest wear depth of inner sealing ring, probably the outer sealing ring had relaxed, and the exhaust pressure had directly pressed on the inner sealing ring and influenced the wear. This is most likely due to the high exhaust gas temperature that the outer sealing rings relaxes and then the outer sealing rings cools down quick by the air, metals that are cooling down quick gets harder and more brittle, thereof a higher hardness.

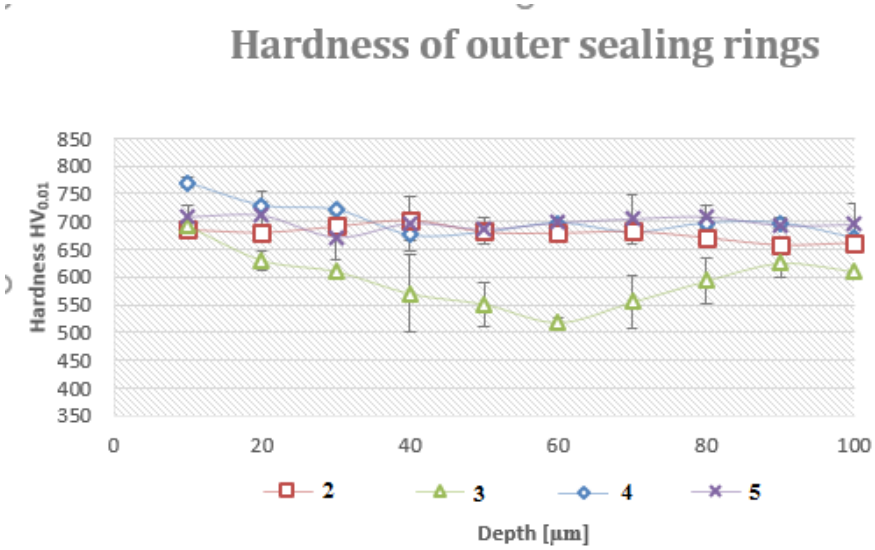

Figure 37. Illustrates the hardness of the outer sealing rings from the surface that had been in contact to the shafts, which it can be seen in Figure 6 at position that's marked with 3.

4.1.8 Hardness of outer sealing rings (from exhaust gases side)

The hardness of the outer sealing rings was measured on the exhaust gases side as it can be seen in Figure 6, position marked with 4. The hardness of the samples is illustrated in Figure 38 where the hardness values are between 740 $HV_{0.01}$ and 772 $HV_{0.01}$ at 10 µm under the surface and continues to decrease along the cross-section of the sealing rings to a constant value around 660 and 670 $HV_{0.01}$. Only one outer sealing ring from truck number 3 has a hardness value of 614 $HV_{0.01}$ at 10 µm under the surface and then the hardness values of it are increasing across the cross-section to a value around 660 $HV_{0.01}$. The lower hardness of the outer sealing ring 3 it is probably that the truck that has this chassis number had been longest driven at this highest exhaust pressure, comparing to the other sealing rings that had been analysed.

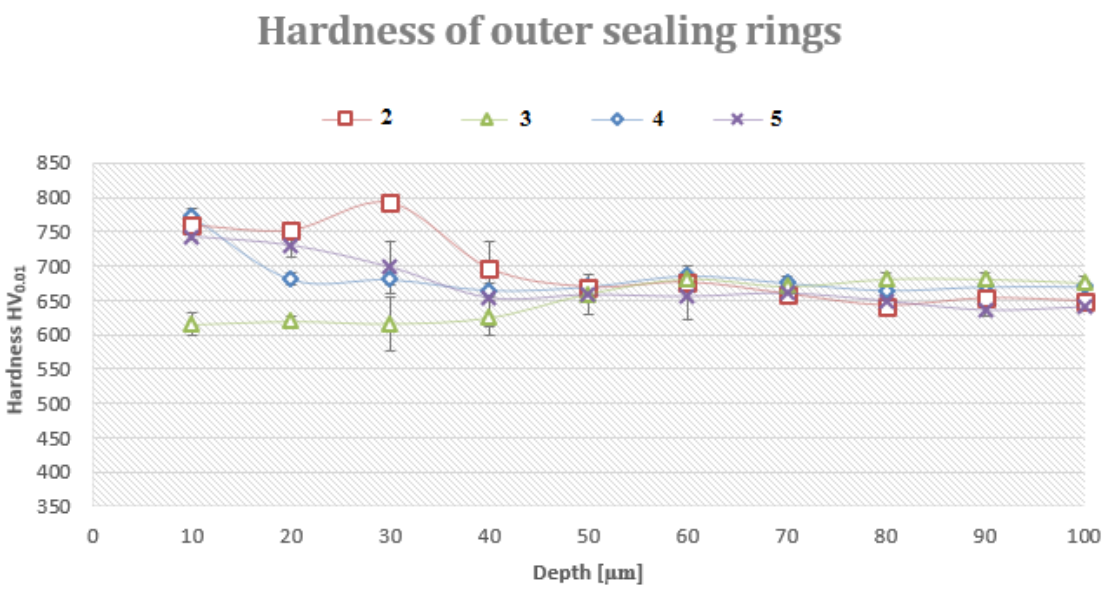

Figure 38. Hardness of outer sealing rings (from exhaust gases side).

4.1.9 SEM analysis of worn inner sealing rings

SEM analysis was performed on the worn surfaces of sealing rings and shafts at positions 1 and 2 as shown in Figure 5. The first inner sealing ring that had been analysed come from truck number 6. In Figure 39 (a), close to the ring gap, there are signs of a patchy layer on the worn surface. Figure 39 (b) is a high magnification of (a) and cracks can be seen along the middle of the worn surface of the sealing ring. The cracks are perpendicular to the sliding direction. The presence of the cracks shows that there were high shear stresses, probably due to the high friction generation between the sliding surfaces of the sealing ring and shaft.

The cracks can also indicate the presence of a thermal fatigue wear mechanism. Thermal fatigue cracking of surfaces results from the rapid alternations in temperature, which may induce stresses high enough to impose an increase of plastic strain in the sealing ring surface [32]. Figure 39 (c) and (d) shows that the cracks are 20 to 30 µm long. Some small particles that had been flattered down on the worn surface of the sealing ring are also seen. Figure 39 shows the SEM image of the inner sealing ring 6 close to the ring gap.

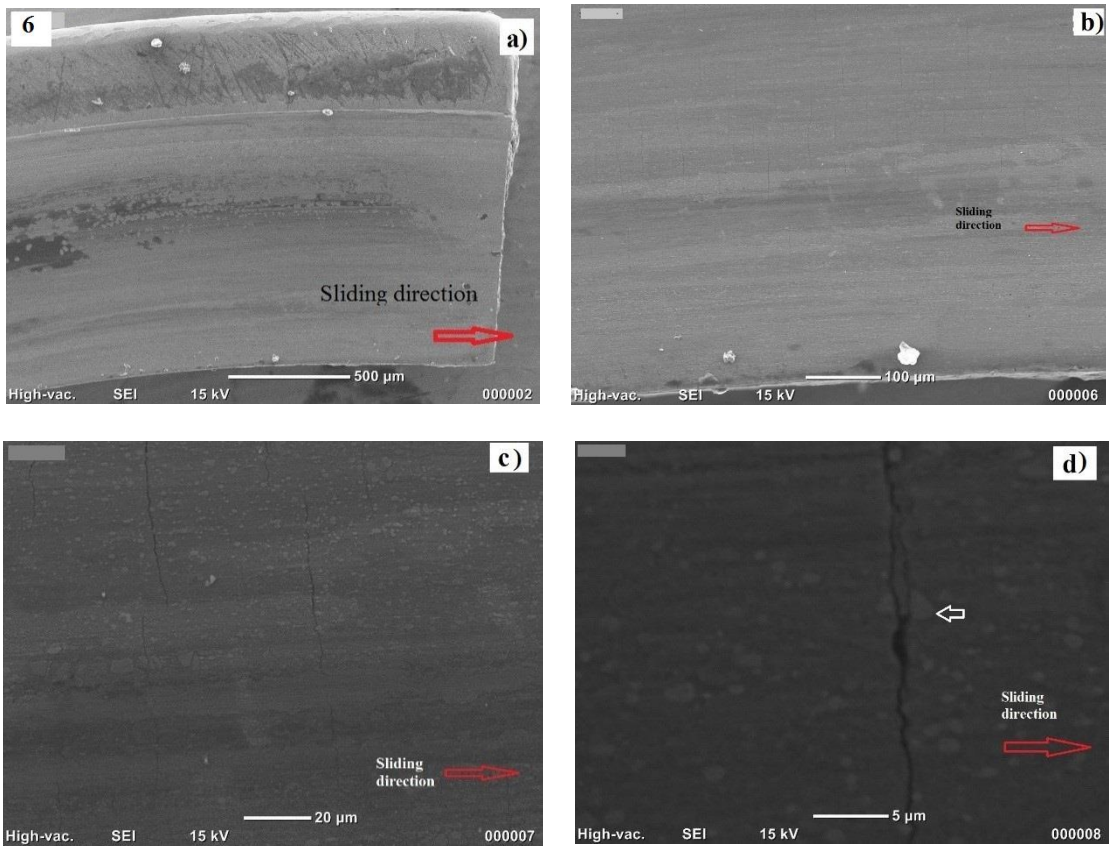

Figure 39. a) is the image of the inner sealing ring 6 close to the ring gap,b) is in zoom of middle of a) as well c) is an in zoom of b) and d) is an high magnification of c), the white arrow in d) shows for example a particle that had been flattered down.

In Figure 40 the SEM micrographs were taken at position 2 on the worn surface of inner sealing ring number 6. In Figure 40 (a) also shows where (b), (c) and (d) are taken. The worn surface shows sign of adhesive wear in (c), some mild abrading grooves parallel to the sliding direction in (d). In Figure 40 (b), a tribo-layer is seen on the surface of the sealing ring.

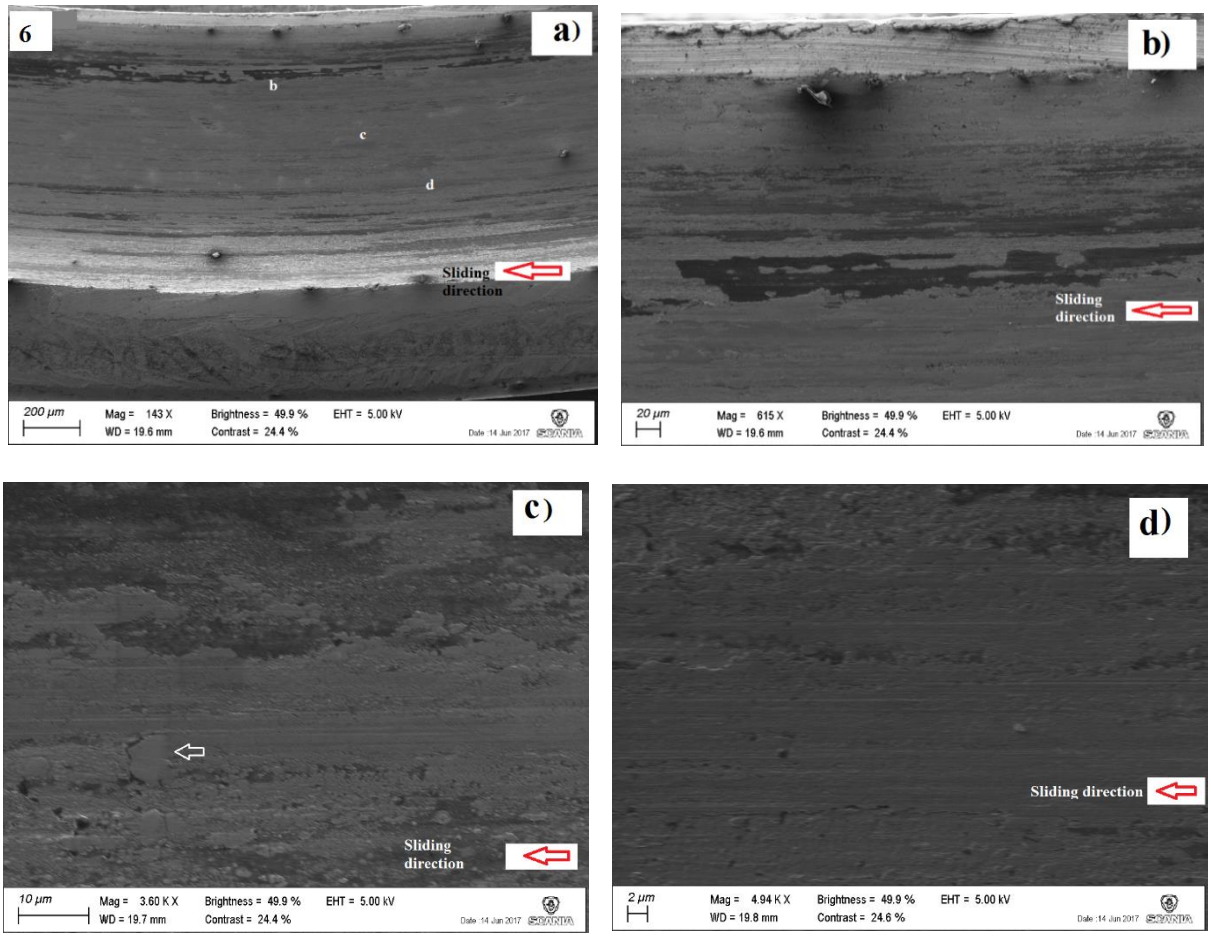

Figure 40. SEM analyses at position 2, in b) and c) it can be seen adhesive wear on the worn surface of the sealing ring.

Figure 41 shows SEM micrographs close to the inner sealing ring gap of truck number 7. Figure 41 (b) a tribo-layer is seen in the upper part of the image while in the lower part of the image it can be seen some adhesive wear. The (c) image illustrates fractured tribo-layer on the surface of the sealing ring. The truck data shows that the truck had been used below average at max load. The exhaust brake pressure percentage of the time is the lowest comparing to the other trucks that had been analysed during the project.

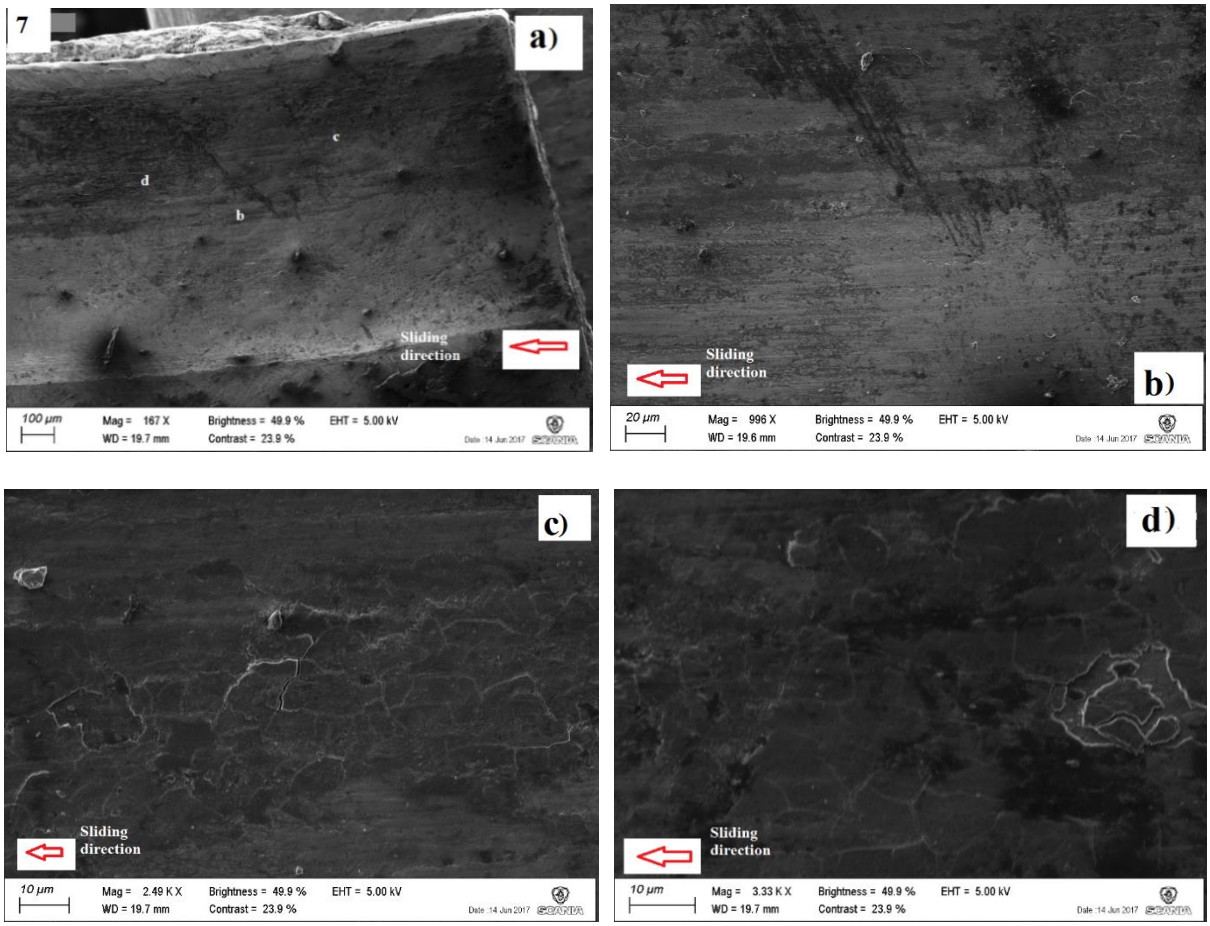

Figure 41. Illustrates the worn surface of the inner sealing ring number 7 close to the ring gap a), while in b), c) and d) are high magnification of a).

At position 2 on the inner sealing ring 7, SEM analyses was done on the worn surface. On the inner edge of the sealing ring some debris is accumulated, Figure 42 (b). In (c) it can be seen a crack that is perpendicular to the sliding direction, the cracks goes trough the tribolayer into the surface of the sealing ring. The cracks look similar to the cracks that were identified in the surface of the inner sealing ring in Figure 39. In (d) can be seen adhesive wear, the blue arrow indicates adhesive particles that had been flattered down.

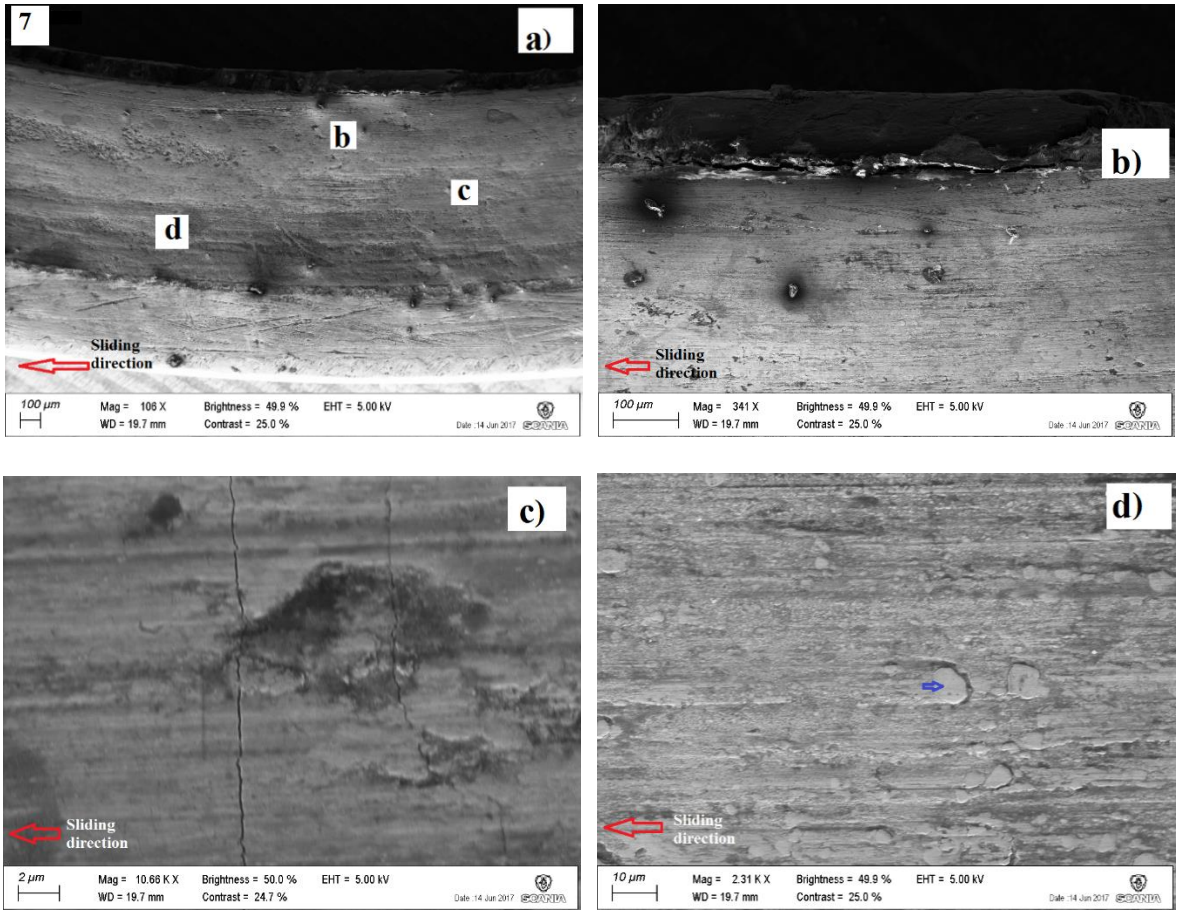

Figure 42. a) shows the position there the analyses had been done on the worn surface of the ring that comes from truck number 7. In b) it can be seen an in zoom of a) and c) is a high magnification of b).

The inner sealing ring that is presented in Figure 43, comes from truck number 1. As it can be seen in (c) there are cracks that are perpendicular to the sliding direction, while in (d) a fractured tribo-layer over the worn surface of the sealing ring is seen. The cracks look like the cracks that are present on the worn surface of the sealing ring that is illustrated in Figure 39. The inner sealing ring 1, which comes form truck number 1, that was driven below average at max load and lowest percentage at medium exhaust brake pressure.

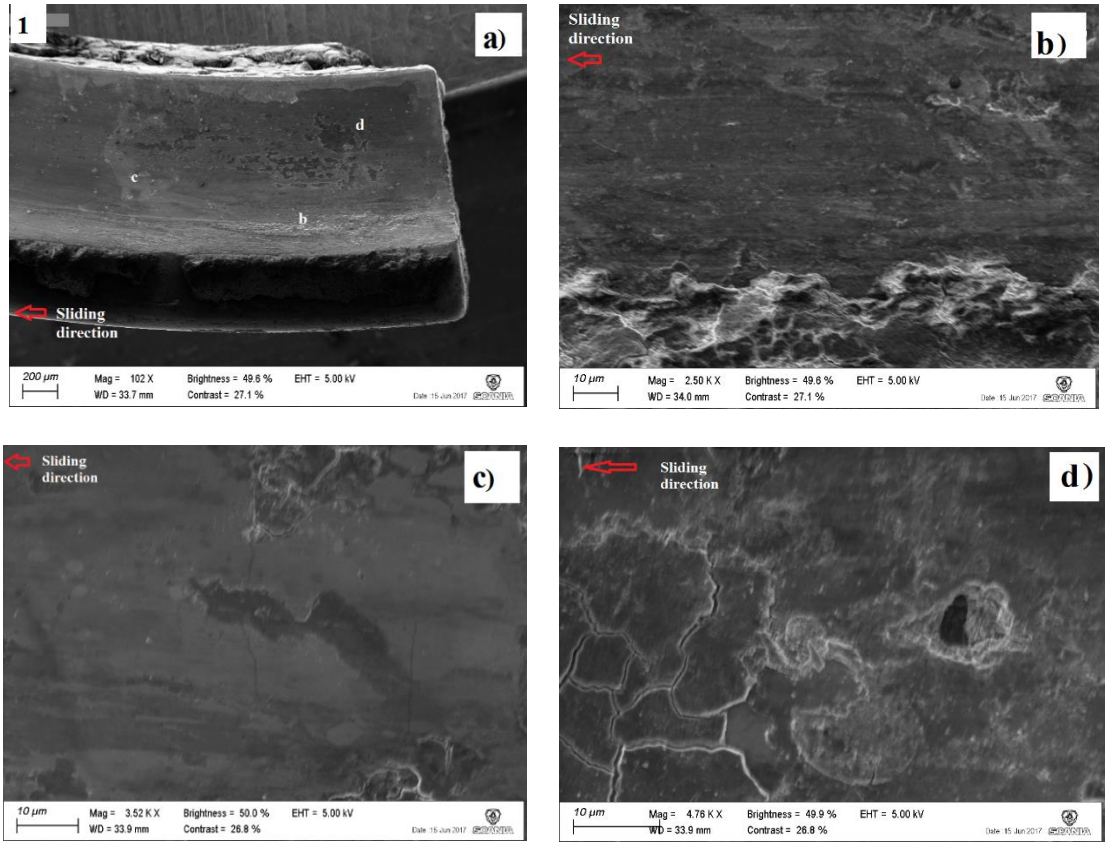

Figure 43. Position 1, analyses of worn surface close to the ring gap.

SEM analysis at position 2 on the inner sealing ring number 1 are shown in in Figure 44. In (b), a crack on the worn surface is seen and the crack looks like the cracks that were found on the worn surface of the sealing rings in Figure 39 and Figure 42. In (c), it can be seen adhesive particles that had been flattered down on the worn surface of the sealing ring. The presence of cracks on the worn surfaces of the inner sealing rings can be due to high friction forces and /or due to the thermal fatigue.

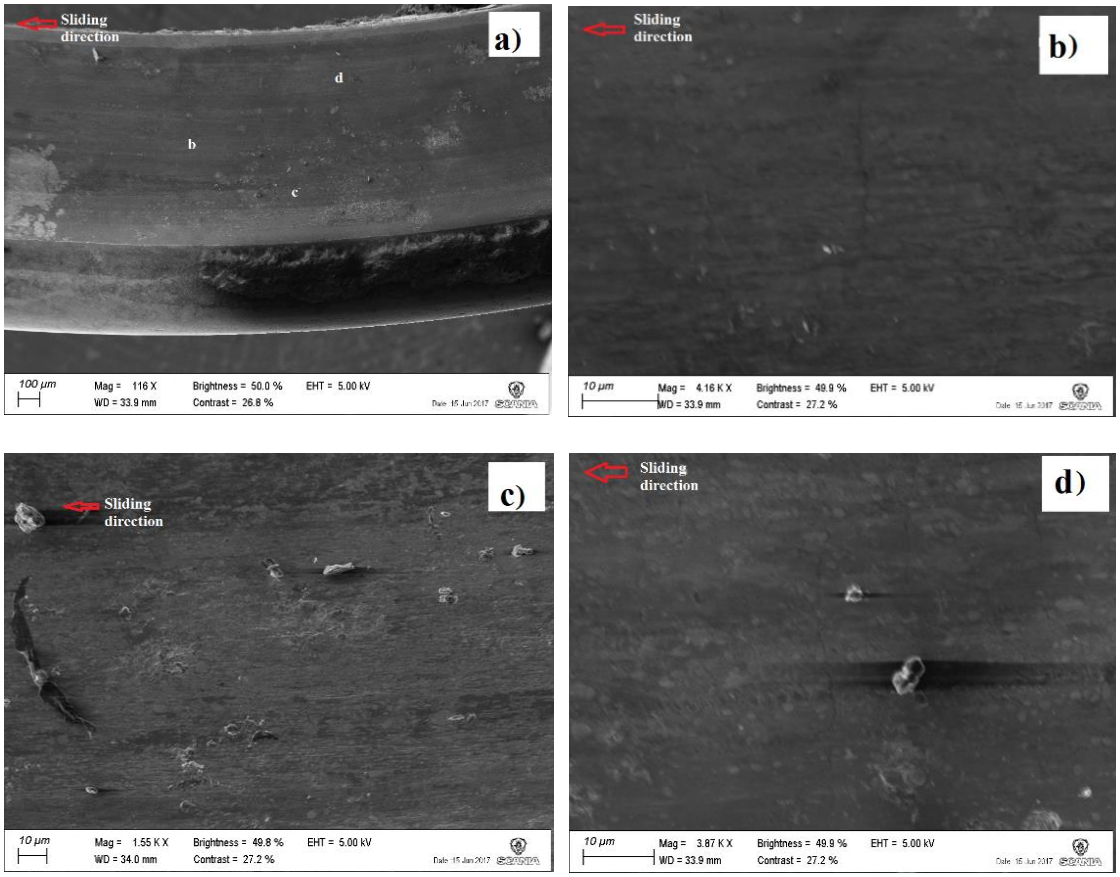

Figure 44. Position 2, analyses of the worn surface at the middle along the worn surface.

4.1.10 SEM analysis of shafts

The worn surfaces of the shafts that had been in contact with the inner sealing rings was also analysed. The first shaft that was analysed comes from truck number 6. In Figure 45 (a), can be seen where the analysis was done. The red arrow indicates the rotational direction of the shaft. In (c) and (d), it can be seen how the surface asperities had been flattered down and how these asperities had plastically deformed. The white arrow shows plastic deformation of such asperities on the middle of the worn surface of the shaft. In c) and d) there are some small cracks that are perpendicular to the rotational direction. The cracks are along the worn surface of the shaft. The presence of these cracks and plastic deformation of the surface of the shaft shows that there was high friction generation and high shear stresses between the sliding surfaces of the sealing rings and shafts. As it was shown in 3D surface profile analyses, the worn surfaces of the shafts, generally have a convex shape while the worn surfaces of the sealing rings got concave shape during the operation, probably due to the high heat and friction generation between the sliding surfaces and probably even due to the high pressure.

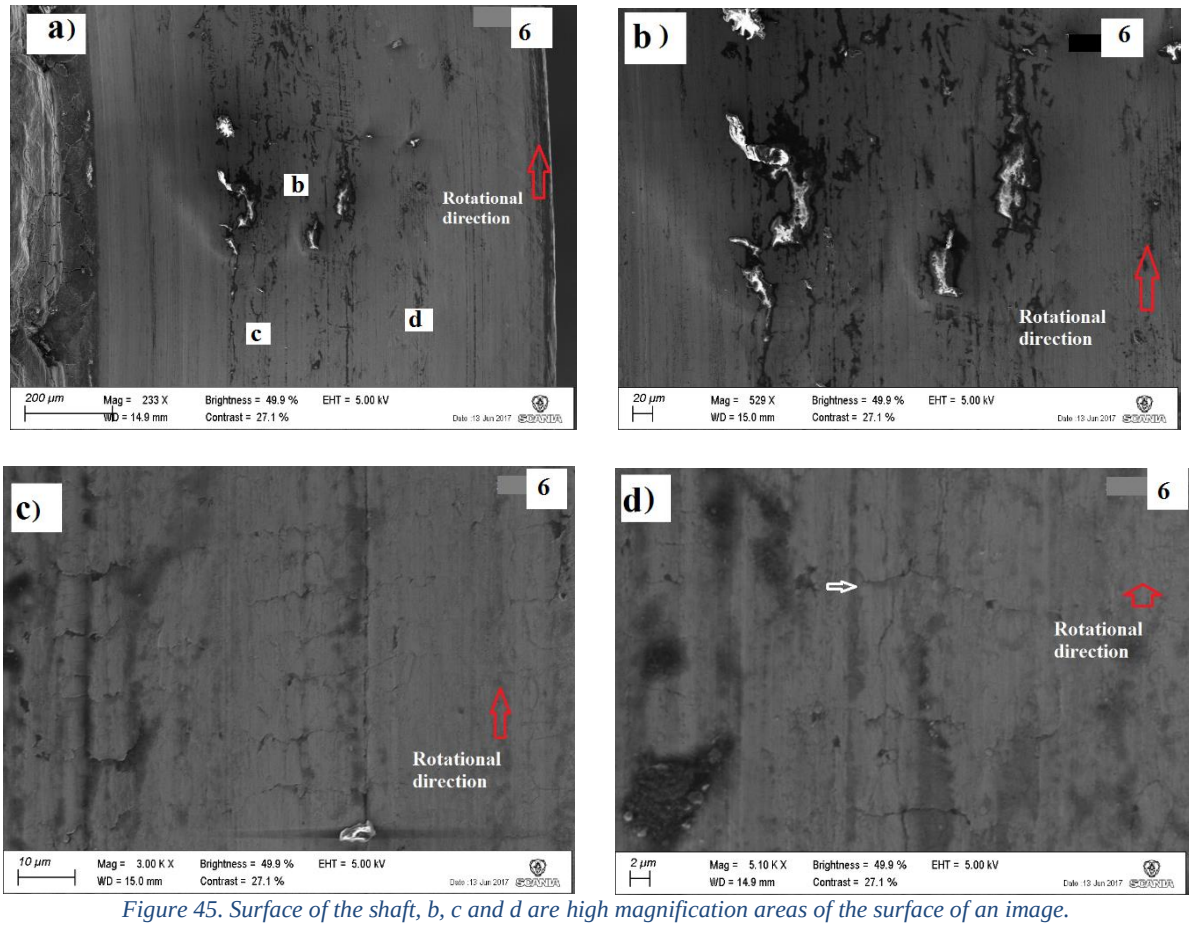

Figure 45. Surface of the shaft, b, c and d are high magnification areas of the surface of an image.

Figure 46 shows the analysis of the worn surface of shaft that comes from truck number 7. In (a), it can be seen where the worn surface of the shaft was closer analysed and where (b), (c) and (d) were magnified on the surface. The red arrow shows the rotational direction of the shaft while the white arrow in (d) shows asperities that was flattered down, probably due to the high pressure during the operation. In (d) and (c) it can also be seen some small parallel grooves to the rotational direction which means that there is abrasive wear on the worn surface of the shaft. In (b) it can be seen how the surface was plastically deformed and even that there was adhesive wear during the using of turbocharger.

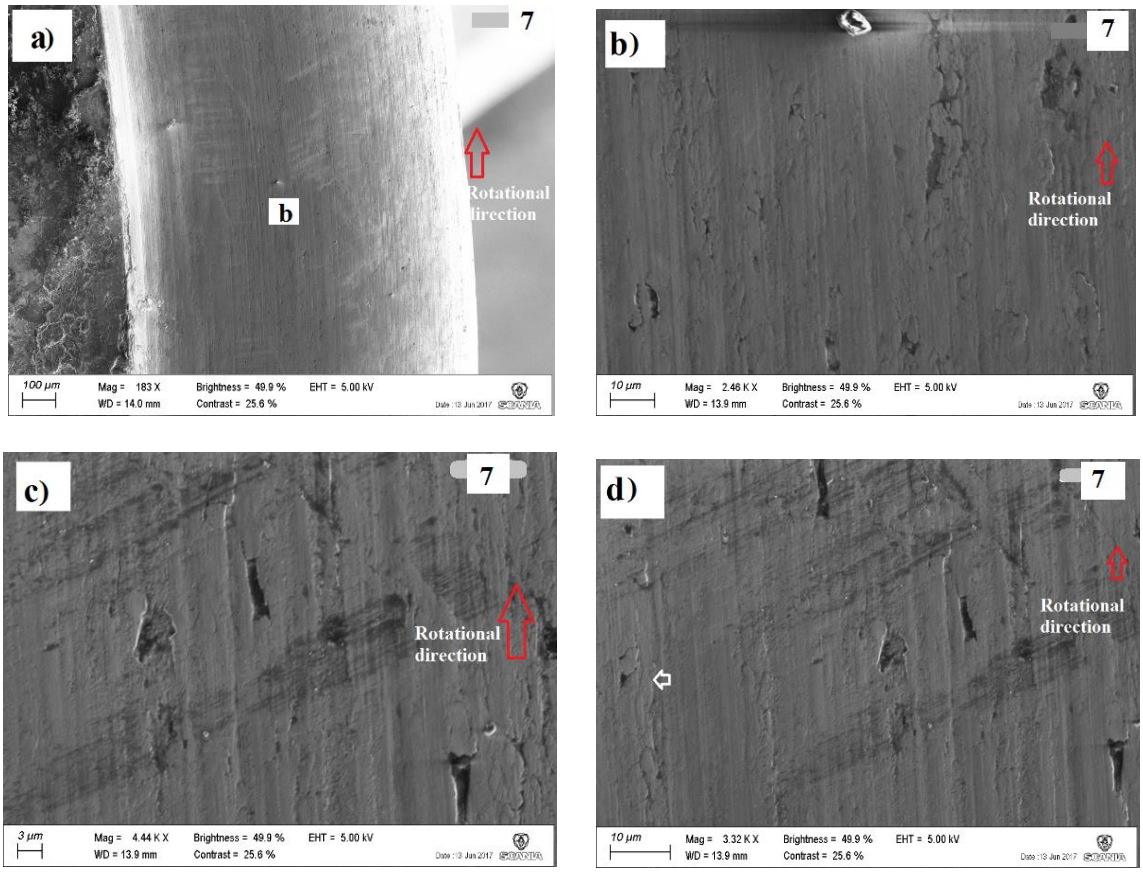

Figure 46. Illustrates the worn surface of the shaft, there the shaft had been in contact with the worn inner sealing ring.

4.1.11 Cross-section analysis of the inner sealing rings and shafts

The cross-section analysis of the inner sealing rings was done along the sliding direction to identify any possible changes to the microstructure and how deep the cracks were. The analysis was done along the worn surface of the inner sealing ring 6. In Figure 47 the crack is going through the tribo-layer into the sealing ring material and has a depth of around 4µm in the cross-section of the sealing ring. The crack that is marked with a white arrow in image (b) has a depth around 3-4 µm into the cross-section of the ring. A fractured carbide at the top surface is also shown in (b) but carbides further down in the material are not affected and the crack propagates around the carbides. In (b) it can even be seen that the tribo-layer is thicker than in (a) and the crack is hidden under the tribo-layer. Both (a) and (b) in Figure 47 come from the inner sealing ring 6 that was cut along the cross-section close to the sealing ring gap to identify how deep the cracks are in the ring material. The cracks can be seen on the surface of the sealing ring in Figure 39, where the surface analysis was done on the same inner sealing ring close to the inner ring gap. These cracks network were identified only in the inner sealing ring material along the cross-section, the depth and intensity of these cracks is probably one of the main reasons why the rings worn more than the shafts, there were not any cracks in the shafts material and the shafts worn less. These perpendicular cracks to the sliding direction of the shaft that are going deep in the ring material.

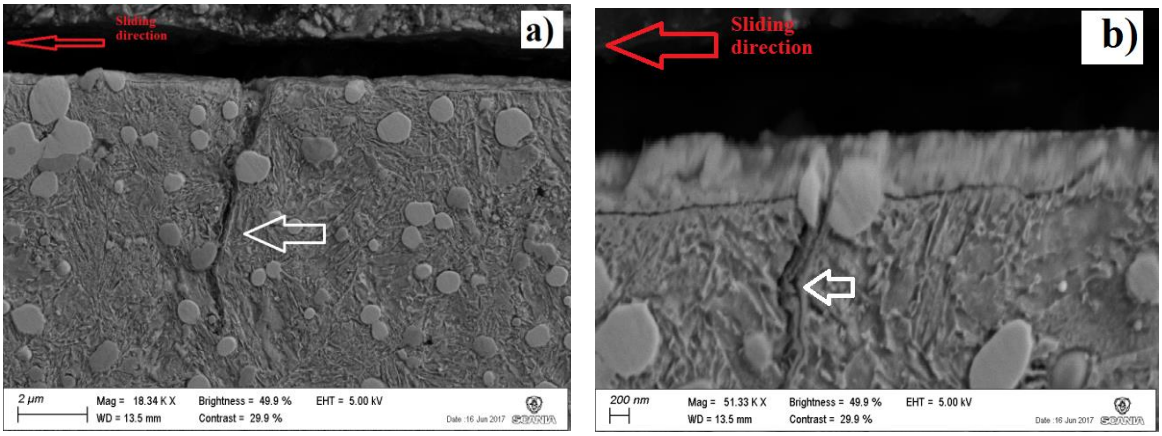

Figure 47. Cross-section analyses of the inner sealing ring 6, the analyses had been done along the sliding direction.

4.1.12 Cross-section analysis of the used shafts

The cross-section of the worn shafts was analysed, both along and perpendicular to the rotational direction. In Figure 48 (a) the cross-section of the new shaft perpendicular to the rotational direction is shown and in (b) it can be seen how the grains of the used shaft had been plastically deformed and parallel oriented due to the friction generation and high contact pressure between the inner sealing ring and the shaft sliding surfaces. In (a) the red line shows how the inner sealing ring surface should be placed according to the shaft. The grains of the new shaft in (a) has the same grain size and orientation. In (b) it can be seen the cross-section of the used shaft number 3 perpendicular to the rotational direction, and it can also be seen that the orientation and the size of the grains under the worn surface of the shaft has changed (red arrow).

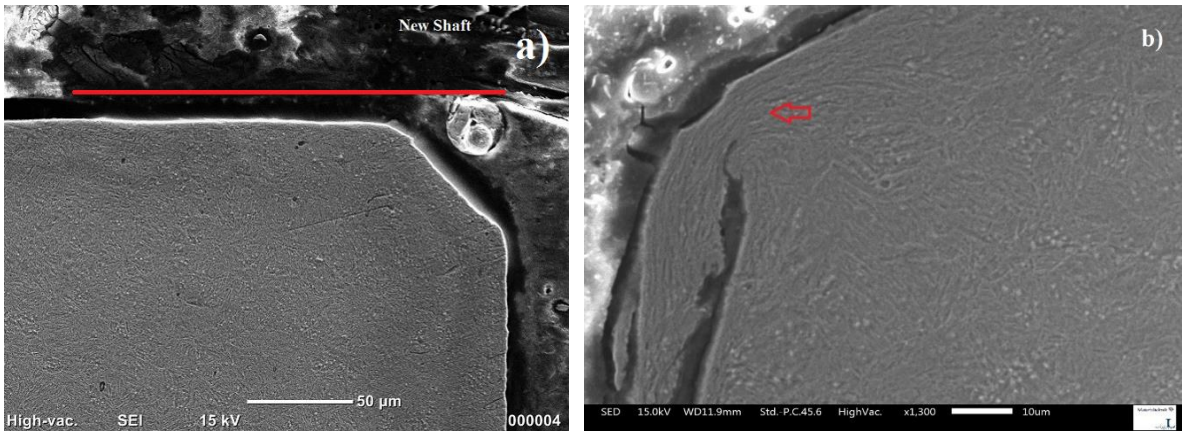

Figure 48. In image a) it can be seen the cross-section of the new shaft perpendicular to the rotational direction, the rotational direction in a) is into the screen. While in b) it can be seen the cross-section of the shaft that has the number 3, the rotational direction of it is out of the screen.

The cross-section analysis on the used shafts had also been done along the rotation direction of the shafts. The red arrows in Figure 49 (a) and (b) below shows the rotational direction of the shafts. A blue arrow shows oriented grains under the worn surface of the shaft that had been in contact with the inner sealing rings. As it can be seen in (a) the grains had been more oriented than in (b). Truck number 6 in (a) had been driven longer distance at highest exhaust brake pressure comparing to the truck that has the number 7 in (b).

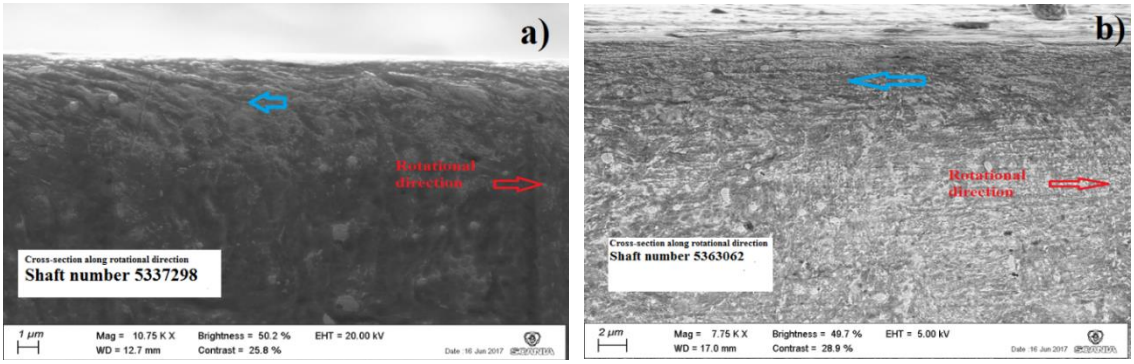

Figure 49. Shows the cross section of two different shaft, 6 in a) and 7 in b) respectively

4.1.13 EDS analysis shaft and sealing ring

The EDS analysis was done to identify the elements that were present on the worn surfaces of the used sealing rings and shafts. Elements that are in the composition of the sealing rings had been found on the surfaces of the shafts, which it indicates that adhesive wear took place between the sliding surface of the inner sealing ring and shafts.

In Figure 50 below (a) Spectrum 1 are the EDS analysis on the surface of the inner sealing ring 6, while in (c), there it can be seen the elements that were found on the worn surface of the sealing ring, Spectrum 1. In (b) Spectrum 3 is illustrated where the EDS analysis were taken on the worn surface of the shaft that was into contact with the inner sealing ring presented in (a) and in (d). It can be seen the elements that were found at Spectrum 3 on the worn surface of the shaft. The shaft has not any W or V in the composition, the analyses and elements in (d) show that there are elements that had been transferred from the surfaces of sealing ring to contacting shaft surface, if the material from the sealing ring was transferred to the surface of the shaft, means that adhesive wear occurred during the material transfer from the inner sealing ring.

There are some other elements that were identified in (c), elements that are not in the chemical composition of the sealing rings or shafts of turbochargers. These elements come most probably from the lubricant additives, elements like, Zn and Ca are often used as additives in oil lubricants, that means that the black tribo-layers that were found on the worn surfaces of turbocharger components (sealing rings and shafts) from LOM analyses are most probably coming from the residual lubricant.

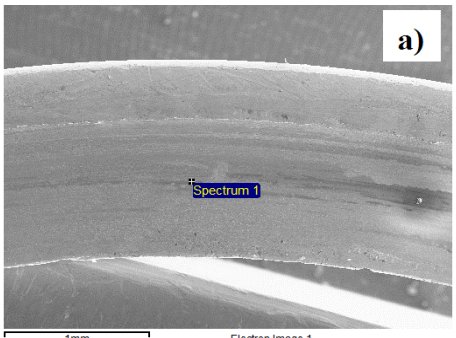

c)

Element	Weight%	Atomic%
C K	537.29	77.70
O K	87.72	9.52
P K	2.45	0.14
S K	5.62	0.30
Ca K	4.15	0.18
V K	11.06	0.38
Cr K	16.36	0.55
Mn K	1.75	0.06
Fe K	354.01	11.01
Zn K	1.47	0.04
W M	13.93	0.13
Totals	1035.82	

d)

Element	Weight%	Atomic%
C K	34.80	38.51
O K	13.26	11.02
V K	1.42	0.37
Cr K	3.35	0.86
Mn K	1.43	0.35
Fe K	202.62	48.22
Mo L	2.86	0.40
W M	3.98	0.29
Totals	263.73	

Figure 50. EDS analysis of used shaft and sealing ring, in(a) surface of the used inner sealing ring while in (c) are the elements that were found on the surface of the used sealing ring in (a). In (b) the used shaft and in (d) the elements from used shaft (b).

4.2 Friction and wear behaviour from tribological tests

The friction and wear behaviour are analysed by replication of the operating conditions in the turbocharger. The tests were performed in Pin on Disc TE67 tribological test machine. The tests are performed at different conditions to evaluate the influence of each parameter on friction and wear behaviour.

4.2.1 Friction behaviour

Test under two loads at two different speeds were performed. The tests performed at two temperatures which results in 8 different setups. The friction results can be seen in Figure 51.

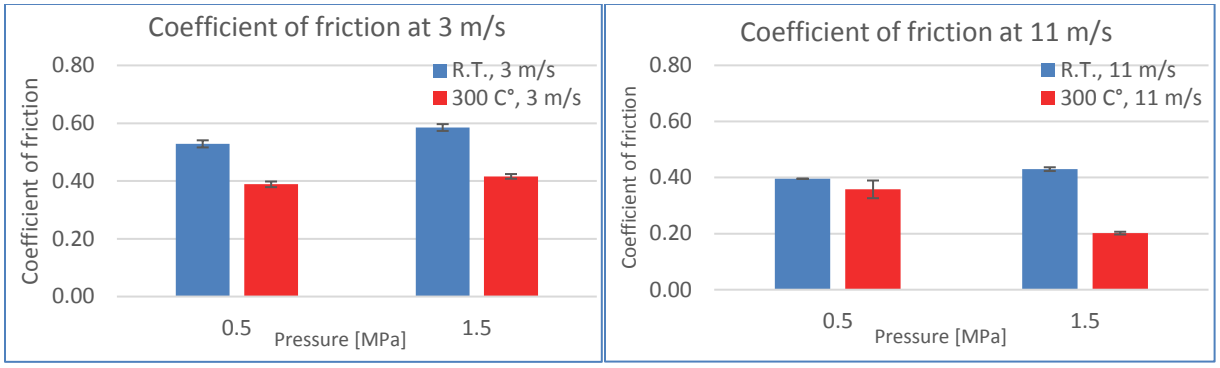

Figure 51. Average coefficient of friction for all test conditions.

The observations show that increased load lead to insignificant changes in frictional behaviour. The only condition where load dependency have considerable influence on coefficient of friction is high temperature (HT) with high sliding speed.

The reason of decreased resistance to sliding may be explained by the equation for coefficient of friction

$$F_\mu = \mu * N$$

where the increased normal load N should increase the resisting force of gliding F_μ with the factor μ, which is coefficient of friction. If the force F_μ is not increased enough compare to the normal load N the coefficient of friction should decrease. This is being observed during this experiment at high speed HT.

The second explanation for the decreased coefficient of friction may be the wear mechanism. The condition of high load and high speed at room temperature (RT) . have extreme difference to other conditions. During the test run sparks were observed. The sparks usually are a heated material that leaves the contact area. The difference can be seen in Figure 52 and Figure 53.

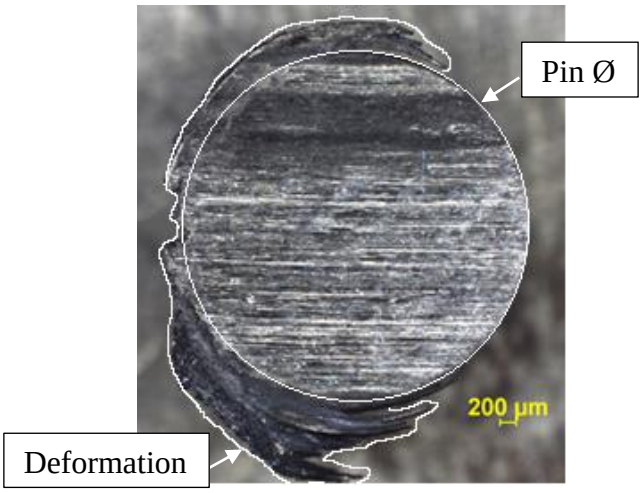

Figure 52. LOM picture of deformation on pin test 9, high load high speed R.T.

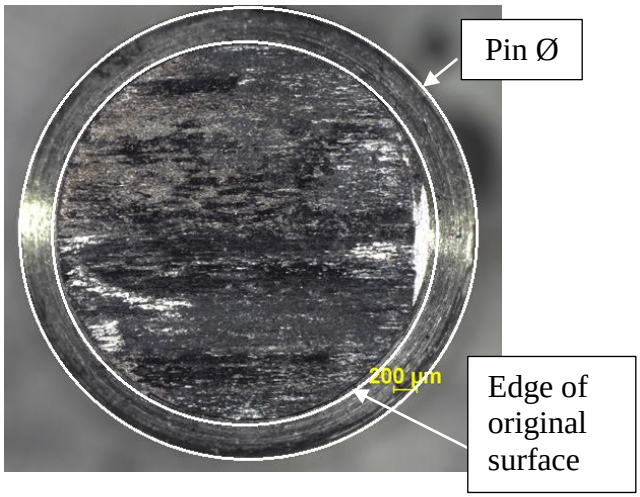

Figure 53. Wear surface of pin test 7, low load high speed R.T.

The LOM examination of pins shows that there is significant difference in deformation. The rest of the conditions did not have the same deformation except for the condition with high load and high speed in RT . The rest of conditions looked like the pin of test 7, Figure 53 where the grading is left and not worn out. This may be the main reason why there is a significant difference in friction behaviour.

The conditions where the speed and/or temperature increased resulted in a lower coefficient of friction for all cases. This means that the lowest coefficient of friction can be found at highest load, highest speed at highest temperature. The results shows small scatter which means that it is repeatable.

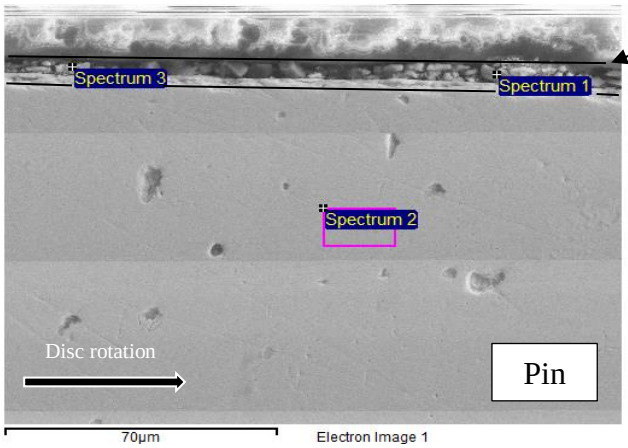

Oxide layer

Spectrum	C	O	Si	Cr	Mn	Fe	Total
Spectrum 1	100.21	27.83	0.66	3.54	1.65	231.59	365.47
Spectrum 2	29.07		1.03	3.71	2.97	291.05	327.83
Spectrum 3	76.32	78.00	0.78	3.48	2.03	220.05	380.65
All results in weight%							

Figure 54. Cross-section view along sliding direction of pin test 23, low speed high load HT and EDS analysis.

The reason to reduced resistance to sliding with higher speed and HT is because of formation of an oxide layer that is building up on the surface. The EDS show that the surface of the pin (Spectrum 1&3) contains more oxygen than the core of the pin (Spectrum 2) which is sign of oxidized surface, see Figure 54. The surface of steels tends to oxidise more rapidly with higher temperature [33], because a higher temperature promotes chemical reaction between steel and oxygen. Higher speed

increases contact energy which increase the temperature. Therefore, an oxidation process is increased on the surface and creates the oxide layer which protect the surface from severe wear.

Wear behaviour

A detailed understanding of the wear behaviour under different operating conditions is a crucial part in development of a new design/material selection of the sealing rings that should withstand the harsh conditions in the turbocharger.

The worn surface of the discs showed material build-up as shown in Figure 55 for some of the test conditions. This is due to higher wear of the softer pin (shaft material), formation and oxidation of wear debris and subsequent compaction of the particles on the harder disc surface. This resulted in very little to no wear on the disc except for tests at low load and low temperature where a distinct wear track was observed.

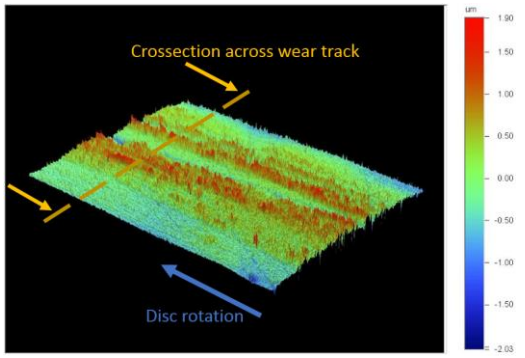

Figure 55. Surface of the disc after test, low load high speed HT.

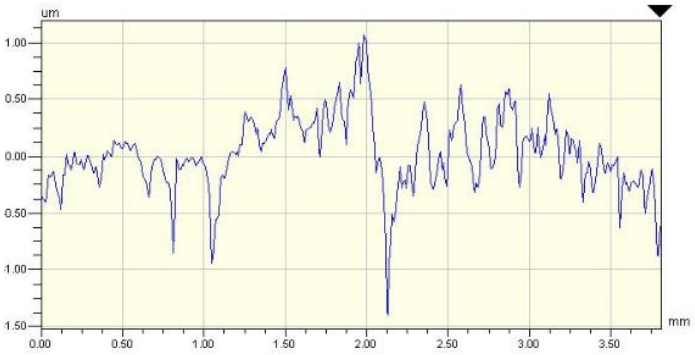

Figure 56. Disc profile measurement.

The wear behaviour of the discs varies. On the surface of discs with wear condition 3 m/s, high load and RT show an thin and brittle oxide layer, see Figure 58. The SEM analysis show some particles that have adhered on surface. The same conditions but HT shows a thicker oxide layer, where with magnification carbides cannot be seen. The main wear mechanism is abrasion and adhesion. For HT disc, it seems that the adhesion happens first. An oxide layer is building up on the surface and then breaks which remove both the oxide layer and surface material (or disc material), see Figure 57. The cross-section view shows an orientation of microstructure of material at low speeds. The friction coefficient is lower at HT, compare to RT, where a thicker oxide layer is observed. The SEM analyse of the HT tests shows clearly that the top of the surface roughness are the first to contact with the pin surface. It can be seen how asperities are flattened out to create a larger oxidised contact area. The oxide then is growing and becoming larger until it breaks from the surface.

The EDS analysis shows a higher content of Si and Mn compared to the surface of the disc. This means that observed material on surface of a disc is coming from the pin. The second observation of EDS is high amount of oxygen on the wear track, which confirms an oxide layer on the disc surface. The EDS analyse can be seen in Appendix D.

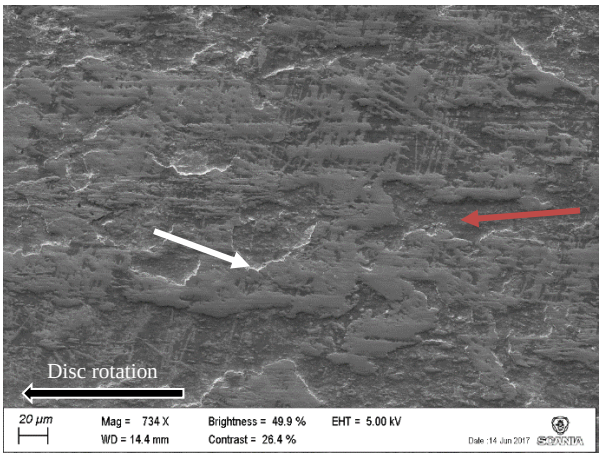

Figure 57. Disc of test 22, 3m/s High load HT. White arrow show brittle oxide layer. Red arrow pointing on original surface.

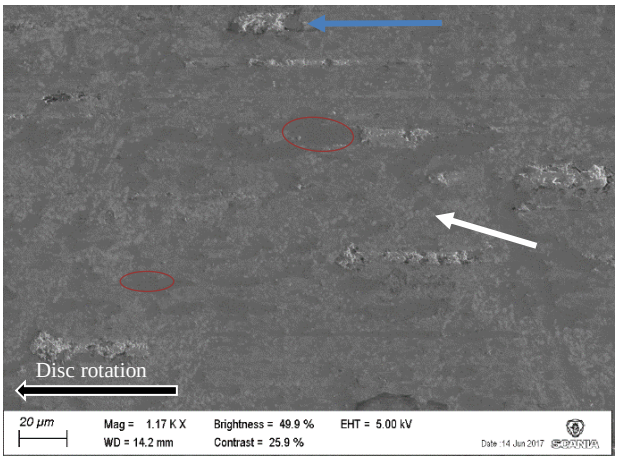

Figure 58. Disc of test 19. 3 m/s High load RT. Oxide layer appears as darker surface (red rings). White arrow shows a broken oxide layer. Blue arrow shows an embedded particle.

Hardness of discs have been measured before and after the tests. The hardness of discs has not changed even after HT tests, but the hardness of oxide-layer is a bit harder compare to original material hardness. The original measurements of tool steel give hardness 640-680 $HV_{0.025}$. It is hard to measure but after HT tests the oxide layers have hardness of 800 $HV_{0.025}$. Measurements of disc hardness can be seen in Appendix C.

Measurement of existing wear track show an insignificant wear compare to the pin (soft material). It is known that in the turbochargers harder ring have higher wear compare to the soft shaft. The effect of higher wear rate of the harder material is not observed in the tribological tests. The results of mass loss of material on pin and disc, where it could be measured, is shown in Figure 59 and standard deviation value in shown in Appendix B.

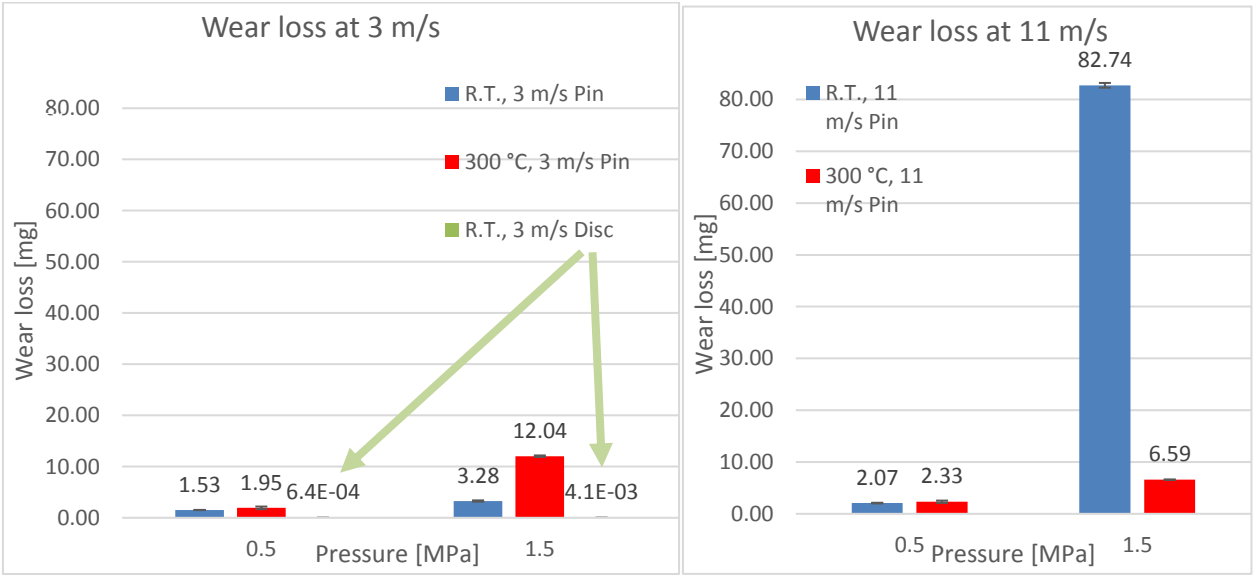

Figure 59. The wear loss of pins and discs in mg for all conditions.

Tribological tests show a higher wear rate of softer material. The reason for the different wear behaviours between turbocharger and tribological experiments may be due to different conditions in the experiments. The first reason is limitations in this project: the sliding speed is not high enough and the duration of the test may be too short. The second reason is pins surface is always in contact, but the surface of the disc is not in contact the whole time. This gives the opportunity for surface to cool down.

The lubricant conditions are different between turbocharger and tribological tests that were performed. The parts in turbocharger have been showed to contain remains of the oil. The tribological tests are performed in dry conditions. Another difference is that the tight space in turbocharger lead to accumulation of debris in contact area.

The debris in turbocharger contained oil contaminants. It is mentioned above that high speed tests moved the pin material to the surface of the disc. The EDS of discs (Appendix D) showed a high oxygen rate on the surface, especially high temperature. The wear of pins is decreasing with higher speed at high temperatures. This can occurred because of time to weld the pin to the disc.

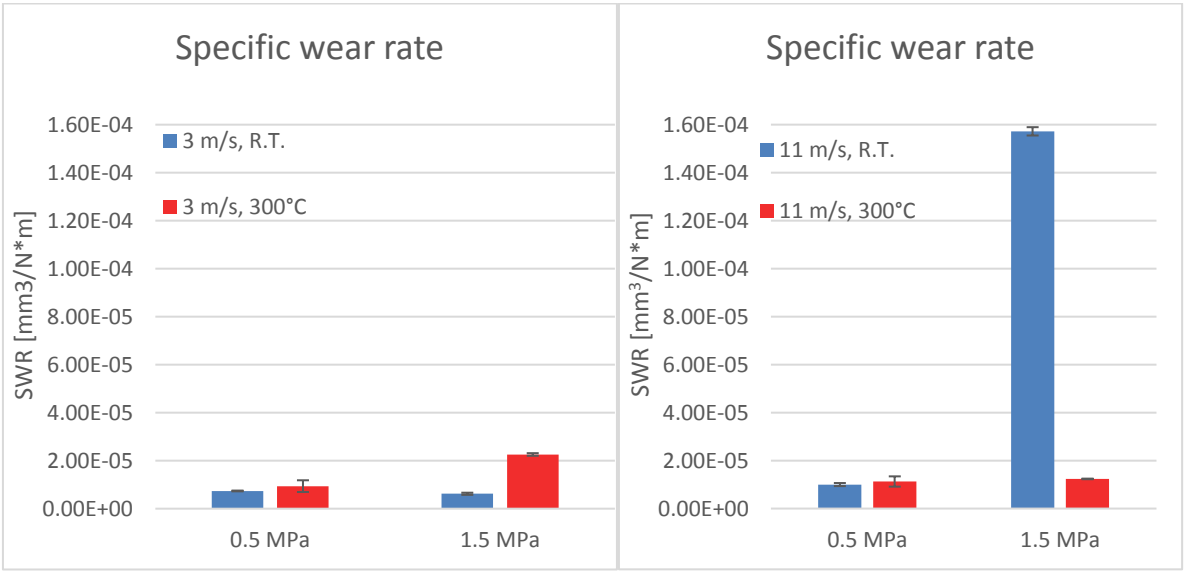

Figure 60. Result of specific wear rate.

The specific wear rates for the pin specimens are shown in Figure 60. The wear results show that the wear rate is reduced when the load is increased at low speed and low temperature. At high speed and low temperature, the pin wear rate increased by one order of magnitude. Under high speed, high temperature an increase in load did not affect the wear rate. Under constant load and speed, an increase in temperature led to an increase in wear rate. Speed did not affect the wear behaviour extensively at low loads but at high loads and high temperature a significant reduction of the wear rate was observed for high speed.

The worn surface of the pin is covered by an oxide layer, see EDS in Figure 54. The oxide layer is observed on all tests. At low temperature tests oxide layer is less brittle and have more continuous surface. The difference can be seen in Figure 61 and Figure 62, or Figure 63 and Figure 64.

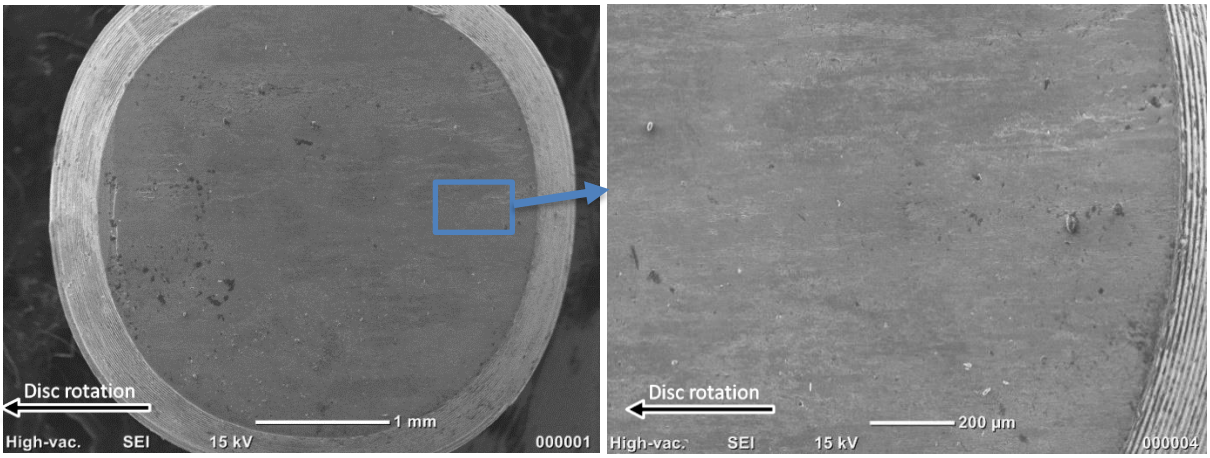

Figure 61. SEM picture of pin test 7, high speed low load RT.

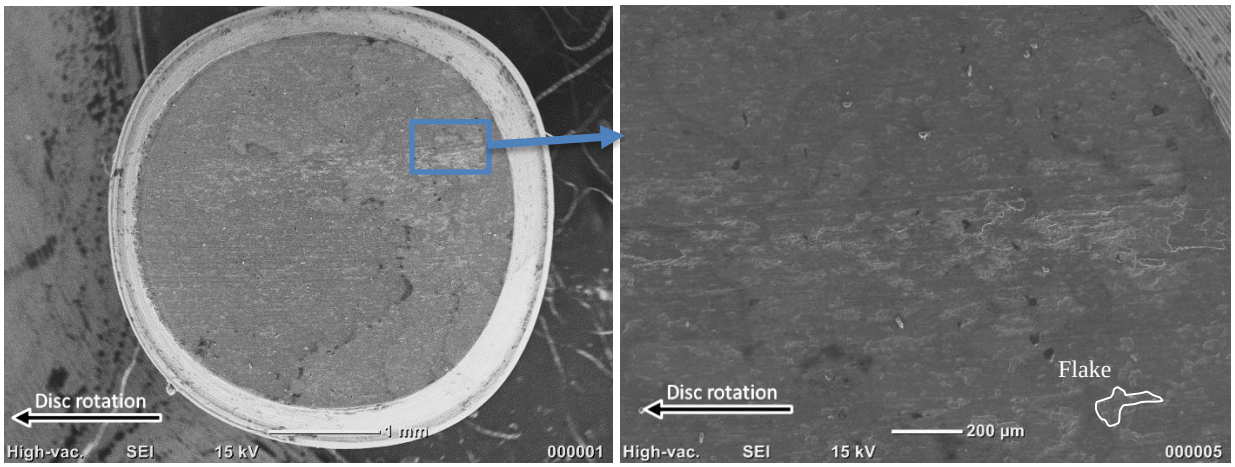

Figure 62. SEM picture of pin worn surface after test 20 at low speed low load HT.

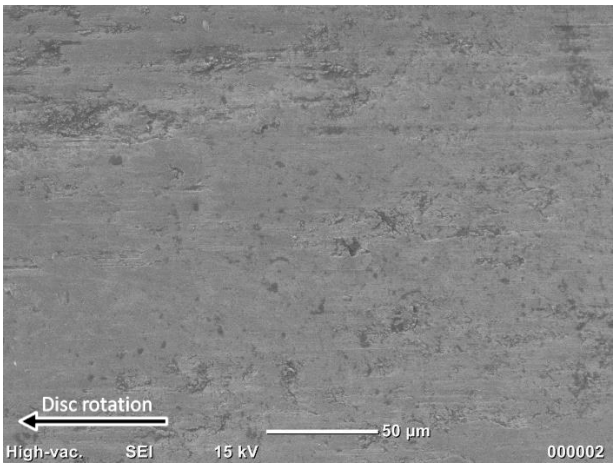

Figure 63. SEM picture of pin worn surface after test 7, high speed low load RT.

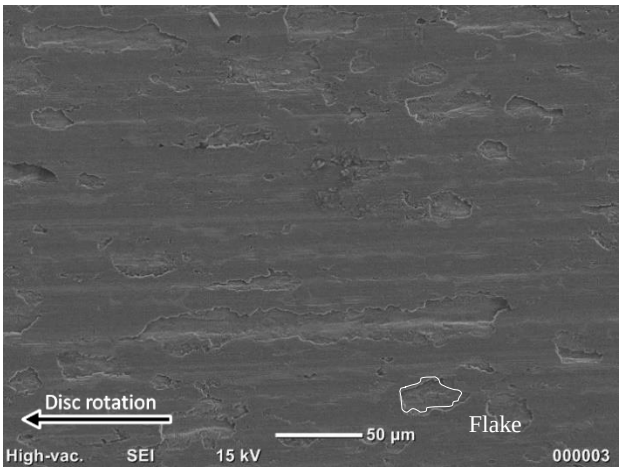

Figure 64. SEM picture of pin worn surface after test 20, low speed low load HT.

At low speeds and low loads adhesive wear is dominant. The surface is more continuous and have no flakes, like the one marked with white in Figure 64. With increased temperature flakes are more common. The oxide layers created after high temperature tests in average tend to be harder than the RT tests, 740HV_{10} HT against 570HV_{10} for RT tests. The hardness measurement itself varies a lot because of the inhomogeneous tribolayer. This gives a conclusion that the oxide layer is more brittle with higher temperature. Increased speed has a big influence on size of the flakes. Flakes are much larger, see Figure 65.

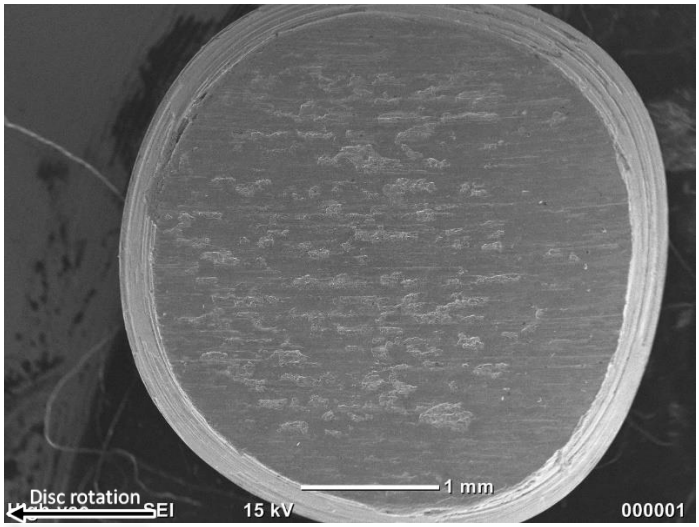

Figure 65. SEM image of surface of the pin after test 27, high speed high load HT.

A cross-section view of the pins have showed an orientation of grains within the material. The orientation is observed both along and across of sliding direction, see Figure 66 and Figure 67. An angle of orientation showed in Figure 66 varies with the load. Figure 67 demonstrates an image of a pin at high speeds, where no wear of the disc is observed. The material moves from the surface of the pin to the surface of the disc. The current view shows a grain orientation to the point where original pin surface contacts the disc. This means that the oxide layer prevent extensive adhesive wear.

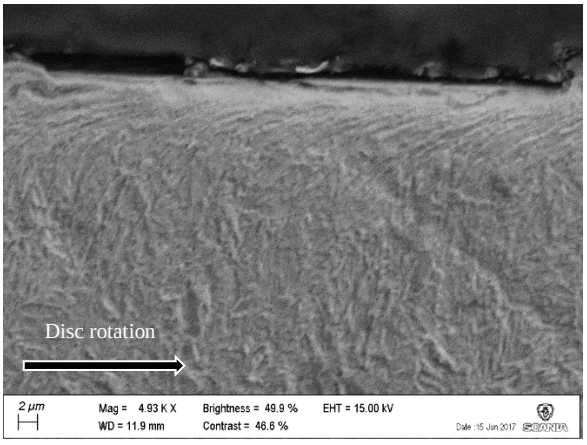

Figure 66. SEM image of cutting view along sliding direction of the pin test 5, low speed low load RT.

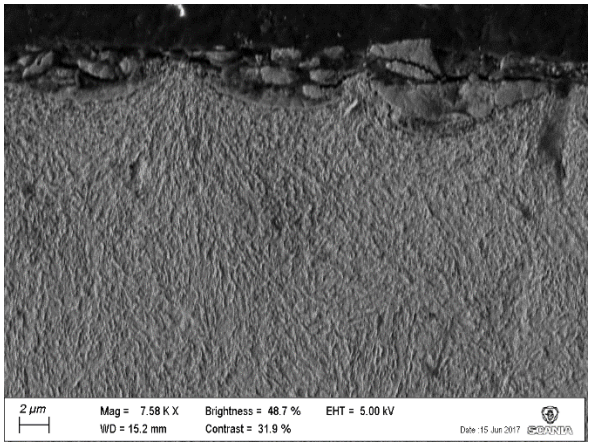

Figure 67. SEM image of cutting view across sliding direction of the pin test 26, high speed high load HT.

There has been research about how the content of hard carbides in tool steel affect the adhesive wear resistance [34]. The tests showed that the carbide content and the distance between carbides have a considerable influence on wear resistance against adhesive wear. The optimum of the carbide state theoretically should be about 21vol% but the test result showed the best resistance achieved at 16vol%.

The wear of high speed and low temperature with high pressure have a significantly lager wear rate than other conditions. It is mentioned above that wear debris are observed during this particular condition. The same behaviour has been observed before. Wear resistance of materials decrease rapidly when certain levels of pressure, speed and temperature are achieved [35]. The breaking point of ring material may be achieved in the turbocharger. The shaft is cooled by the supply of oil to the thrust bearing which gives the ring a possibility to reach a much higher temperature. The difference in conditions may affect the wear in such way that the harder material of the sealing ring is easier to wear than the softer shaft. The cracks observed on sealing rings are larger than the shafts which proves that the rings may have e.g. much higher thermal stresses than the shaft.

Analyse of field data

During the project, the correlation between truck usage and sealing ring wear was studied. The parameters which are analysed are mileage, number of km in high load, number of km during exhaust brake and number of gearshifts. The result showed that there is no clear dependency for neither of those parameters, for an example see mileage in Figure 68.

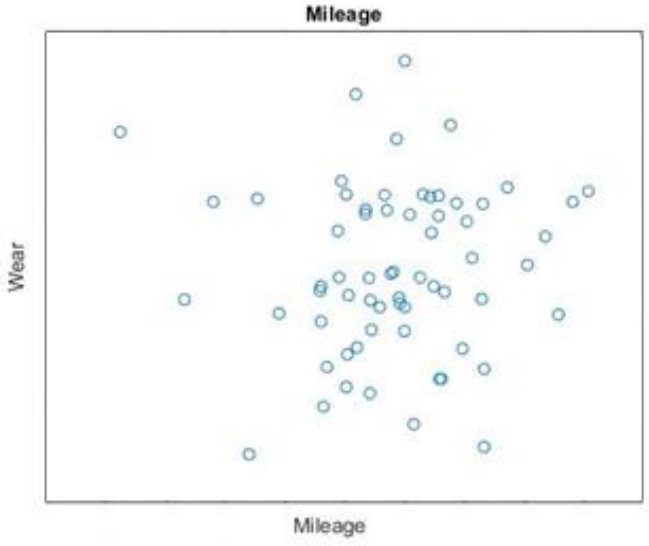

Figure 68. Wear of inner sealing ring in customer trucks.

The customers are using trucks in various conditions with different loads applied on engine. A filter was created to narrow the usage of the engine to choose trucks with similar load conditions. The available data supplied as a matrix, where it is available percentage of mileage at specific engine load at each engine RPM span. The filter was designed to calculate total percentage at each engine load, neglecting the RPM. The average use of trucks at each engine load is calculated (average along vertical line in Figure 69). Then the average value is multiplied with a value to get the upper and lower limit of engine use. An example of boundary conditions can be seen in Figure 69. The values in the Figure 69 are representative.

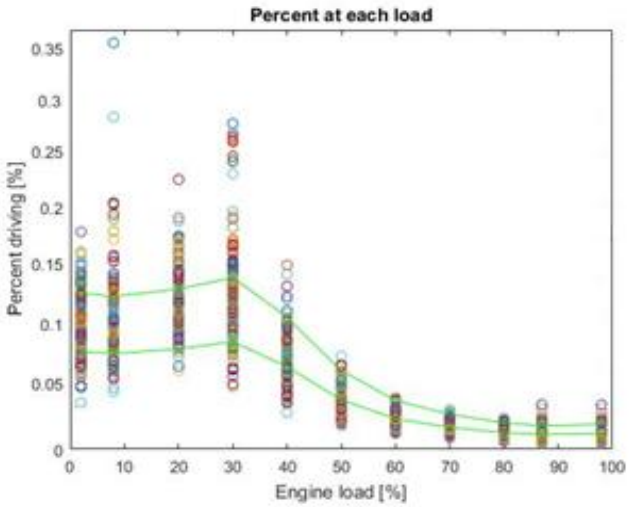

Figure 69. The dots represent engine use at each engine load and the green line show the conditions of average use with 23% margin.

The same method is applied for engine revolution by neglecting the engine load. The data of wear of inner sealing ring and mileage is taken from the selected trucks. The result from filtering by revolution didn't showed any pattern, but the 10 trucks selected with similar engine load conditions may follow a linear pattern, see Figure 70.

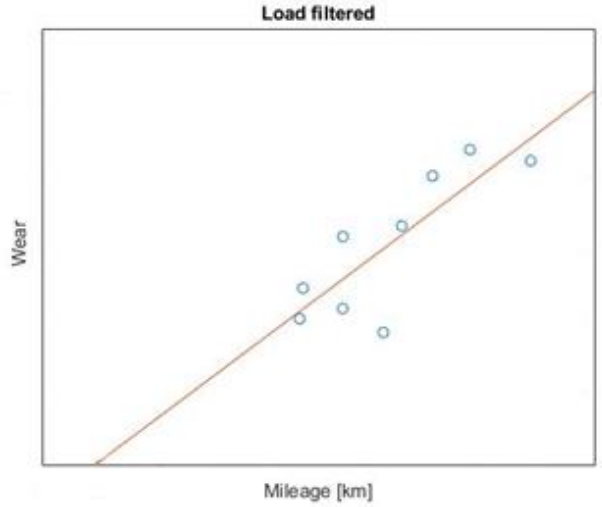

Figure 70. The trucks filtered by engine load conditions.

The result represents the average load conditions. A further investigation of different load conditions showed that there is a possible dependency between mileage and wear. Same load conditions are critical to confirm the wear prediction. The revolution of the engine has not the same influence on the sealing rings wear.

The study is performed on a few trucks. A mechanical condition in the turbocharger, provides an inaccuracy in the linear models. Different load conditions show a linear dependency as well.

4.3 Suggestions for improved durability of sealing rings

The durability of the sealing rings can be improved by several methods. Here it is discussed to change the material or operating condition. The change of material is possible. An alternative material should be resistant to higher temperatures than the sealing rings material. The tool steel that is used today uses Fe matrix with hard tungsten carbides. The carbides can potentially be removed from matrix before they were worn out. The cracks through tungsten carbides show that the carbides may be to brittle for this kind of conditions.

The second possible improvement is changing the working conditions. During the tribological experiments it was found that materials have breaking points due to conditions [35]. There is a specific combination of contact pressure, sliding velocity, temperature and lubricant that gives the highest wear rate. The wear resistance may decrease with higher value of for example pressure. A smaller diameter could be an option to reduce the sliding speed between the surfaces in the future turbocharger.

There can be several methods to reduce the contact pressure. For example, a larger contact area is the most straight forward way to bring down the contact pressure. The problem is that the blow by may increase because of the unsealed contact. A geometry of least efficient flow can be applied to decrease the blow by.

There is a possibility to reduce the pressure over sealing rings is by creating cuttings on the shaft, turbo wheel or cuttings on the bearing house to push the gases away from sealing rings. The gases are moving at the same rotational speed of the shaft which means that a specially formed stationary heat shield may decrease the pressure near the sealing rings. This decrease the contact pressure and may decrease the temperature as well. The thermal problem of relaxation of the ring and wear of the ring is main mechanisms of increased blow by.

The improvement of turbocharger and sealing rings performance can be improved by implementing a ball bearing design. It is decreasing frictional losses up to 50% [36] and increase durability of the sealing rings. With improvement of this technology a turbocharger can decrease pollution and increase durability of heavy duty diesel engines.

5. Conclusions

From the results that are presented in chapter 4.1, the plastic deformation of shafts worn surfaces are showing that there was high friction between the sliding surfaces. The friction, is in turn influenced by high contact pressure between the sliding surfaces in turbocharger components. Both the turboshafts and the turbo sealing rings in turbochargers are made of steel.

Steel has good material properties at high pressure and high temperatures and it is probably one of the main reasons why sealing rings and shafts were made of this material. When two surfaces that are made of same materials and sliding against each other, generally high friction generates which in turn leads to high adhesive wear.

Both the sealing rings and shafts from the turbochargers that were analysed in chapter 4.1 are showing that there was both adhesive and abrasive wear on the worn surfaces. The worn surfaces of shafts were plastically deformed, while on the worn surfaces of the sealing rings was a network of small cracks perpendicular to the sliding direction, these small cracks are from the high friction generation and contacting pressure between the sliding surfaces, by rapidly changing the driving conditions then the friction and pressure between sliding surfaces in turbochargers, suddenly change. The sudden changing of friction and pressure between the sliding surfaces due to different driving conditions then the sliding surfaces temperature also suddenly is changing which in turn leads to thermal fatigue cracks of the sealing rings worn surfaces.

The tribo-tests in chapter 4.2 are also showing the presence of plastic deformation on the worn surfaces of the pins, which are made of the same material as turbocharger shafts. The plastic deformation of the material shows also a presence of high adhesive friction due to the high contacting pressure.

The pins and the disc from the tribo-tests both show adhesive and abrasive wear. An oxide layer was observed which varies with the operating conditions. The tool steel in some conditions did not show any wear. There were not any thermal fatigue cracks on the worn surfaces from the tribo-tests components, probably because there was not any sudden increase or decrease in the surface temperature.

One of the main parameters that is influencing the damage of the turbocharger sealing rings and shafts is the high contact pressure that arises during exhaust braking and high engine load. During tribological tests it was confirmed that the breaking point of material can be achieved by increasing pressure only.

To minimize the contact pressure between the inner sealing rings and shafts the geometry of the sealing rings and shafts can be changed by having a larger contact area between the components. In this way, the pressure would probably have a lower influence on the lifetime of the turbocharger components. To minimize the high friction and high adhesive wear, the turbocharger sealing rings can be made of other material, for example, materials that can better resist to relaxation and the high temperatures from the exhaust gases and temperature from the high exhaust gas pressure in turbine house. For example, the rings can be made of such called nickel superalloys.

6. Future work

More measurements of working conditions of sealing rings can be performed. It is crucial for further research that the conditions are known. Measurements of pressure between sealing ring or movement of sealing rings are needed for better evaluation of wear and friction. A measurement of friction force between sealing ring and bearing house at high temperatures can be made. This measurement will help to understand the contact pressure, which is estimated by calculation today. The temperature of the sealing is to be estimated or measured. Several tests can be performed with both higher and lower carbide content to estimate wear rate of the material in a turbocharger.

The future tribological tests can be performed on ring-on-ring contact. This will eliminate a cooling cycle for the disc material. A temperature measurement of sealing rings combined with ring-on-ring contact may better recreate the wear cycle in the actual turbocharger. This will give a possibility to estimate breaking point for tool steel. This may give a possibility to explain why a harder material is worn more than a soft material.

A continuous work on wear model to estimate a wear dependency on different parameters. A filter for available wear data that is taking into account a turbocharger performance instead of engine performance, which was performed in this project. It may show the influence of driving on wear behaviour of the rings.

7. Acknowledgements

This master thesis was done in collaboration between Lulea University of Technology and Scania. The work was done for Scania, but the largest period of the time the work was done at Lulea University of Technology. The work comprises a 20 weeks' fulltime work and was done during the spring semester 2017 at Lulea University of Technology.

We want to thank Jens Hardell from the Division of Machine Elements at Lulea University of Technology. Jens was our supervisor and examiner and he assisted with a lot of help and knowledge during this thesis time. Jens helped a lot to choose the right analysis methods and even with the examination of the components. As well we want to thank Madeleine Ekström our supervisor from Scania. Madeleine helped a lot with material data from trucks and even knowledge about the driving conditions of diesel engines turbochargers.

We would also thank Pouria Valizadeh Moghaddam for his help in tribology lab. Thanks to Leonardo Pelcastre, Lars Hammerström and the NMGG department for their help during the project.

8. References

1. BHUSHAN, Bharat. *Introduction to tribology*. John Wiley & Sons, 2013.
2. GODFREY, Douglas. Friction oscillations with a pin-on-disc tribometer. *Tribology International*, 1995, 28.2: 119-126.
3. Burwell, John T. "Survey of possible wear mechanisms." *Wear* 1.2 (1957): 119-141.
4. Van Beek, Anton. "Advanced engineering design." *TU Delft, Delft, The Netherlands* (2006).
5. Hurricks, P. L. "Some metallurgical factors controlling the adhesive and abrasive wear resistance of steels. A review." *Wear* 26.3 (1973): 285-304.
6. Hardell, Jens, and Braham Prakash. "High-temperature friction and wear behaviour of different tool steels during sliding against Al–Si-coated high-strength steel." *Tribology International* 41.7 (2008): 663-671.
7. Runkle, Joseph C. "Method for making tool steel with high thermal fatigue resistance." U.S. Patent No. 5,290,507. 1 Mar. 1994.
8. Roberts, George Adam, Richard Kennedy, and George Krauss. *Tool steels*. ASM international, 1998.
9. Eyre, T. S. "Wear characteristics of metals." *Tribology International* 9.5 (1976): 203-212.
10. Neale, Michael, and Mark Gee. *A Guide to Wear Problems and Testing for Industry*. William Andrew, 2001.
11. Williams, John. *Engineering tribology*. Cambridge University Press, 2005.
12. Stott, F. H. "High-temperature sliding wear of metals." *Tribology International* 35.8 (2002): 489-495.
13. Soemantri, Satryo, A. C. McGee, and Iain Finnie. "Some aspects of abrasive wear at elevated temperatures." *Wear* 104.1 (1985): 77-91.
14. Quinn, T. F. J. "Oxidational wear modelling: Part II. The general theory of oxidational wear." *Wear* 175.1-2 (1994): 199-208.
15. Quinn, T. F. J. "Oxidational wear." *Wear* 18.5 (1971): 413-419.
16. Waterhouse, R. B., and D. E. Taylor. "Fretting debris and the delamination theory of wear." *Wear* 29.3 (1974): 337-344.
17. Quinn, T. F. J. "Oxidational wear modelling: I." *Wear* 153.1 (1992): 179-200.
18. Blau, Peter J. "Elevated-temperature tribology of metallic materials." *Tribology international* 43.7 (2010): 1203-1208.
19. Dohda, Kuniaki, et al. "Tribology in metal forming at elevated temperatures." *Friction* 3.1 (2015): 1-27.
20. Ganesan, V. *Internal combustion engines*. McGraw Hill Education (India) Pvt Ltd, 2012.
21. Gjika, Kostandin, L. San Andrés, and G. D. Larue. "Nonlinear dynamic behavior of turbocharger rotor-bearing systems with hydrodynamic oil film and squeeze film damper in series: prediction and experiment." *Journal of Computational and Nonlinear Dynamics* 5.4 (2010): 041006.
22. FERGUSON, Colin R.; KIRKPATRICK, Allan T. *Internal combustion engines: applied thermosciences*. John Wiley & Sons, 2015.

23. FABIŚ-DOMAGAŁA, Joanna. FMEA analysis of potential failures of turbochargers for combustion engines by the use of the simularity method. *Czasopismo Techniczne*, 2015.
24. SAN ANDRES, Luis; KERTH, Jason. Thermal effects on the performance of floating ring bearings for turbochargers. *Proceedings of the Institution of Mechanical Engineers, Part J: Journal of Engineering Tribology*, 2004, 218.5: 437-450.
25. HOWARD, Samuel A. Rotordynamics and Design Methods of an Oil-Free Turbocharger©. *Tribology transactions*, 1999, 42.1: 174-179.
26. BORICEAN, C. C.; RADU, Gh A. Diesel engine turbochargers: analysis and testing. *Bulletin of the Transilvania University of Brasov, Series I: Engineering Sciences*, 2012, 5.1.
27. KOUTSOVASILIS, P.; DRIOT, N. Turbocharger rotors with oil-film bearings: Sensitivity and optimization analysis in virtual prototyping. In: *Proceedings of the 11th International Conference on Vibrations in Rotating Machines, Wiesbaden, Germany*. 2015. p. 23-25.
28. KNOTEK, J., et al. Influence of Turbine and Compressor Wheel Mass and Inertia on the Rotor Dynamics of Turbocharger. *Tribology in Industry*, 2016, 38.1.
29. ΜΠΌΜΠΟΣ, Δημήτριος. *Tribological design of nano/magnetorheological fluid journal bearings*. 2016. PhD Thesis.
30. Tanimoto, K., Kajihara, K. and Yanai, K., 2000. Performance of hybrid ceramic ball bearing for turbochargers. *Koyo Engineering Journal*, *157*, pp.21-31.
31. ZEPPEI, Dieter; KOCH, Silvio; ROHI, Amir. Ball Bearing Technology for Passenger Car Turbochargers. *MTZ worldwide*, 2016, 77.11: 26-31.
32. Persson, Anders, Sture Hogmark, and Jens Bergström. "Thermal fatigue cracking of surface engineered hot work tool steels." *Surface and Coatings Technology* 191.2 (2005): 216-227.
33. Garza-Montes-de-Oca, N.F. and Rainforth, W.M., 2009. Wear mechanisms experienced by a work roll grade high speed steel under different environmental conditions. *Wear*, *267*(1), pp.441-448.
34. Fontalvo, G.A., Humer, R., Mitterer, C., Sammt, K. and Schemmel, I., 2006. Microstructural aspects determining the adhesive wear of tool steels. Wear, 260(9), pp.1028-1034.
35. So, H., 1996. Characteristics of wear results tested by pin-on-disc at moderate to high speeds. *Tribology international*, *29*(5), pp.415-423.
36. MILLER, Jay K. *Turbo: Real world high-performance turbocharger systems*. CarTech Inc, 2008.

9. Appendix

A. Tribological conditions for each test

Cold tests					Warm tests				
	test_1	test_2	test_3	test_4		test_14			
Distance [m]	3000	6000	6000	6000	Distance [m]	6000			
Rotational speed [RPM]	1900.0	1500.0	1239.1	1583.3	Rotational speed [RPM]	1910			
Diameter [mm]	30	38	46	54	Diameter [mm]	110			
1 rev [m]	0.094248	0.11938	0.144513	0.169646	1 rev [m]	545.4			
Distance per minut [m/min]	179.07	179.07	179.07	268.61	Distance per minut [m/min]	11.0			
Duration of the test [sec]	1005.19	2010.379	2010.379	1340.252	Duration of the test [sec]	0.9			
Relativ speed	2.98	2.98	2.98	4.48	Relativ speed	17362.36			
Total number of revolution	31831	50259	41519	35368	Total number of revolution				
Load [kg]	0.7	0.7	1.2	0.7	Load [kg]	0.9			
Disc nr_side	prov	prov	prov	prov	Disc nr_side	prov			
	test_5	test_6	test_7	test_8		test_20	test_21	test_22	test_23
Distance [m]	6000	6000	6000	6000	Distance [m]	6000	6000	6000	6000
RPM	1910	1193.662	1910	1910	RPM	1194	1194	1194	1194
Diameter wear track [m]	30	48	110	110	Diameter wear track [m]	48	48	48	48
Duration of the test [sec]	1999.9	2000.0	545.4	545.4	Duration of the test [sec]	1999.4	1999.4	1999.4	1999.4
Relative speed [m/s]	3.0	3.0	11.0	11.0	Relative speed [m/s]	3.0	3.0	3.0	3.0
Load [kg]	0.2	0.2	0.2	0.2	Load [kg]	0.2	0.2	0.9	0.9
Total number of laps	63662	39789	17362	17362	Total number of laps	39789	39789	39789	39789
Disc nr_side	1_1	1_1	1_1	1_2	Disc nr_side	1a_1	2a_1	3a_1	4a_1
	test_9	test_10	test_11	test_12		test_24	test_25	test_26	test_27
Distance [m]	6000	6000	6000	6000	Distance [m]	6000	6000	6000	6000
RPM	1910	1910	1194	1910	RPM	1910	1910	1910	1910
Diameter wear track [m]	110	30	48	30	Diameter wear track [m]	110	110	110	110
Duration of the test [sec]	545.4	1999.9	1999.4	1999.9	Duration of the test [sec]	545.4	545.4	545.4	545.4
Relative speed [m/s]	11.0	3.0	3.0	3.0	Relative speed [m/s]	11.0	11.0	11.0	11.0
Load [kg]	0.9	0.9	0.9	0.2	Load [kg]	0.2	0.2	0.9	0.9
Total number of laps	17362	63662	39789	63662	Total number of laps	17362	17362	17362	17362
Disc nr_side	2_1	2_1	2_1	3_1	Disc nr_side	2a_2	1a_2	3a_2	4a_2
	test_13		test_15	test_16		test_28	test_29		
Distance [m]	6000		6000	6000	Distance [m]	6000	6000		
RPM	1910		1910	1910	RPM	1910	1910		
Diameter wear track [m]	110		30	30	Diameter wear track [m]	110	110		
Duration of the test [sec]	545.4		1999.9	1999.9	Duration of the test [sec]	545.4	545.4		
Relative speed [m/s]	11.0		3.0	3.0	Relative speed [m/s]	11.0	11.0		
Load [kg]	0.9		1.1	1.1	Load [kg]	0.2	0.2		
Total number of laps	17362		63662	63662	Total number of laps	17362	17362		
Disc nr_side	3_1		1a_2	3a_2	Disc nr_side	1a_1	2a_1		
	test_17	test_18	test_19						
Distance [m]	6000	6000	6000						
RPM	1910	1910	1194						
Diameter wear track [m]	30	110	48						
Duration of the test [sec]	1999.9	545.4	1999.4						
Relative speed [m/s]	3.0	11.0	3.0						
Load [kg]	1.1	0.2	0.9						
Total number of laps	63662	17362	39789						
Disc nr_side	5_1	5_1	5_1						

B. Wear data from tribological experiments

The wear data collected during the tribological testing is shown in Table 3. Each test has a test number and a condition at which it was running. A wear loss of the pin is calculated by weighing pins before and after the test. Wear loss of the disc is estimated with 3D-surface measurement. The measurements calculate a worn volume on the disc surface which gives an information about worn mass. Friction coefficient consist of calculated average of levelled out friction coefficient measured during each test. Specific wear rate (SWR) is calculated by formula

$$SWR = \frac{Wear\ volume}{Normal\ load * Sliding\ distance}.$$

Calculated average of wear, friction coefficient and standard deviation for each wear conditions (Table 4) are shown in Table 5 and Table 6. A density of carbon and tool steel used in calculations is 7900 kg/m^3.

Table 3. Wear data sampled from each tribological test.

Test NR	Conditions				Weigth loss		Friction coefficient	SWR Pin
	Speed [m/s]	Diameter [mm]	Distance [m]	Pressure [MPa]	Pin [mg]	Disc [mg]	[-]	[m^3/N*m]
RT								
5	3	30	6000	0.5	1.48	7.21E-04	0.546	7.16E-15
6	3	48	6000	0.5	1.58	5.51E-04	0.511	7.61E-15
7	11	110	6000	0.5	1.91		0.394	9.23E-15
8	11	110	6000	0.5	2.38		0.396	1.15E-14
9	11	110	6000	1.5	84.03		0.439	1.60E-13
10	3	30	6000	1.5	2.65	4.25E-03	0.599	5.03E-15
11	3	48	6000	1.5	3.17	3.68E-03	0.598	6.02E-15
12	3	30	6000	1.5	3.56	2.47E-03	1.453	6.76E-15
13	11	110	6000	1.5	81.45		0.420	1.55E-13
18	11	110	6000	0.5	1.93		0.397	9.31E-15
19	3	48	6000	1.5	3.75	6.19E-03	0.558	7.04E-15
HT								
20	3	48	6000	0.5	1.23		0.402	5.94E-15
21	3	48	6000	0.5	2.66		0.375	1.28E-14
22	3	48	6000	1.5	12.45		0.404	2.34E-14
23	3	48	6000	1.5	11.62		0.427	2.18E-14
24	11	110	6000	0.5	1.71		0.313	8.24E-15
25	11	110	6000	0.5	2.96		0.403	1.43E-14
26	11	110	6000	1.5	6.49		0.195	1.22E-14
27	11	110	6000	1.5	6.68		0.209	1.25E-14
28	11	110	6000	0.5	4.81		0.223	2.32E-14
29	11	110	6000	0.5	2.73		0.237	1.32E-14

Table 4. Eight conditions at which tribological wear tests were performed.

Wear condition	Temperature	Speed	Diameter	Distance	Pressure	Load
NR	[°C]	[m/s]	[mm]	[m]	[MPa]	[kg]
1	25	3	30-48	6000	0.5	0.2
2	25	3	30-48	6000	1.5	0.9
3	25	11	110	6000	0.5	0.2
4	25	11	110	6000	1.5	0.9
5	300	3	48	6000	0.5	0.2
6	300	3	48	6000	1.5	0.9
7	300	11	110	6000	0.5	0.2
8	300	11	110	6000	1.5	0.9

Table 5. The calculated average value at each tribological wear condition.

Wear condition	Mean value			
	Pin	Disc	Friction	Pin SWR
NR	[mg]	[mg]	coefficient	[mm^3/N*m]
1	1.53	6.36E-04	0.53	7.39E-06
2	3.28	4.15E-03	0.59	6.21E-06
3	2.07		0.40	1.00E-05
4	82.74		0.43	1.57E-04
5	1.95		0.39	9.40E-06
6	12.04		0.42	2.26E-05
7	2.33		0.36	1.13E-05
8	6.59		0.20	1.24E-05

Table 6. Calculated standard deviation of average value at each tribological wear condition.

Wear condition	Standard deviation			
	Mass pin	Mass Disc	Friction	Pin SWR
NR	[mg]	[mg]	coefficient	[mm^3/N*m]
1	0.03	6.01E-05	0.01	1.61E-07
2	0.24	7.75E-04	0.01	4.50E-07
3	0.13		0.00	6.40E-07
4	0.91		0.01	1.73E-06
5	0.51		0.01	2.44E-06
6	0.29		0.01	5.48E-07
7	0.44		0.03	2.15E-06
8	0.07		0.00	1.23E-07

C. Disc hardness measurement

The hardness of discs is taken before and after tribological tests. Four hardness measurements are performed at randomly selected discs at random places before tests. After the HT tests the hardness of discs surface taken on three discs at three randomly selected places, see Table 7. Hardness measurements of wear track after the tests can be seen in Table 8. The measurement is taken on brittle oxide layer which in some cases broke during the measurement.

Table 7. Hardness of disc tool steel material.

	All measurements in $HV_{0.025}$			
Original discs	688	647	672	672
Disc 1a	672	672	549	
Disc 2a	642	633	672	
Disc 3a	633	683	672	

Table 8. Hardness measurement of disc wear tracks after performed tribological test.

Test NR	All measurements in $HV_{0.025}$				Mean value	STD
5	633	619	642	647	635	12
6	652	667	652	652	656	8
7	496	483	503	493	494	8
8	580	576	638	593	597	28
9	683	683	638	693	674	25
10	642	615	624	610	623	14
17	783	775	801	763	781	16
18	704	683	693	672	688	14
20	815	843	788	937	846	65
21	829	775	858	715	794	63
22	683	1008	858	904	863	136
23	858	801	788	801	812	31
24	888	815	815	693	803	81
25	1047	872	815	971	926	103
26	1027	788	662	715	798	161
27	1252	801	954	843	963	204
28	704	888	872	937	850	101
29	920	801	750	715	797	90

D. EDS analysis of disc surface

The EDS analysis have been performed on the discs. To perform the analyse discs were cut along wear track. The cut surface was polished and cleaned with acetone. Further it was taken pictures of the cut surface in SEM with 30 kV, see in Table 9. The EDS analyse is performed at two points to compare a content of material.

Table 9. Cutting view of Disc 3a test 22, 3m/s high load HT.

Spectrum 1

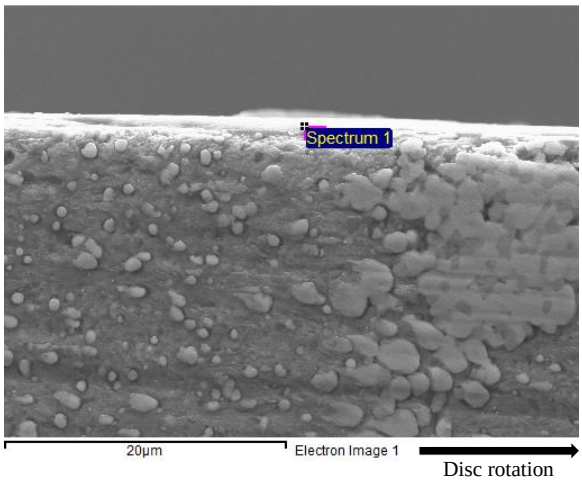

Element	Weight%	Atomic%
C K	46.03	28.90
O K	84.16	39.67
V K	6.70	0.99
Cr K	11.77	1.71
Fe K	195.17	26.35
Mo L	17.65	1.39
W M	24.46	1.00
Totals	385.93	

Spectrum 3

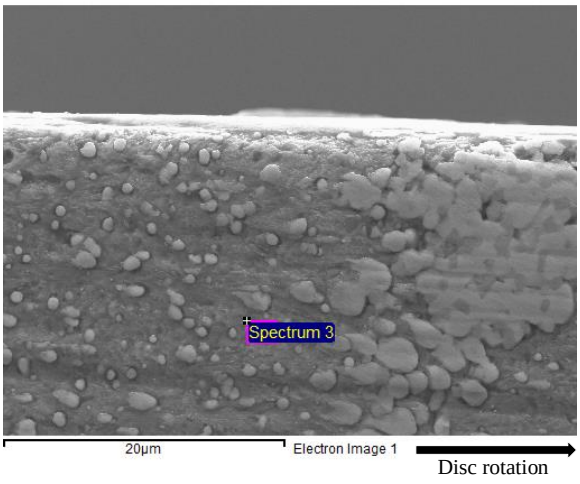

Element	Weight%	Atomic%
C K	71.95	37.84
O K	9.89	3.91
V K	10.22	1.27
Cr K	25.42	3.09
Mn K	2.44	0.28
Fe K	450.19	50.92
Mo L	24.37	1.60
W M	32.05	1.10
Totals	626.54	

Additional EDS analyse is performed on the surface of the disc where a wear track is created. The test focus on analysing the content of material that have been applied to the surface of the disc. The EDS performed at three different point to be able to confirm the difference in content, see Table 10. The analyse is performed at 30kV.

Table 10. EDS analysis of surface of the disc test 24, High speed Low load HT.

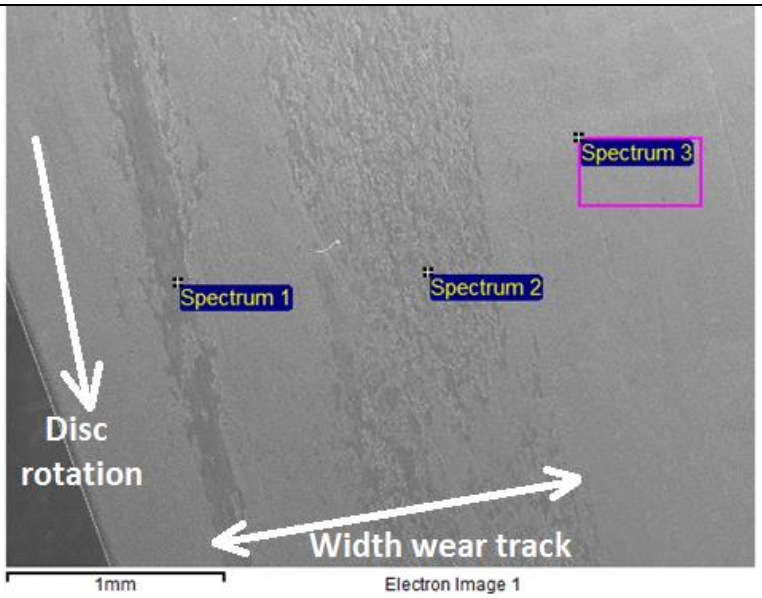

Spectrum	In stats.	C	O	Si	V	Cr	Mn	Fe	Mo	W	Total
Spectrum 1	Yes	16.11	147.39	1.24	0.90	5.13	1.93	241.37			414.0
Spectrum 2	Yes	16.99	129.23	0.79	1.21	5.00	1.26	192.46	3.59	3.03	353.5
Spectrum 3	Yes	31.80	17.34		6.09	10.18		166.57	15.37	24.06	271.4
Max.		31.80	147.39	1.24	6.09	10.18	1.93	241.37	15.37	24.06	
Min.		16.11	17.34	0.79	0.90	5.00	1.26	166.57	3.59	3.03	

All results in weight%

E. Hardness measurements across cross-section of turbocharger components.

In Figure 71 are the hardness values measurements of used shafts.

a)

depth	Value 1	value 2	value3	average	STD
10	440	443	443	442	1,732051
20	443	435	443	440,3333	4,618802
30	435	435	443	437,6667	4,618802
40	426	411	419	418,6667	7,505553
50	430	445	435	436,6667	7,637626
60	426	419	418	421	4,358899
70	418	426	381	408,3333	24,00694
80	388	394	410	397,3333	11,37248
90	409	404	410	407,6667	3,21455
100	406	409	409	408	1,732051

b)

depth	value1	value2	value3	average	STD
10	435	435	427	432,3333	4,618802
20	426	426	438	430	6,928203
30	429	432	424	428,3333	4,041452
40	420	400	420	413,3333	11,54701
50	414	419	419	417,3333	2,886751
60	409	419	405	411	7,211103
70	409	409	404	407,3333	2,886751
80	403	415	411	409,6667	6,110101
90	404	405	411	406,6667	3,785939
100	414	409	405	409,3333	4,50925

c)

depth	value 1	value 2	value 3	average	STD
10	435	426	426	429	5,196152
20	420	426	418	421,3333	4,163332
30	418	420	418	418,6667	1,154701
40	416	414	410	413,3333	3,05505
50	410	414	410	411,3333	2,309401
60	414	419	416	416,3333	2,516611
70	410	404	408	407,3333	3,05505
80	406	404	408	406	2
90	406	409	404	406,3333	2,516611
100	409	409	404	407,3333	2,886751

d)

depth	value 1	value 2	value 3	average	STD
10	444	471	470	461,3333	15,30795
20	443	460	430	433	15,04438
30	409	390	394	391,3333	10,01665
40	390	385	378	381,6667	6,027714
50	382	372	390	382,3333	9,0185
60	385	390	390	398,3333	2,886751
70	415	414	385	405	17,03917
80	416	420	409	416,3333	5,567764
90	420	415	410	413	5
100	414	414	420	417	3,464102

Figure 71. Hardness values that were taken across cross-section of the shafts.

Figure 72 shows the hardness values of the inner sealing rings, each three different values, the mean value and standard deviation STD.

a)

depth	value 1	value 2	value 3	average	STD
10	654	654	654	654	0
20	652	662	662	658,6667	5,773503
30	760	704	704	722,6667	32,33162
40	662	683	693	679,3333	15,82193
50	606	652	642	633,3333	24,19366
60	606	606	600	604	3,464102
70	606	606	606	606	0
80	606	606	624	612	10,3923
90	620	606	606	610,6667	8,082904
100	606	606	606	606	0

b)

depth	value 1	value 2	value 3	average	STD
10	670	670	670	670	0
20	662	683	660	668,3333	12,74101
30	650	662	650	654	6,928203
40	624	624	624	624	0
50	624	618	618	620	3,464102
60	618	618	618	618	0
70	610	610	610	610	0
80	608	610	610	609,3333	1,154701
90	608	608	609	608,3333	0,57735
100	608	610	608	608,6667	1,154701

c)

depth	value 1	value 2	value 3	average	STD
10	640	660	640	646,6667	11,54701
20	683	633	633	649,6667	28,86751
30	624	624	624	624	0
40	624	624	624	624	0
50	624	624	624	624	0
60	624	624	633	627	5,196152
70	618	618	618	618	0
80	618	610	610	612,6667	4,618802
90	610	610	610	610	0
100	610	610	610	610	0

b)

depth	value 1	value 2	value 3	average	STD
10	670	670	686	675,3333	9,237604
20	650	670	650	656,6667	11,54701
30	610	650	650	636,6667	23,09401
40	620	630	650	633,3333	15,27525
50	620	640	620	626,6667	11,54701
60	630	620	630	626,6667	5,773503
70	616	620	616	617,3333	2,309401
80	610	610	610	610	0
90	610	610	610	610	0
100	610	610	610	610	0

Figure 72. Hardness values of inner sealing rings.

Hardness values of outer sealing rings, the values that are shown in Figure 73 below are taken from the part that is closer to the inner sealing ring, can be seen in Figure 6 marked with 4.

a)

depth	value 1	value 2	value 3	average	STD
10	686	703	686	691,6667	9,814955
20	640	640	610	630	17,32051
30	610	610	610	610	0
40	610	610	490	570	69,28203
50	596	535	522	551	39,50949
60	522	511	522	518,3333	6,350853
70	522	533	610	555	47,94789
80	557	583	639	593	41,90465
90	610	654	610	624,6667	25,40341
100	610	610	610	610	0

b)

depth	value 1	value 2	value 3	average	STD
10	686	686	686	686	0
20	686	686	670	680,6667	9,237604
30	703	686	686	691,6667	9,814955
40	703	703	703	703	0
50	703	656	686	681,6667	23,79776
60	686	670	683	679,6667	8,504901
70	703	673	672	682,6667	17,61628
80	673	670	670	671	1,732051
90	650	662	662	658	6,928203
100	662	662	662	662	0

c)

depth	value1	value 2	value 3	average	STD
10	779	770	760	769,6667	9,504385
20	721	735	730	728,6667	7,094599
30	721	721	721	721	0
40	670	686	670	675,3333	9,237604
50	670	686	686	680,6667	9,237604
60	703	686	703	697,3333	9,814955
70	686	670	686	680,6667	9,237604
80	686	703	703	697,3333	9,814955
90	703	686	703	697,3333	9,814955
100	670	670	670	670	0

d)

depth	value 1	value 2	value 3	average	STD
10	686	720	720	708,6667	19,62991
20	760	687	686	711	42,43819
30	624	686	704	671,3333	41,96824
40	640	720	730	696,6667	49,32883
50	686	686	686	686	0
60	704	686	704	698	10,3923
70	740	654	720	704,6667	45,0037
80	720	686	720	708,6667	19,62991
90	690	703	686	693	8,888194
100	730	654	700	694,6667	38,27967

Figure 73. Hardness values of outer sealing rings, from the side of the outer rings that's closer to the inner sealing rings.

Hardness of the outer sealing rings was measured even from the turbine wheel. The measurements values are shown in Figure 74. The hardness from the turbine wheel side are shown in Figure 6 the position is marked with 4.

a)

depth	value1	value 2	value 3	average	STD
10	759	759	759	759	0
20	759	739	759	752,3333	11,54701
30	799	799	778	792	12,12436
40	740	686	662	696	39,94997
50	683	662	662	669	12,12436
60	683	662	683	676	12,12436
70	662	670	645	659	12,76715
80	642	642	642	642	0
90	662	654	642	652,6667	10,06645
100	662	642	642	648,6667	11,54701

b)

depth	value1	value 2	value 3	average	STD
10	596	624	624	614,6667	16,16581
20	624	610	624	619,3333	8,082904
30	570	639	639	616	39,83717
40	639	639	596	624,6667	24,82606
50	670	654	654	659,3333	9,237604
60	670	670	703	681	19,05256
70	670	670	670	670	0
80	670	686	686	680,6667	9,237604
90	670	686	686	680,6667	9,237604
100	670	670	686	675,3333	9,237604

c)

depth	value1	value 2	value 3	average	STD
10	778	760	778	772	10,3923
20	686	670	686	680,6667	9,237604
30	686	670	686	680,6667	9,237604
40	670	654	670	664,6667	9,237604
50	670	670	670	670	0
60	686	686	686	686	0
70	670	670	686	675,3333	9,237604
80	670	654	670	664,6667	9,237604
90	670	670	670	670	0
100	670	670	670	670	0

d)

depth	value 1	value 2	value 3	average	STD
10	739	750	740	743	6,082763
20	750	720	720	730	17,32051
30	720	720	654	698	38,10512
40	630	630	700	653,3333	40,41452
50	670	624	680	658	29,86637
60	686	660	620	655,3333	33,24655
70	660	650	670	660	10
80	650	636	660	648,6667	12,05543
90	640	626	640	635,3333	8,082904
100	640	640	640	640	0

Figure 74. Hardness values of outer sealing rings, the measurements are taken from the turbine/exhaust gas side, as it can be seen the hardness values are generally higher than the hardness values of inner sealing rings.

F. Parameters influence on wear behavior of AISI 4140

Here is shown graphic representation of results of tribological tests performed with carbon steel AISI 4140 and tool steel HS 6-5-2. Discs were made of tool steel and pins are made of carbon steel. There are two gliding speeds: 3m/s (low) and 11m/s (high). The temperatures were 25°C and 300°C. Contact pressure was 0.5 and 1.5 MPa. Result of specific wear rate dependency can be seen below in Figure 75, Figure 76 and Figure 77.

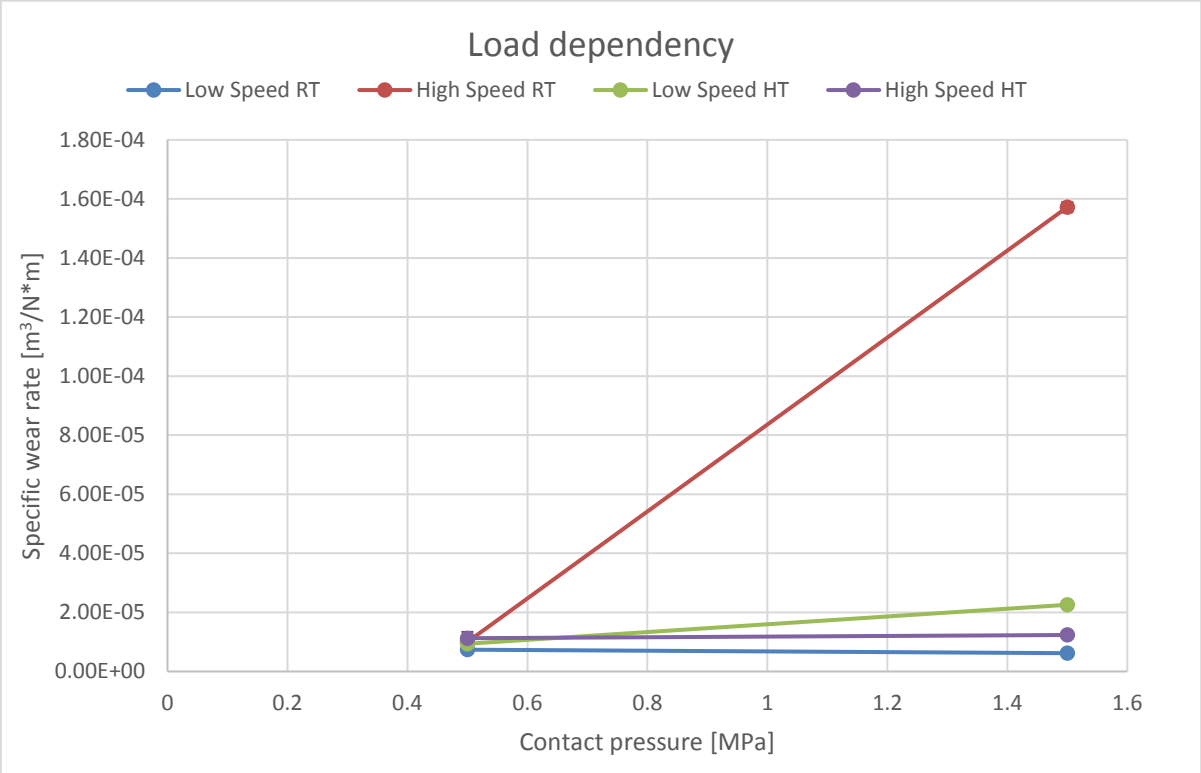

Figure 75. Specific wear rate of carbon steel AISI 4140 as function of load.

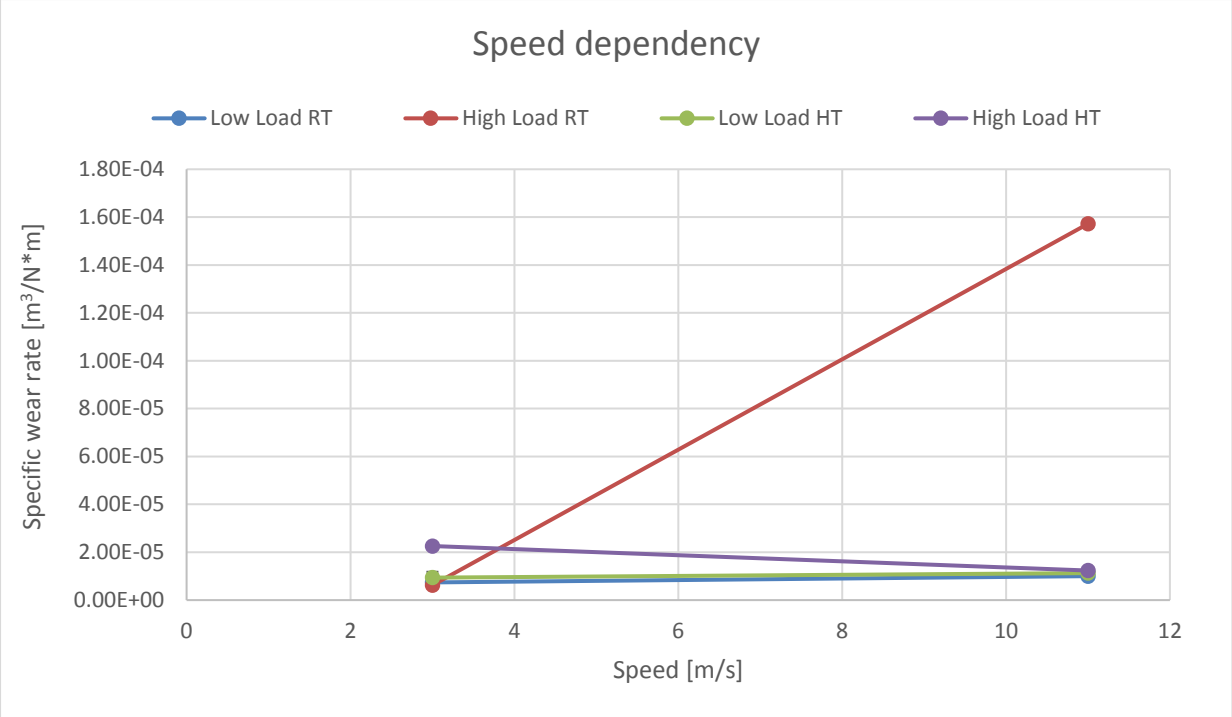

Figure 76. Specific wear rate of carbon steel AISI 4140 as function of gliding speed.

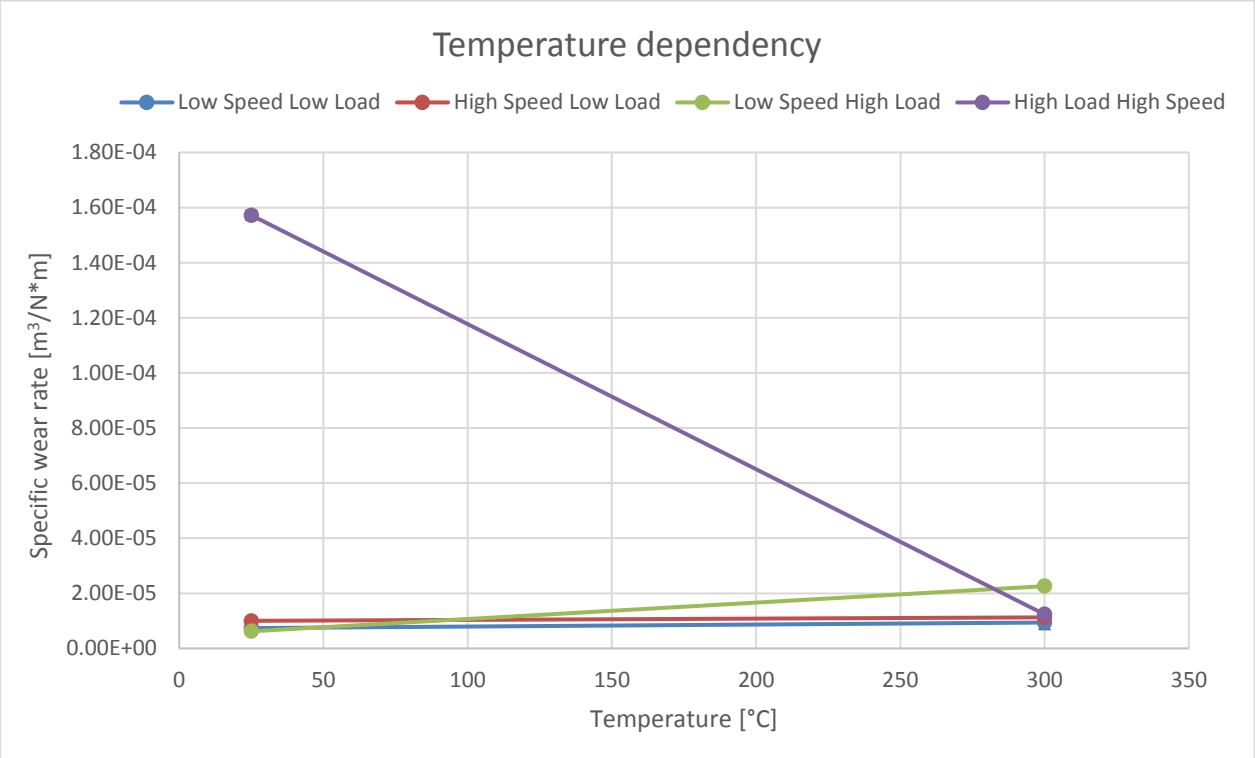

Figure 77. Specific wear rate of carbon steel AISI 4140 as function of temperature.